THE GEOMAGNETIC FIELD(A REVISION OF CHAPTER 11, HANDBOOK OF GEOPHYSICS AND SPACE ENVIRONMENTS)

David J. Knecht

Air Force Cambridge Research Laboratories
L. G. Hanscom Field, Massachusetts

26 September 1972

AFCRL-72-0570
26 SEPTEMBER 1972
AIR FORCE SURVEYS IN GEOPHYSICS, NO. 246

AIR FORCE CAMBRIDGE RESEARCH LABORATORIES
L. G. HANSCOM FIELD, BEDFORD, MASSACHUSETTS

The Geomagnetic Field

(A Revision of Chapter 11, Handbook of Geophysics and Space Environments)

DAVID J. KNECHT

AIR FORCE SYSTEMS COMMAND
United States Air Force

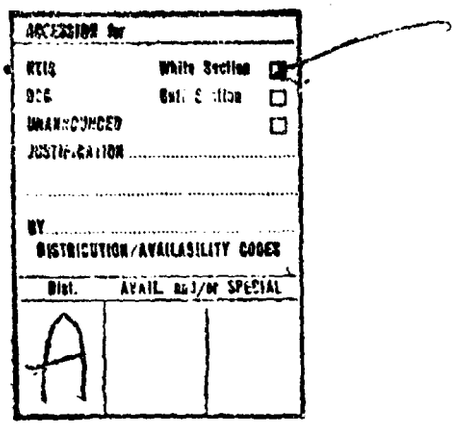

Qualified requestors may obtain additional copies from the Defense Documentation Center. All others should apply to the National Technical Information Service.

[redacted]

Unclassified

Security Classification

DOCUMENT CONTROL DATA - R&D

(Security classification of title, body of abstract and indexing annotation must be entered when the overall report is classified)

1. ORIGINATING ACTIVITY *(Corporate author)*
Air Force Cambridge Research Laboratories (PHG)
L. G. Hanscom Field
Bedford, Massachusetts 01730

2a. REPORT SECURITY CLASSIFICATION
Unclassified

2b. GROUP

3. REPORT TITLE
THE GEOMAGNETIC FIELD (A Revision of Chapter 11, Handbook of Geophysics and Space Environments)

4. DESCRIPTIVE NOTES *(Type of report and inclusive dates)*
Scientific. Interim.

5. AUTHOR(S) *(First name, middle initial, last name)*
David J. Knecht

6. REPORT DATE	7a. TOTAL NO. OF PAGES	7b. NO. OF REFS
26 September 1972	130 131	66

8a. CONTRACT OR GRANT NO.		9a. ORIGINATOR'S REPORT NUMBER(S)
b. PROJECT, TASK, WORK UNIT NOS.	76010801	AFCRL-72-0570
c. DOD ELEMENT	62101F	9b. OTHER REPORT NO(S) *(Any other numbers that may be assigned this report)*
d. DOD SUBELEMENT	681000	AFSG No. 246

10. DISTRIBUTION STATEMENT
Approved for public release; distribution unlimited.

11. SUPPLEMENTARY NOTES	12. SPONSORING MILITARY ACTIVITY
TECH, OTHER	Air Force Cambridge Research Laboratories (PHG) L. G. Hanscom Field Bedford, Massachusetts 01730

13. ABSTRACT

This survey summarizes what is known about the magnetic field of the earth, based on information available through 1971. Observed phenomena are described and interpreted in terms of the most widely accepted physical explanations. An overview of the geomagnetic field and its dynamic relationship with its terrestrial and interplanetary environment is first presented as briefly as possible, followed by more detailed descriptions of geomagnetic measurements and experimental methods, precise current models and past behavior of the main field, regular variations in the field resulting from the motion of the earth, disturbance variations of the field produced by the interplanetary environment, and dynamic processes occurring in the outer magnetosphere. Extensive references to sources of data and more detailed publications are provided. This survey is a replacement for Chapter 11 of Handbook of Geophysics and Space Environments (Shea L. Valley, ed.), Air Force Cambridge Research Laboratories and McGraw-Hill Book Co., New York, 1965.

DD FORM 1 NOV 65 1473

Unclassified

Security Classification

Unclassified

Security Classification

14. KEY WORDS	LINK A		LINK B		LINK C	
	ROLE	WT	ROLE	WT	ROLE	WT
Geomagnetism Magnetic storms Magnetosphere Disturbance Magnetometers Paleomagnetism						

Unclassified

Security Classification

AFCRL-72-0570
26 SEPTEMBER 1972
AIR FORCE SURVEYS IN GEOPHYSICS, NO. 246

SPACE PHYSICS LABORATORY PROJECT 7601

AIR FORCE CAMBRIDGE RESEARCH LABORATORIES

L. G. HANSCOM FIELD, BEDFORD, MASSACHUSETTS

The Geomagnetic Field

(A Revision of Chapter 11, Handbook of Geophysics and Space Environments)

DAVID J. KNECHT

AIR FORCE SYSTEMS COMMAND

United States Air Force

Abstract

This survey summarizes what is known about the magnetic field of the earth, based on information available through 1971. Observed phenomena are described and interpreted in terms of the most widely accepted physical explanations. An overview of the geomagnetic field and its dynamic relationship with its terrestrial and interplanetary environment is first presented as briefly as possible, followed by more detailed descriptions of geomagnetic measurements and experimental methods, precise current models and past behavior of the main field, regular variations in the field resulting from the motion of the earth, disturbance variations of the field produced by the interplanetary environment, and dynamic processes occurring in the outer magnetosphere. Extensive reference to sources of data and more detailed publications are provided. This survey is a replacement for Chapter 11 of Handbook of Geophysics and Space Environment (Shea L. Valley, ed.), Air Force Cambridge Research Laboratories and McGraw-Hill Book Co., New York, 1965.

Preface

This survey is a replacement for Chapter 11, "The Geomagnetic Field", of the Handbook of Geophysics and Space Environments, Air Force Cambridge Research Laboratories and McGraw-Hill Book Company, 1965. Numbering of sections does not correspond to the previous numbering, so the cross-referencing system in other chapters will not be valid. This survey summarizes what is known about the magnetic field of the earth, based on information available through the end of 1971 when the manuscript was written.

Contents

Illustrations

Tables

The Geomagnetic Field

(A Revision of Chapter 11, Handbook of Geophysics and Space Environments)

11.1 INTRODUCTION

11.1.1 Historical Perspective

The existence of the geomagnetic field has been recognized for a very long time. The usefulness of a magnet as a directional reference was probably known in China more than 1000 years ago and in Europe at least 800 years ago. As early as the 15th century, the earlier belief that a compass needle points true north was found to be incorrect, and mariners and mapmakers took account of this. Recorded measurements of the magnetic declination (the deviation of the compass from true north) at various locations on the earth date back to the early 16th century, which also saw the discovery of the magnetic dip (the deviation of a compass needle from horizontal when unconstrained). Although experiments with magnets had been carried out since the 13th century, the concept that the earth itself is a magnet was not advanced until the end of the 16th century, by Gilbert. From these beginnings, geomagnetism, as a branch of science, was developed. It was first assumed that the magnetism of the earth was like that of a solid permanent magnet, and it was therefore expected to be constant in the absence of major geological changes, but this view was soon proved wrong; the secular variation (changes in the field over time intervals of years or centuries) was discovered in the 17th century. Transient

(Received for publication 22 September 1972)

variations of the field (geomagnetic disturbance) were observed during the 18th century, and geomagnetism was increasingly appreciated to be a dynamic phenomenon. By the early 19th century, a large number of magnetic observatories had been established, both in European countries and in the distant lands of their empires. Through coordinated measurements by many stations, the geographic dependence of some geomagnetic phenomena was discovered and the worldwide nature of major disturbances was established. The increasing volume and precision of accumulated data made discouragingly clear how complex were the phenomena being studied. Increasing international cooperation included investigations during the first International Polar Year (1882-1883). By this time, the correlation between the 11-year periodicities of sunspot occurrence and geomagnetic phenomena had been noted. Early in the 20th century, the intimate connection between solar and geomagnetic phenomena was further established by the correlation of recurrent disturbances with the 27-day solar rotation and, later, by the correlation of magnetic storms with solar flares. However, the most important connection, the fact that the geomagnetic field interacts with a continuous stream of solar plasma, was established only within the last ten years. As a result of satellite investigations, these recent years have seen drastic revisions in many of the fundamental concepts of geomagnetism.

11.1.2 Current Perspective and Scope

It is clear from this brief historical account that, while the dynamic nature of the geomagnetic field has long been appreciated, the basic outlines of a unified explanation of geomagnetic phenomena have been rather obscure almost to the present time. This was so, of course, mainly because the generating processes take place either deep inside the earth or high in space, while experimental measurements could be made only on or close to the surface of the earth. Now, in the last decade, a picture has emerged in which the geomagnetic field is seen as a complex feature of the planet interacting with its environment in the solar system. Rigorous theoretical treatment and important detail are still lacking for some portions of the picture, and even some of the basic concepts are not firmly established. However, there is sufficient agreement and consistency to justify basing the present discussion on this picture, placing less emphasis on the traditional ground-based description of the field.

The complexity of the geomagnetic field, extending over large regions of space, entering into many types of interactions, and intruding into a variety of disciplines from geology to plasma physics, suggests that a brief review of the entire field might be of questionable value because of the omissions and oversimplification which would be necessary. Against this difficulty, however, is

weighed the desirability of presenting a unified physical picture to clarify the relationships which exist between geomagnetic phenomena of vastly differing type, magnitude, and location. Therefore, the following sections are intended to summarize for the nonspecialist the current understanding in most of the major areas of geomagnetism, with emphasis on providing the simplest possible explanation of the physics involved. Discussion of fundamentals and clarifying description have been included, while most rigorous mathematical theory has been omitted. Similarly, the space limitation has permitted reproducing only a few of the quantitative numerical and graphical data which should be included in a handbook, and, of the tables and charts included, most are intended for illustrative purposes rather than reference use. To compensate, references are given to more detailed reviews and data sources, along with information on the availability of these.

11.2 A SUMMARY OF CURRENT UNDERSTANDING

The material of this section presents a broad and somewhat simplified overview of the geomagnetic field by listing and discussing briefly the processes which contribute significantly to the static and dynamic nature of the field and indicating how these processes are related in a unified picture of geomagnetic phenomena. Terminology, conventions, coordinate systems, and units are introduced. Important phenomena and processes are taken up again in greater detail in subsequent sections.

11.2.1 Physical and Geometric-Temporal Descriptions

Theory, in attempting to account for the geomagnetic field in terms of physical processes going on within the earth, the magnetosphere, and the interplanetary environment, leads to a physical description of the field. To the extent possible, such a description is presented here. Experiment, on the other hand, most often produces measurements of the field which constitute a geometric-temporal description. Recognizable characteristics of data (taken as a function of location and time, with varying frequency response) are usually assigned a terminology or otherwise classified long before they can be attributed to specific physical causes, since the latter is often accomplished only with difficulty and after repeated attempts. Therefore, the two descriptions are always mixed in the literature, and they are mixed in the following discussions; it must be kept clearly in mind whether the discussion and terminology relate to a physical or to a geometric-temporal description.

11.2.2 Units, Terminology, and Conventions

The geomagnetic field is characterized at any point by its direction and magnitude, which can be specified by two direction angles and the magnitude, the magnitude of three perpendicular components, or some other set of three independent parameters. Angles are commonly measured in degrees, minutes, and seconds. The magnitude is usually given in units of oersted (magnetic intensity) or gauss (magnetic induction). Since the field is less than one oersted everywhere, the unit gamma is often used; one gamma equals 10^{-5} oersted or 10^{-5} gauss, being used interchangeably for intensity and induction. Some of the angles and components commonly employed are shown in Figure 11-1. Standard terminology is as follows. The vector geomagnetic field is the vector $\overline{F}$. Its magnitude F is called the total intensity or the total field. The magnitude H of the horizontal component vector $\overline{H}$ is called the horizontal intensity; the magnitude Z of the vertical component vector $\overline{Z}$ is called the vertical intensity. The northward, eastward, and downward components of the field are designated by the magnitudes X, Y, and Z, respectively, the Cartesian components of the field. The magnitude D of the angle between $\overline{X}$ and $\overline{H}$ is called the declination, the magnetic variation, or the variation of the compass. The magnitude I of the angle between $\overline{H}$ and $\overline{F}$ is called the inclination or the dip. The

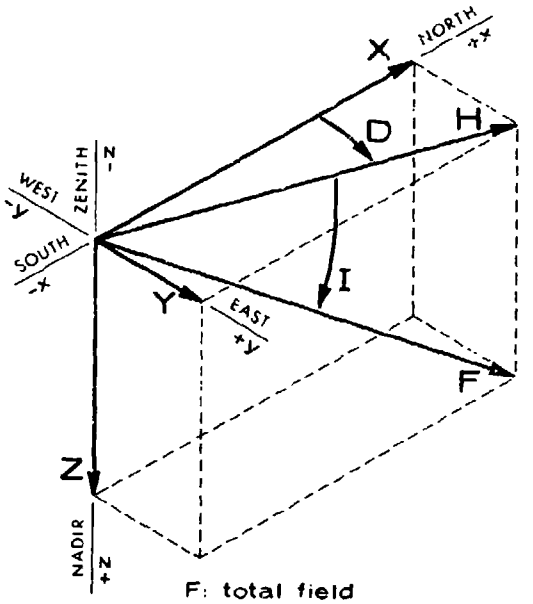

F: total field
H: horizontal component
X: northward component
Y: eastward component
Z: vertical component
D: declination
I: inclination

Figure 11-1. Definition and Sign Convention for the Magnetic Elements

quantities F, H, X, Y, Z, D, and I are called magnetic elements. The sets of elements used most commonly to specify the field are (H, D, Z); (F, I, D); and (X, Y, Z). The sign convention for each parameter is shown in the figure, all vectors and angles being positive as drawn.

11.2.3 Coordinate Systems

A number of coordinate systems have been employed in the description of geomagnetic phenomena. Four of the most useful are the geographic, geomagnetic, solar-ecliptic, and solar-magnetospheric systems. They are shown in Figure 11-2

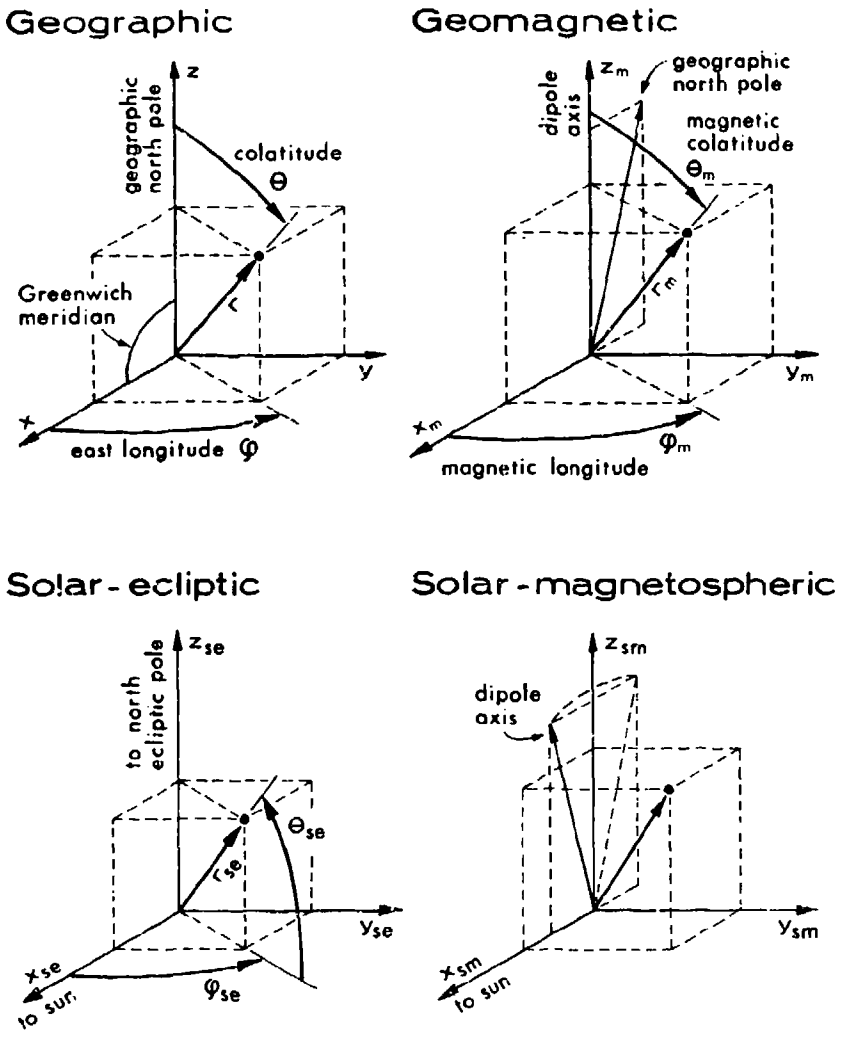

Figure 11-2. Coordinate Systems Useful in Geomagnetism

and are defined as follows:

A geographic coordinate system is one which is fixed with respect to the rotating earth and aligned with the axis of rotation. Most commonly used are the spherical polar coordinates r, θ, and φ, where r is geocentric distance, θ is colatitude (measured from the north geographic pole), and φ is east longitude (measured from the Greenwich meridian), with the earth assumed spherical. Sometimes altitude (above the surface of the earth) is specified in place of r, north or south latitude is specified in place of θ, and west longitude is specified in place of φ for values greater than 180 degrees. (Care is necessary in using geodetic coordinates which are defined relative to the nonspherical earth ellipsoid.)

The geomagnetic coordinate system is also a spherical polar system fixed relative to the earth, but the polar axis is the axis inclined 11.5 degrees to the axis of rotation, intersecting the earth surface at the point 78.5°N, 291.0°E, which is the geomagnetic north pole. As detailed below in Section 11.4.2, this is the axis of the best centered-dipole approximation to the field. Geomagnetic coordinates r, θ_m, and φ_m (and geomagnetic latitude and longitude) are defined by analogy with geographic coordinates, with φ_m (or geomagnetic longitude) measured from the American half of the great circle which passes through both the geographic and geomagnetic poles (that is, the zero-degree geomagnetic meridian coincides with 291.0°E geographic longitude over most of its length).

The solar-ecliptic coordinate system is a right-handed Cartesian system with coordinates x_{se}, y_{se}, and z_{se}, and the center of the earth as origin. The positive x_{se} axis is directed toward the sun. The z_{se} axis is directed toward the northern ecliptic pole, so both the x_{se} and y_{se} axes lie in the ecliptic plane. This system therefore rotates slowly in space with the orbital period of the earth. In this system, field vectors are often resolved into two components, one lying in and the other perpendicular to the ecliptic plane; the direction of the former is specified by the angle φ between it and the x_{se} axis (positive counterclockwise when viewed from the northern pole). The direction of the total field is specified by φ and θ, where θ is the angle between the vector and the ecliptic plane (positive northward). This system is particularly useful for referencing data from interplanetary space, such as measurements of the undisturbed solar wind and the interplanetary magnetic field.

The solar-magnetospheric coordinate system is also a right-handed Cartesian system, with coordinates x_{sm}, y_{sm}, and z_{sm}, and its origin at the center of the

earth. The positive x_{sm} axis is also directed toward the sun. It differs from the solar-ecliptic system in that the z_{sm} axis lies in the plane containing both the x_{sm} axis and the geomagnetic dipole axis defined above. The system therefore not only rotates with the orbital period of the earth but also rocks back and forth through 23 degrees (a rotation about the x_{sm} axis) with a period of one day. This system is particularly useful for referencing data from distant regions of the magnetosphere, since time-dependent features which result from the conical motion of the dipole axis are, to a large extent, eliminated; that is, to a first approximation, the entire magnetosphere, in its main features, may be expected to rock back and forth in this way.

In addition to strictly spatial coordinate systems, several so-called magnetic systems have been found useful in studying the motion of charged particles trapped in the magnetic field; these coordinates generally locate particles by reference to surfaces on which some magnetic parameter is constant, and since most particles are strongly controlled magnetically, a great simplification of the data often results. Most widely used is the B-L coordinate system of McIlwain; as shown in Figure 11-3, surfaces of constant B (magnetic field intensity) are concentric, roughly ellipsoidal shells encircling the earth, while surfaces of constant L (a magnetic parameter) approximate the concentric shells generated by dipole field lines rotating with the earth. The mathematical definition of L arises from the equations of motion of particles in the field; to some degree of approximation, particles move to conserve three adiabatic invariants, to which B and L are simply related. Since these coordinates are more useful to the study of trapped particles than to the study of the field itself, the reader is referred to standard texts on trapped-particle physics for a complete discussion (for example, see Chapter 2 of Hess [1968]).

11.2.4 Sources of the Field

In considering a physical description of the field, a useful point of view to adopt is that of energy balance. A static field represents an energy density $B^2/8\pi$, and any change in the field implies a transfer of energy to or from the field. Understanding the field therefore implies identifying the energy sources and the causative physical mechanisms through which this energy generates (or is generated by) the field. Except in the case of permanent residual magnetism, a magnetic field is generated only by the macroscopic motion of electric charge, so the final step in any physical process affecting the field will involve electric currents, though the energy driving the currents may be drawn from various sources. At present, the terrestrial and extraterrestrial sources known to contribute appreciably to the geomagnetic field are the following:

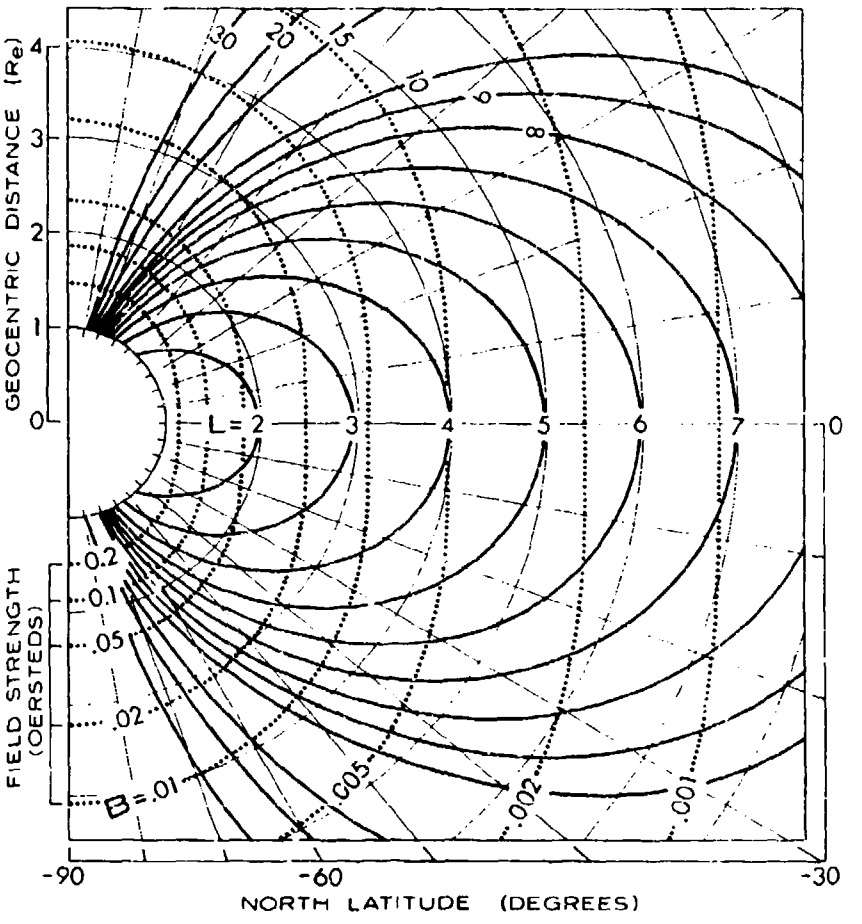

Figure 11-3. The B-L Coordinate System. The curves are the intersection with a magnetic meridian plane of surfaces of constant B and constant L. The departure of these curves, plotted for a dipole field, from those of the actual field is too small to be apparent in a figure of this scale

Core Motion. Convective motion of the conducting fluid core of the earth constitutes a self-exciting dynamo.

Crustal Magnetization. Residual permanent magnetism exists in the crust of the earth.

Solar Electromagnetic Radiation. Atmospheric winds produced by solar heating move charged particles produced by solar ionizing radiation, constituting ionospheric currents which generate a field.

Gravitation. The gravitational field of the sun and moon produces a tidal motion of air masses which generates a field in the same way as does the air motion from solar heating.

Solar Corpuscular Radiation. A number of field contributions arise directly or indirectly from the interaction of solar plasma with the main field; important effects include compression of the main field by external plasma pressure, the intrusion of solar plasma into the main field, and the heating of plasma already within the field.

Solar Interplanetary Field. This field is relatively weak, but at large distances from the earth it has a major effect on the interaction of the solar plasma with the geomagnetic field.

There are a number of other obvious possible sources which, in fact, do not contribute appreciably; examples are the earth's mantle and energetic cosmic rays.

11.2.5 The Steady Field

A geometric-temporal description of the field is constructed from measurements made by observatories, stations, ships, rockets, satellites, etc., all of which are restricted in geometric coverage (geographic or spatial location) and temporal coverage (time period and frequency response). Observed phenomena tend to be classified accordingly. The traditional classification by frequency is very useful and is retained here.

The steady (nonvarying or dc) component of the field may be considered first. Although it is true that the entire field has been varying drastically over geological time scales, that portion which varies with periodicities greater than about a year is customarily considered to be the steady field, while the remainder is considered the variation field.

Most of the steady field arises from internal terrestrial sources (that is, below the surface of the earth, but excluding currents induced in the earth by external current systems) and is known as the main field. This field results primarily from convective motion of the core and is approximately of dipole configuration, having a strength at the surface of the earth of a fraction of an oersted. The dipole is centered close to the geographic center of the earth, with its axis inclined about 11.5 degrees to the axis of rotation. About ten percent of the main field, often termed the residual field, is nondipolar; it consists of both large-scale anomalies (up to thousands of kilometers), believed to be generated by eddy currents in the fluid core, and small-scale irregularities (down to ten kilometers), arising from residual magnetism in the crust. Changes in the main field, the so-called secular variation, are slow, with time constants of tens to thousands of years.

If the earth were in a perfect vacuum, its dipole field would extend outward without limit, merging smoothly with the fields of the sun and other planets in a simple additive fashion, the field strength declining inversely with the third power of the geocentric distance. However, interplanetary space is not a vacuum but is

filled with the ionized corona of the sun, the solar wind, which flows continuously outward past the planets. On a quiet day, near the earth, this plasma typically has a density of a few ions/cm^3 and a velocity of about 400 km/sec. An important feature of the plasma is its high electrical conductivity. One result of applicable theory is that the magnetic field will be "frozen into" such a plasma; that is, the ions, electrons, and magnetic field will move together as a compressible fluid medium. When such a moving fluid encounters a stationary entity with which it can interact, such as the geomagnetic field, one or the other will be deflected, swept away, or otherwise modified by the collision. The total pressure of the solar wind is the sum of the pressure exerted by the momentum of the particles and the Maxwell pressure $B^2/8\pi$ of the frozen-in field. The geomagnetic field also contains highly conductive plasma, and this medium similarly sustains a pressure equal to the sum of the ambient-plasma and Maxwell pressures. When the pressures of the interplanetary medium and the geomagnetic field are compared, it is clear that at great distances the geomagnetic field will be swept away by the solar wind and that close to the earth the wind will be excluded by the field. At intermediate distances there must exist a region of interaction where the pressures are comparable and where rather complicated features may be expected. In the last decade, satellite experiments and theoretical development have discovered and clarified the principal features of this interaction. Some of them are illustrated in Figure 11-4. (In this figure and much of the following discussion, the 23-degree tilt of the rotational axis and the 11.5-degree tilt of the dipole axis have been neglected for simplicity.) The field of the earth extends to about 10 R_e geocentric distance toward the sun (R_e being a unit of length equal to the radius of the earth), at which distance it terminates abruptly in a thin layer known as the magnetopause. The region interior to this layer is known as the magnetosphere. The region exterior to it contains the solar wind, which is "piled up", that is, compressed, deflected, heated, and made turbulent by the collision. These effects propagate some distance upstream, with the result that the wind is slowed over a distance of a few R_e. Since the velocity of the undisturbed wind is "supersonic", there exists a surface at which the velocity is just "sonic", and a stationary shock front, the bow shock, is created. The magnetopause is typically at about 10 R_e and the bow shock at about 14 R_e on the sun-earth line. The region between these is called the magnetosheath. In the plane of the dawn-dusk meridian, the solar wind exerts less pressure on the magnetopause because of its oblique incidence, and the magnetopause and bow shock typically intersect this plane at about 14 and 21 R_e respectively. Field lines from the high-latitude (polar-cap) regions are swept back toward the night side and form a long geomagnetic tail. Although it might be expected that solar-wind pressure perpendicular to the direction of its bulk flow should close the magnetosphere within a few tens of earth radii behind the earth,

this is not the case: the combined pressure of field and plasma within the tail is sufficient to prevent closing, and the tail has been observed at a distance of more than 1000 R_e behind the earth. It might also be expected that the north polar field lines (at least the more sunward of them) would be connected to the corresponding south polar field lines, crossing the equatorial plane smoothly within the tail, but this too does not happen; these field lines are also drawn out into the tail, directed toward the earth above the plane and away from the earth below it. Thus, in the tail (beyond a geocentric distance of about 10 R_e) the equatorial plane (neglecting tilts) is a sort of neutral sheet, across which there is an abrupt field reversal. (This is, in fact, only approximately true; the component perpendicular to the neutral sheet is not quite zero.)

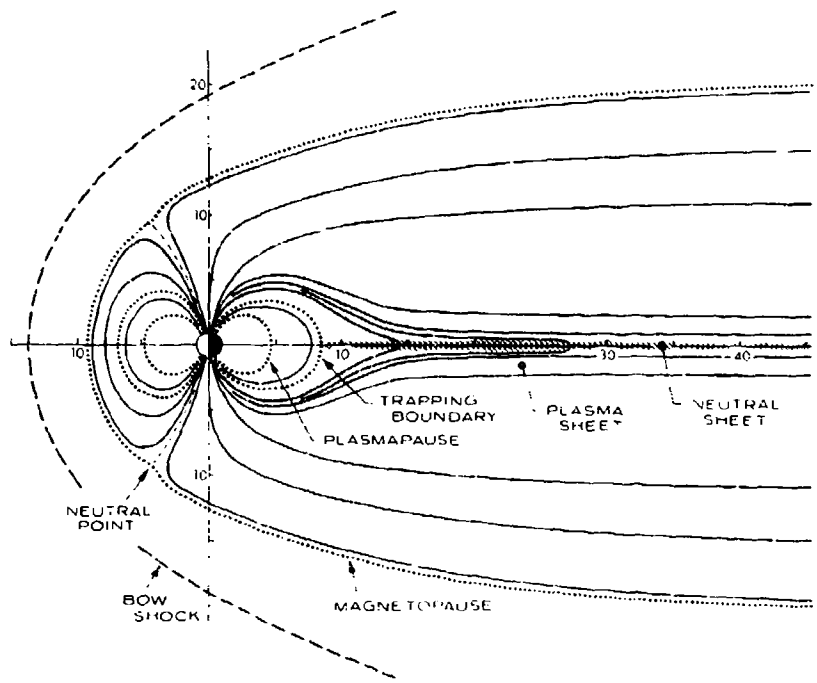

Figure 11-4. General Configuration of the Magnetosphere, Shown in a Noon-Meridian Section

A surface of discontinuity in the magnetic field implies the existence of a current flow in the surface, and the current pattern can be inferred from the field. On the sunward magnetopause the flow is characterized by an eastward current sheet (dawn-to-dusk) across the nose (subsolar point) of the magnetosphere. In the neutral sheet the flow is westward across the tail (also dawn-to-dusk), with return loops on the tailward part of the magnetopause. These currents are shown schematically in Figure 11-5. (The composite magnetopause current is not shown.)

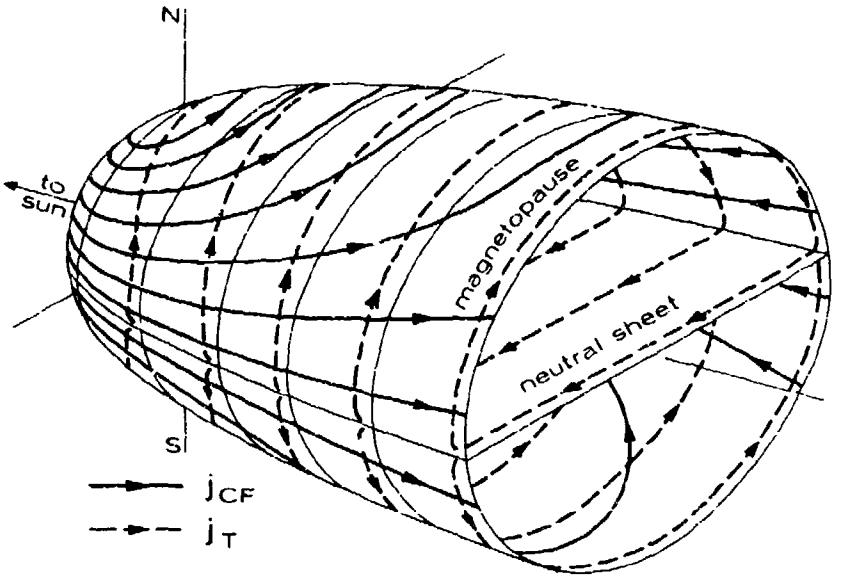

Figure 11-5. Flow Patterns of the Two Current Systems Which Determine the Configuration of the Magnetosphere. The Chapman-Ferraro current j_{CF} confines the field on the sunward side, and the tail current j_T produces the extended geomagnetic tail [adapted after Axford, 1965]

The current system of the magnetopause acts to cancel the dipole field outside and enhance the field inside the magnetopause. This is equivalent to a compression of the geomagnetic field by the cavity to which it is confined. Because the cavity almost totally surrounds the earth, the field is compressed on all sides, but since the tail is open and the highest pressure is on the nose of the cavity, the compression is somewhat less on the night side. The compression results in an average increase of the equatorial surface field of about 0.1% (about 30 gammas); just inside

the magnetopause the increase is 100% (which is about 30 gammas when the magnetopause is at 10 R_e but about 60 gammas if it has been pushed in to 8 R_e). About a third of the surface increase results from diamagnetism in the solid earth.

The steady field, then, consists basically of the main field of the earth compressed by the cavity to which it is confined. In addition, each of the time-varying field contributions discussed below is also (like the magnetopause current) likely to have an average dc value which may be thought of as part of the steady field, but at present such distinctions are not often useful nor made. For example, convection of the outer magnetosphere and the flowing of a ring current are processes which continue even on the quietest days, but their quantitative contributions to the steady field are small and not well established.

11.2.6 Quiet Variation Fields

The earth, with its core, atmosphere, and main field, rotates in the interplanetary environment and moves along its orbit so that any point stationary in geographic coordinates experiences periodic variations in gravity force, solar illumination, and compression or other modification by solar-wind effects. The field contributions which result from these motions vary diurnally and seasonally. Field contributions which vary this slowly and regularly and do not result from disturbances in the interplanetary environment are known as quiet variation fields. The analysis of experimental data to determine the quiet variation fields, is, of course, difficult in the presence of magnetospheric disturbances, and criteria for separating field contributions are somewhat arbitrary and subject to personal judgment. These fields were originally defined on the basis of data taken during a few quietest days per month, but with better understanding of magnetospheric disturbance, improved measurements, and an awareness that quietness is only relative (any day being only more or less disturbed), it is now more common to consider them in an idealized sense as being those variations which would exist if the earth were subjected only to an absolutely quiet external environment.

Quiet variation fields include several contributions. The so-called Sq (solar quiet) variation field results almost entirely from solar electromagnetic radiation, which heats and ionizes the atmosphere, producing convective flow and high conductivity in the ionosphere; this motion of a conducting fluid in the presence of the main field generates currents which produce the field. The Sq field at most surface locations has a peak-to-peak amplitude of several tens of gammas. Similarly, the tidal flow of the atmosphere arising from the luni-solar gravitational field generates currents which produce the so-called L (lunar daily) variation field, which has an amplitude at the surface of a few gammas (about a tenth that of the Sq field). Another contribution results from the confinement of the main field by

the solar wind; since this compression is stronger on the day side than on the night side, there is a diurnal variation; its amplitude is also a few gammas at the surface, while in the more distant regions of the magnetosphere it is, of course, dominant, completely altering the field configuration. However, in discussing these distant regions, it is common to employ a coordinate system (such as solar-magnetospheric coordinates) which does not rotate with the earth, and most of the diurnal effect is eliminated.

Quiet variation fields are discussed in Section 11.5, which, for both historical and practical reasons, retains a ground-based perspective.

11.2.7 Disturbed Variation Fields

Variations in the geomagnetic field which do not have a simple periodicity and which appear to result from changes in the interplanetary environment are termed disturbed variation fields or geomagnetic disturbance and are denoted by D. The D field is that remaining after the steady and the quiet variation fields have been subtracted from the total. Large disturbances of relatively long duration, the behavior of which suggests some magnetospheric event as the cause, are termed geomagnetic storms. Except for some fluctuations attributable to irregular motion of the upper atmosphere, the sun is responsible for all disturbance effects recognized at present, and, with only two exceptions, it is the solar wind, with the frozen-in solar magnetic field, which transmits the disturbance to the vicinity of the earth. The two exceptions are disturbances associated with solar flares: polar-cap absorption events (PCA) result from low-energy protons from the flare, and so-called solar flare effects (SFE) apparently result from X-ray emissions from the flare. Both affect the field by enhancing ionospheric conductivity; they are discussed in Section 11.6.5.

Historically, the disturbance field has been studied by ground observation, with the hope of separating the observed surface field into components which could be explained in terms of current systems above the earth. A useful geometric-temporal distinction has been the separation of the component which depends only on universal time (UT) from that which depends on local time (LT); the former, usually called the storm-time variation and denoted by Dst, is symmetric about the polar axis, while the latter, called the disturbance-daily variation and denoted by DS (or Ds), is asymmetric. Then D = Dst + DS. The component Dst was attributed to a ring current encircling the earth a few earth-radii above the equator, while DS was attributed to ionospheric currents generated by auroral particles precipitated from the ring current. Although better knowledge of the magnetosphere has made clear that ionospheric and magnetospheric current systems are intimately related, this separation is still useful. Other separations have been made or

proposed, usually relating to a physical rather than a geometric-temporal description and often applicable only to a specific theoretical model. Many are currently in use in the literature, but it is likely that they will be revised as the description improves.

Apart from the exceptions noted, geomagnetic disturbance results from the interaction of the solar wind with the geomagnetic field. Some minimum level of disturbance might be expected to result from turbulence generated by instabilities in the flow of plasma around the magnetosphere, even if solar-wind properties were absolutely constant. However, the usual disturbance phenomena, having characteristic times of minutes to days and observable in ground-based measurements of the field, result from variations (often abrupt) in one or more of the solar-wind parameters, for example, the density or velocity of the plasma or the direction or intensity of the interplanetary field. The larger events are called geomagnetic storms, and although phenomena vary greatly from storm to storm, the average or typical behavior (the "classic" magnetic storm) may be described. It is likely that the classic storm involves all or most of the processes which contribute to any magnetic disturbance and that the different types of events which have been distinguished and described in the literature are members of a single family. An understanding of the classic storm, which stands out above the background of ever-present smaller disturbances, is therefore likely to explain most other disturbance phenomena as well.

The progress of a storm is most clearly observable in recordings of the surface field (magnetograms), particularly of the horizontal component. Figure 11-6 shows the average behavior of the horizontal components of Dst and of the daily range of DS for 346 magnetic storms observed at 30° geomagnetic latitude. The classic storm begins with a sudden commencement (ssc or SC), which (at low-latitude observatories) is an impulsive increase in H, typically having a rise time of one to six minutes and an amplitude of several tens of gammas. (The ssc is not observable in Figure 11-6.) The ssc is observed over the entire earth with a spread in arrival time of less than one minute and, depending on location and the particular storm, may be positive, negative, double-valued, or absent entirely. It is apparently caused by the impact on the magnetosphere of a discontinuity in the solar wind, normally a sharp increase in pressure, which compresses the magnetosphere more strongly. The rise time of the observed surface-field increase is the time required for the discontinuity to reach all points of the magnetopause and to be transmitted to the ground as a hydromagnetic wave. An event of this type which is not followed by the later phases of a storm is called a sudden impulse (SI). The initial phase of the storm follows the ssc and typically lasts two to eight hours, during which the field remains compressed by the increased pressure behind the discontinuity. The initial phase is terminated by the main phase, seen at low

latitudes as a rapid decrease in the field to values below the prestorm level; the main-phase decrease often approaches or exceeds 100 gammas, developing over a period of a few hours to a day. It is characterized by noise (large fluctuations with a broad spectrum of rise times) and an asymmetry in local time, often developing first in the afternoon-evening sector. It represents an expansion or inflation of the field by a ring current (of charged particles trapped in the field), which must arise either from the heating of plasma already trapped or from the injection of new plasma. The recovery phase, which follows the main phase, consists of a quiet increase of the field toward the prestorm value. The recovery often proceeds more rapidly at first than later, suggesting that more than one process is involved. The recovery typically has a characteristic time of about one day, but it may take much longer. Recovery results from the termination of the process supplying the heated plasma and a cooling (or removal) of the plasma which had inflated the field. Geomagnetic storms are discussed more fully in Section 11.6.1.

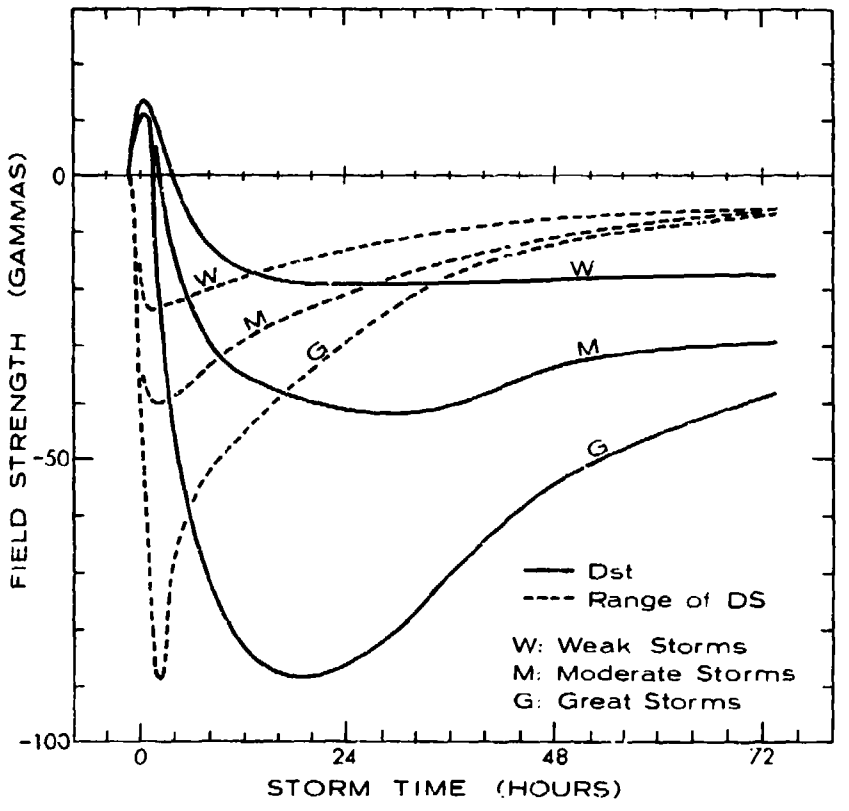

Figure 11-6. Characteristic Development of the Classic Geomagnetic Storm, as Shown by the Storm-Time (Dst) and Disturbance-Daily (DS) Variations at Low Latitudes, Averaged for 346 Storms [after Sugiura and Chapman, 1960]

Because the magnetosphere is an elastic entity, its dynamic behavior includes oscillations, especially during magnetic disturbances. Periodic and aperiodic field fluctuations with frequencies covering nearly 8 decades (10^{-3} to 10^{5} Hz) have been observed. In the lower frequency range (.0016 to 5 Hz) they are called micropulsations. Rapid fluctuations are discussed in Section 11.6.4.

11.2.8 Other Magnetospheric Phenomena

In the magnetosphere, particle and field phenomena are intimately related. Magnetospheric processes typically involve the transfer of energy back and forth between the magnetic field, electric fields, and charged-particle populations, and a determination of how much energy resides in each depends, of course, upon the choice of coordinate system. Therefore, it is impossible to study the magnetic field without considering the nature of electric fields and the behavior of charged particles. Even when these do not enter appreciably into the energetics, they serve as useful diagnostic indicators.

Auroras are the visible result of the precipitation of charged particles into the atmosphere. The motion of the particles is strongly controlled by the magnetic field; some auroral particles result from the release of normal trapped particles by scattering or field changes, but most must be guided by the magnetic field into the atmosphere from a newly introduced population. Visible and nonvisible radiation results following the excitation of atmospheric constituents by the charged particles. Although there is always some precipitation of auroral particles, active auroral displays are intimately associated with geomagnetic disturbance. Energies of auroral particles typically range from less than one to more than ten keV. The total energy expended around the world in auroras is significant, the average being about 10^{18} ergs/sec or one percent of the total energy of the solar wind which collides with the magnetosphere. In large auroral events a considerably higher percentage is expended.

Trapped radiation, almost entirely protons and electrons, is a constant feature of the inner magnetosphere. Particle energies extend upward (with decreasing intensity) to tens and hundreds of MeV. The more energetic particles often have long trapping lifetimes and a fairly constant intensity, but their energy density is small compared with that of the magnetic field which holds them and their importance in geomagnetic phenomena is therefore relatively minor. Populations of charged particles with energies less than 100 keV are important, however. They have a much greater density and variability, their energy density is often appreciable compared with that of the field, and their energies are comparable with electric-field potentials which can exist over magnetospheric dimensions. The magnetic-storm ring current (that is, the plasma which inflates the field during the

main phase of a storm) consists of protons and electrons with energies of the order of tens of keV.

Thermal plasma surrounds the earth from ionospheric altitudes outward to about 4 or 5 R_e (on the equator) where the density typically suffers a fairly sharp decrease by about two orders of magnitude. The surface on which this occurs is shaped like a magnetic shell, but with a characteristic deformation; it is known as the plasmapause. (See Figure 11-4.) Its location clearly is intimately related to the pattern of convection of the magnetic field in the inner magnetosphere. The concept of convection is a useful one. It may intuitively be considered to be the motion, as a fluid, of the field lines and the particles confined to them; the motion is perpendicular to the direction of the field, the lines not remaining anchored to the earth.

Picturing the magnetopause as a surface which rigorously confines the geomagnetic field and excludes the interplanetary field is an oversimplification. Because geomagnetic disturbance is observed to be dependent on the direction of the interplanetary field in the solar wind, it is apparent that some reconnection of geomagnetic and interplanetary field lines occurs across this surface. This permits solar particles to enter the magnetosphere, a process which is observed to occur. Particles can also enter at the two neutral lines on the sunward portion of the magnetosphere, where the lower-latitude dipole-like field lines turn one way and polar field lines forming the geomagnetic tail turn the other, making the field tangential to the magnetopause zero. Field-line reconnection at the magnetopause is discussed in Section 11.7.2.

The existence of electric fields in the magnetosphere, with strengths as high as 100 mv/m or more, has been observed experimentally, and electric fields are required for any theory of ionospheric currents and convection of the magnetic field. Outside the magnetosphere, the sweeping of an interplanetary field $\overline{B}$ past the earth by a solar wind of velocity $\overline{v}$ implies that an electric field $\overline{E} = -(\overline{v} \times \overline{B})/c$ will be observed in a coordinate system fixed at the earth. Electric fields are of great importance both energetically and as diagnostic indicators.

The dynamic behavior of the magnetosphere is complex, and a unified picture of the many processes involved is only beginning to emerge. Most of the processes and phenomena noted above are highly interdependent. Because of such properties as the high conductivity along field lines and the high speed of hydromagnetic-wave propagation, effects of a process at one location propagate easily to distant regions, often causing a very different process to occur there. For example, the Sq electric field, produced by an ionospheric dynamo, propagates throughout the magnetosphere where it results in convection. But the reverse is also true; convection driven by another source implies electric fields which are transmitted to the ionosphere, contributing to the Sq currents. Correctly identifying the actual situation is difficult.

Throughout most of the magnetosphere, the magnetic field, electric fields, and low-energy-particle populations are in constant interaction, being required to satisfy Maxwell's equations and the resulting laws of magnetohydrodynamics. This interdependency of phenomena must be borne in mind in the discussion of individual processes below.

11.3 MEASUREMENTS OF THE GEOMAGNETIC FIELD

Geomagnetic phenomena, discussed in the preceding and following sections in terms of theoretical explanations, are studied experimentally through data obtained by ground stations, ships, aircraft, and space vehicles. Since experimental data are often pertinent to more than one area of study, this section identifies and reviews major sources, noting experimental techniques, accuracies, geographical and temporal coverage, and availability.

11.3.1 Instrumentation

Instruments used over the past several hundred years to measure the intensity and direction of the magnetic field have been few in number and simple in principle. However, during the past century they have been made very reliable and fairly precise. Although greater precision and sensitivity were needed earlier, major developments of new instruments came only in the past 25 years, partially because the older instruments were not adaptable for use on rockets and satellites. The principal instruments currently in use may be listed as follows.

Ground-based instruments exploit several physical principles. Several are based on the alignment or oscillation of a permanently magnetized needle in the field; these include the compass, dip circle, and magnetic theodolite, which measure D, I, and H, respectively, the three elements usually measured at observatories to determine the field. Several others rely on the induction of a voltage in a coil of wire. The coil may be rotated in the field as in the dip inductor, or may be fixed, as in the induction coils of large area used to measure micropulsations. Two widely used magnetometers are based on the cancellation of a component of the earth's field by the known field of an electromagnet; these are the H-magnetometer of Schuster and Smith and the Z-magnetometer of Dye. To these older instruments, there have been added more recently several instruments based on atomic resonance techniques, the proton precession (and proton vector), rubidium-vapor, and helium magnetometers, as well as instruments which exploit the saturation characteristics of a ferromagnetic core, the fluxgate or saturable-core magnetometers.

Satellite and rocket measurements currently rely mainly on the rubidium-vapor, search-coil (that is, induction-coil), and fluxgate magnetometers. These have the

inherent characteristics of small size, low weight, modest power requirements, and an electrical output signal which is easily telemetered, and reliable and precise versions for satellite use have been developed over the past decade. Since most older observatory instruments are read optically or require mechanical adjustment during use, adapting them for satellite applications would entail unwarranted complexity.

Two magnetometer types which have not yet been developed for geomagnetic work are those based on the Hall effect and electron-beam deflection. Two indirect methods of studying the geomagnetic field are the measurement of the electron cyclotron frequency of particles trapped in the field and the measurement of telluric currents.

A brief description of these instruments and methods follows. The observatory instrument used to measure declination is essentially a compass. The needle is suspended by a fiber at a point displaced from its center of mass enough that the dip is counterbalanced and the needle is horizontal. The fiber can be turned to remove almost all torsion; an unmagnetized needle is used to check this condition, and residual torsion is corrected for by extrapolating readings for two or more needles of differing moments. With care and skill, the uncertainty can be less than 10 seconds of arc.

The corresponding instrument for measuring inclination is the dip circle, which consists of a magnetized needle lying in the plane of the magnetic meridian and pivoted about a horizontal axis through its center of mass. Precision scales and appropriate optics facilitate reading the angle of the needle, and several procedures are followed to correct for instrumental errors, but the measurement is inherently less precise than the declination measurement.

The classical method of measuring the horizontal intensity H is the so-called oscillation and deflection experiment, which consists of two separate measurements made with a single standard magnet of moment M. In the oscillation measurement, the magnet is suspended and allowed to oscillate horizontally about the magnetic meridian. The period T is measured and the product HM is found from the equation $HM = 4\pi^2 I/T^2$, where I is the moment of inertia of the magnet. Both M and H are presumed to be unknown. In the deflection experiment, a magnetic theodolite, shown schematically in Figure 11-7, is used. Two arms and a telescope, spaced 90 degrees apart, can be rotated together about a vertical axis on which a magnetized needle is suspended horizontally. The angular position of the needle axis is read by aligning the telescope axis with it (using the reflection of telescope cross hairs in a mirror attached to the needle), both with and without the magnet in position on one of the arms (its magnetic axis directed toward the center). The difference is the deflection φ. The quotient H/M may be computed from the equation $H/M = 2K/(r^3 \sin \varphi)$, where r is the distance between centers of

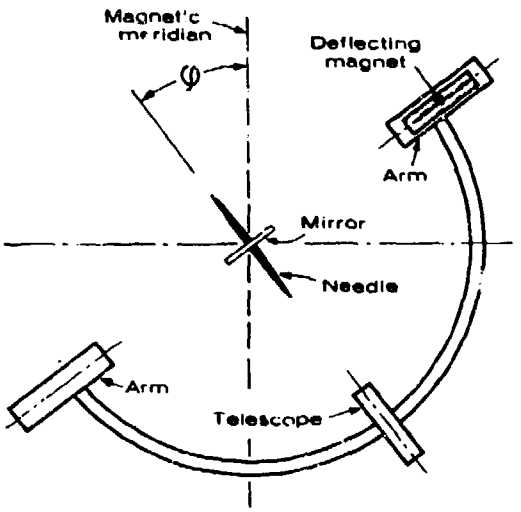

Figure 11-7. The Magnetic Theodolite [after Chapman and Bartels, 1940]

the magnet ard needle and K is the so-called deflection constant of the magnet. From the values of the product and the quotient of the two unknowns obtained by the two experiments, the horizontal intensity may be computed: $H = [(HM) \times (H/M)]^{1/2}$. With care, H can be measured with an uncertainty of less than 1 gamma.

Because of the poor inherent precision of the dip circle, the dip inductor is now more commonly used to measure inclination. This instrument is simply a flat many-turn coil of wire which can be rotated about one of its diameters. With the coil rotating, this axis is adjusted so that the induced voltage is zero, indicating that the axis is aligned with the field vector. The dip angle is read with appropriate scales and optics. The precision is comparable to that of the declination measurement, the uncertainty being less than 10 seconds of arc.

Fixed induction coils of various sizes are used to measure rapid fluctuations in the field. To measure the vertical component, horizontal coils with diameters of nearly 10 km have been laid out on the ground; for the other components, coils a few meters in diameter, but with many turns, are used. Also used for this purpose are much smaller coils which are fitted with laminated mu-metal cores to concentrate magnetic flux for increased sensitivity. The inherent sensitivity of induction coils is proportional to the frequency of the field fluctuation; the detection of .001-gamma variations at 1 Hz is not uncommon. A typical search-coil instrument for spacecraft has a coil two centimeters in diameter and thirty centimeters long enclosing a mu-metal core; its sensitivity is about 1 gamma at 1 Hz and .001 gamma at 3 kHz. Satellite search-coils have also been used as rotating coils, using the satellite spin, to measure two components of the dc field.

The H-magnetometer of Schuster and Smith consists of a Helmholtz coil with its axis horizontal and rotatable about a vertical axis so that the H component of the field may be annulled. The coil is purposely misaligned with the vector $\overline{H}$ by a couple of degrees so that there will be a small residual component exactly perpendicular to $\overline{H}$ when the annulment in the direction of $\overline{H}$ is exact. A small needle suspended at the center indicates null when it is perpendicular to $\overline{H}$. The annulling field is computed from electrical constants and the coil dimensions. The uncertainty of the measurement is typically about 1 gamma.

The Z-magnetometer of Dye is similar; it uses a Helmholtz coil with a vertical axis. The alignment, however, is made as accurate as possible, and null is detected by a vibration galvanometer. This is a small electromagnet, mounted to vibrate freely at some mechanical resonance frequency along its axis (also vertical); when driven with a large electrical current of this frequency it vibrates unless the vertical field is complete annulled. The precision is comparable to that of the H-magnetometer. At high latitude stations, Z is much larger than H, and for better accuracy these stations usually measure Z, I, and D rather than H, I, and D.

The first and best developed of the newer atomic- or nuclear-resonance instruments was the proton-precession magnetometer. The physical principle on which it depends is the following. Individual protons in a hydrogenous material placed in a magnetic field have both a magnetic moment and an angular momentum, which coincide in direction; the field exerts on the proton a torque tending to align its moment with the field, but the existence of angular momentum causes the common vector to precess about the field direction. Normally, the precessing vectors are random in phase and produce no coherent signal, but if they are started with a common phase by suddenly releasing them after polarization by a strong field perpendicular to the field to be measured, they precess for some time in unison, producing, at the precession frequency, a signal which can be detected by a pickup coil surrounding the material. The precession (Larmor) frequency is directly proportional to the field, the constant of proportionality being $1/2\pi$ times the proton gyromagnetic ratio. This physical constant is known to an accuracy of better than one part in 10^5 and has a value of 2.67519×10^4 $(\text{gauss-sec})^{-1}$; the frequency for a field of 0.30000 gauss is therefore 1.2773 kHz. In a typical instrument, the hydrogenous material is a fraction of a liter of water, alcohol, or n-heptane, around which is wound a single coil, used both to produce the polarizing field of about 100 gauss and subsequently to detect the precession signal. The sample is polarized for a few seconds, and the precession signal persists for a few seconds thereafter before thermal agitation destroys the coherence. Several precautions and corrections are required, but the instrument is basically simple and reliable. The resonance line width for water is typically about 1 gamma and absolute measurements of the field may be made with an uncertainty as low as 0.1 gamma.

Versions suitable for use in observatories, aircraft, ships, and rockets have been developed.

The proton vector magnetometer combines the proton-precession magnetometer with two sets of Helmholtz coils arranged to annul the H and Z field components. To measure Z, $\vec{H}$ is first annulled by producing $-\vec{H}$ in the H coils. This null cannot be detected directly but is produced by using just half the current required to generate $-2\vec{H}$; the latter condition can be detected, since the total intensity is then exactly the same as that with zero current in the coil. The current required to annul Z is then measured. First-order instrument errors, of which leveling alignment is most critical, can be corrected by appropriate checks with reversed coils. To keep the field gradient at the sensor low enough with moderate coil dimensions, a four-element Fenselau or Braunbek coil array may replace the simpler Helmholtz coil. Since this instrument uses the proton-precession magnetometer simply as a null detector, the precision of the measurement depends on the accuracy with which the generated field are known; an uncertainty as low as about 0.3 gamma is possible. This instrument is now used to measure H and Z at many observatories.

A newer resonance instrument is the rubidium-vapor magnetometer, which relies on the Zeeman effect and the phenomenon of optical pumping. Any alkali vapor is suitable, but the rubidium isotopes 85 and 87 have been most used. The energy-level diagram for Rb-87, showing the Zeeman splitting in a magnetic field, is shown in Figure 11-8. When light of about 0.79476-micron wavelength is passed through a transparent cell filled with rubidium vapor, resonance absorption and re-emission occurs, involving transitions between the various Zeeman sublevels of the ground and first excited states. If the light is circularly polarized, the absorption transitions must have $\Delta m = +1$, so no transitions from the groundstate sublevel with $m=+2$ can occur. Eventually, all electrons are trapped in this substate and no further absorption can take place; the vapor becomes magnetically polarized and transparent. This process is termed "optical pumping". The polarization can be destroyed by impressing in a direction perpendicular to the ambient field a weak magnetic field, oscillating at a frequency (the Larmor frequency) corresponding exactly to the Zeeman splitting (6.99 Hz/gamma). Forbidden transitions between the various m-sublevels of the groundstate are induced, electrons trapped in the sublevel with $m = +2$ are redistributed to other sublevels, resonance absorption of the light is again possible, and the vapor is no longer transparent. The ambient magnetic field is determined by measuring the Larmor frequency (that is, the oscillating-field frequency which produces maximum light absorption). The simplest magnetometer consists of the rubidum-vapor absorption cell surrounded by a coil to produce the Larmor-frequency field, an rf-excited rubidium-vapor lamp

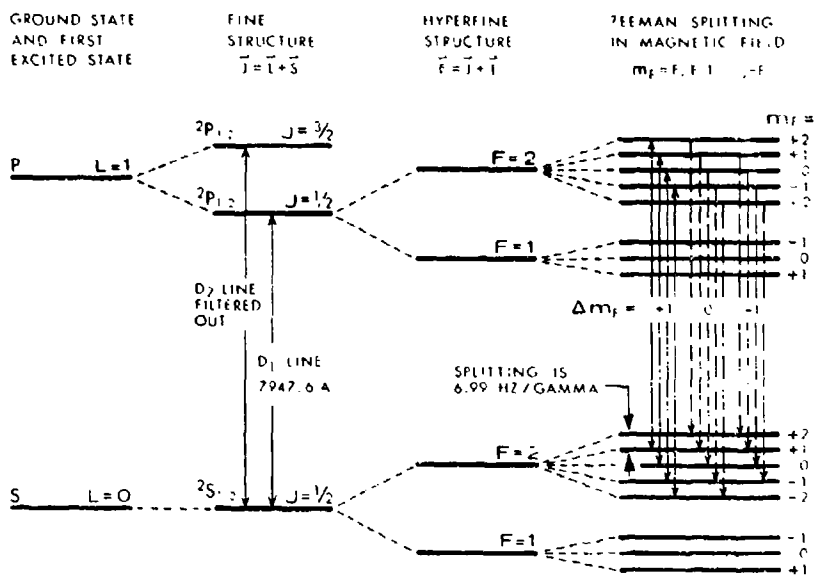

Figure 11-8. Energy-Level Diagram for Rubidium-87

with a filter to absorb all but the 0.79476-micron line, a circular polarizer between the lamp and the cell, and a photodetector to measure the intensity of transmitted light. The frequency of the impressed field may be adjusted manually for minimum transmission of light through the cell. (A 20-percent change in absorption occurs between the pumped and unpumped condition.) In more refined instruments, several corrections and improvements are usually incorporated. For many applications, particularly in spacecraft, self-oscillating instruments have been developed; in these, both the light intensity and the impressed field oscillate with the Larmor frequency, which is established using a feedback signal from the photodetector. The absolute accuracy of rubidium-vapor magnetometers is limited by the inherent line width of the resonance (several gammas) and a further splitting of the Zeeman levels by second-order effects in the coupling of moments; the uncertainty in weak-field measurements (for example, in the distant magnetosphere) is negligible, but in strong-field measurements (for example, near the surface of the earth) it is seldom less than about 2 gammas.

The helium magnetometer is also an optical-pumping instrument. Its operation is similar to that of the rubidium-vapor magnetometer, except that, since the

groundstate of helium has zero magnetic moment, electrons are trapped in a sublevel of the metastable 2^3P_1 state instead, being excited to the metastable state by an rf electric field. The inherent sensitivity is higher because of a greater Zeeman splitting (28 Hz/gamma compared with 7 Hz/gamma for Rb-87), but the line width of the resonance is much broader (about 100 gammas). Practical problems resulting from the higher Larmor frequency have hindered the development of self-oscillating instruments. While rubidium-vapor magnetometers have been used much more extensively to date, several advantages of the helium magnetometer are likely to assure its usefulness in certain applications in the future.

While the fluxgate magnetometer has been in use for about 35 years, its current usefulness in geomagnetism is due to extensive development in recent years. In simplest form, it consists of a highly permeable ferromagnetic core on which primary and secondary coils are wound. The primary winding is driven with a sinusoidal current which has an amplitude sufficient to drive the core material into saturation twice each cycle, thus changing the permeability of the material at a frequency twice that of the primary current. The flux in the core arises from two sources, the exciting field and the ambient external field. The former produces a large component at the driving frequency and, because of the changing permeability, other components at odd-harmonic frequencies. The latter produces a large component at the second-harmonic frequency and smaller components at higher even-harmonic frequencies, all due to the changing permeability; that is, the steady ambient field, which would otherwise produce no signal is "gated" into the secondary winding by the changing permeability of the core. Since the exciting field produces only odd harmonics, the second harmonic is a measure of the ambient field. Its amplitude is proportional to the magnitude of the field component parallel to the core, and its phase indicates the sign. If the core material is separated longitudinally into two halves, the primary winding can encircle the two halves in opposite senses so that the net excitation flux through the secondary is zero. To the degree that cancellation is complete, only the desired even-harmonic signal is detected. A typical fluxgate magnetometer of this type is shown schematically in Figure 11-9. Another scheme to eliminate the drive signal in the secondary winding is to wind the primary and secondary coils to be orthogonal. Since this is an analog instrument with analog output signal, several characteristics of the circuitry and the core material limit the accuracy; until recently, calibration shifts and zero drift have been a problem, and careful satellite measurements still employ auxiliary windings to generate inflight calibration fields and a mechanical device to reverse sensor orientations. Fluxgate magnetometers are particularly useful in satellite experiments for measuring interplanetary and very weak geomagnetic fields and at the surface of the earth for measuring variation fields. With special

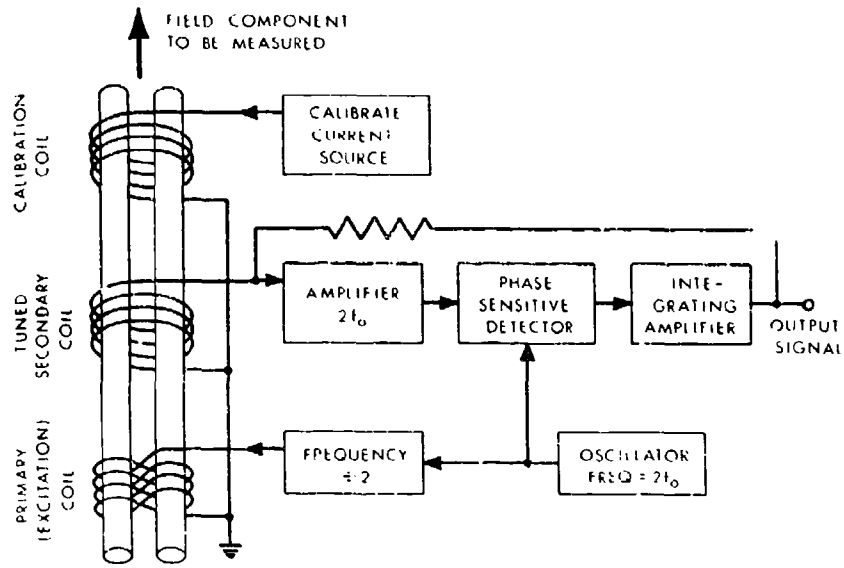

Figure 11-9. Schematic Diagram of a Typical Fluxgate Magnetometer

care, the sensitivity to the former can be a small fraction of a gamma; the sensitivity to the latter is typically about one gamma. Since the excitation field may have a frequency as high as about 10 kHz, field fluctuations with frequencies to 100 Hz or more can be measured. The fluxgate instrument may be combined with a system of Helmholtz coils or permanent magnets to annul all or most of the surface field; this is commonly done for micropulsation measurements. Since a single sensor measures only one component of the field, a three-sensor array is often constructed to measure the total field. A so-called orienting fluxgate has been used for extensive world-wide magnetic mapping by aircraft. This instrument has three orthogonal sensors with a servomechanism to orient the array such that two sensors are perpendicular to the field (reading zero); the third then measures the total intensity, and the servomechanism measures the direction. On spinning spacecraft, one sensor is sometimes mounted at that angle to the spin axis (arctan $\sqrt{2}$) for which the sensor direction describes a cone containing three orthogonal axes, so the sensor measures three field components successively as the spacecraft spins; however, spacecraft dynamics are not usually well enough controlled to permit accurate measurements by this method.

In the Hall-effect magnetometer, the sensing element is a thin slab of semiconductor such as indium antimonide. If a current $\bar{I}$ is caused to flow in such a material placed in an ambient magnetic field $\bar{H}$, a potential gradient is developed

which is porportional to and in the direction of $\bar{I} \times \bar{H}$. With the current held constant, the voltage across the slab is a measure of the field. The very small sensor size is a major advantage, and such magnetometers are widely used to measure strong fields in laboratory experiments, but problems with low signal levels and temperature drifts have discouraged the development of instruments for use in geomagnetism, where field intensities are lower.

A magnetometer based on the deflection of an electron beam by the magnetic field has also received some attention. It consists of a precisely constructed electron tube in which the beam is accelerated from one end and detected at the other on a collector divided into halves so that the current differential is a measure of the deflection and, therefore, the field. High sensitivity (on the order of a milligamma) is possible, but to date such instruments have not been developed for geomagnetic measurements because of the complexity entailed by severe requirements for mechanical and electronic stability and precision.

A measurement of the electron cyclotron frequency of trapped particles has been used to infer the intensity of the geomagnetic field. A trapped electron has a component of motion, in the plane perpendicular to the field, which is circular (cyclotron motion) with a frequency proportional to the field value: $f_c = 2.7994$ F (MHz). It has been found that signals with frequencies which are integral multiples (up to 4 or 5) of this frequency can be detected by a satellite at the location of the particles, and a measurement of the frequency yields the value of the field. The method is neither fully understood nor developed, but may be of value in the future.

Telluric currents (that is, currents flowing in the surface of the earth) can be studied to infer the overhead magnetic-field fluctuations which are presumed to induce them. The quantity measured experimentally is the voltage between one or more pairs of electrodes buried in the ground. (In auroral studies, the voltage induced in long telephone lines has also been used.) The electrodes are typically bare strips of lead or a metal immersed in a solution of one of its salts in a porous container. The surface area which contacts the soil may be several square feet, with the electrodes buried several feet deep and separated by a fraction of a kilometer. Although the method is very sensitive and simple, its usefulness is limited by several difficulties. Self-potentials and contact resistances at the several electrodes are different, are difficult to predict or measure, and vary with time, so that slow fluctuations of the field are obscured. With the relatively low-impedance current meters used earlier, faster fluctuations could not be observed, but with the advent of low-noise high-impedance electronic amplifiers, frequencies to at least 10 Hz can be studied, and currents corresponding to field changes as small as 10^{-5} gamma are detectable. Potentials due to slower fluctuations and drifts in electrode characteristics are usually filtered out. A more fundamental limitation is that irregularities in the ground conductivity pattern and their change

with surface conditions distort the magnitude and direction of the field values inferred from the currents.

The development or selection of suitable magnetometers is not the only problem in making geomagnetic measurements; related considerations often pose greater difficulty and constitute the limiting factor in achieving accurate results. Error in determining the orientation and geographic or spatial location of instruments is a problem common to observatory, ship, aircraft, and spacecraft experiments. At ground locations, surveying, leveling, and establishing true azimuth must be carefully done and monitored, since mounting piers can shift appreciably. Few, if any, experiments conducted with ships or aircraft have established instrument orientation with sufficient accuracy for useful component measurements, and it has been common, therefore, to measure only the total intensity. An orbiting spacecraft is not subjected to appreciable disturbance forces or torques, and star trackers and scanners have been developed to measure accurately the orientation relative to the celestial sphere; the problem of accurately establishing orbital location is also tractable with modern tracking techniques. However, these capabilities have not yet been utilized to make accurate vector field measurements. A problem common to ships, aircraft, and spacecraft is the difficulty of making them highly nonmagnetic. Only two such ships (see Section 11.3.3) have made extensive worldwide surveys. To eliminate the magnetic effect of conventional vessels, measurements at sea have been made by instruments placed on anchored and free-floating buoys or towed at some distance behind a ship, of course, certain other difficulties are encountered with such schemes. Nonmagnetic aircraft have been operated by several countries, with good coverage of ocean areas further than 30 degrees from the poles and some coverage of more poleward regions. A great number of nonmagnetic spacecraft have been built and flown with varying degrees of success. The most stringent requirements are imposed for measurements in the distant magnetosphere or interplanetary space, where the total field may be only a few gammas. A carefully observed program to eliminate magnetic materials and current loops can yield excellent results, but such programs are often compromised because of high cost, the difficulty in exercising adequate control over the many contributors to a satellite, or an important conflicting requirement to use magnetic material for some other purpose. Magnetometers are often mounted outboard of the spacecraft on extendable booms to exploit the fact that the spacecraft field decreases as the cube of the distance. Demagnetizing a spacecraft prior to launch is usually helpful, but the residual moment is likely to be changed unpredictably by shock and vibration in the ambient field at launch and by temperature effects. The moment along the spin axis can never be measured with certainty after launch. Moments of current loops vary because the currents vary; the moment of a solar-cell array

often has a component fixed in space (nonrotating) because the illumination on it is spin modulated.

A final problem area for space experiments involves limitations imposed by telemetry and other spacecraft systems. In the past, data were often transmitted in analog form and the cumulative error from the data telemetry system was often distressingly large, seldom less than one or two percent unless the experiment employed special circuitry. It is now more common to use pulse-code-modulation (PCM) systems, in which data are converted in the satellite for transmission in digital form. The precision of analog-to-digital converters routinely exceeds 10-bit accuracy (0.1%), and special circuitry (for example, frequency counters for resonance magnetometers) may be incorporated into experiments to eliminate completely any error attributable to telemetry. A severe limitation which usually remains is that of telemetry information bandwidth. For a given transmitter power and orbit, the bit rate at which data can be transmitted reliably is limited, and since this capability is divided among several experiments on the same spacecraft, it is often necessary to compromise accuracy or sampling rate or both. Other characteristics of spacecraft systems which are beyond the control of the experimenter (for example, data format, timing and synchronization, power-supply regulation, etc.) also frequently impact adversely on experimental results.

11.3.2 Ground-Station Measurements

Since the beginning of the nineteenth century, the principal source of geomagnetic data has been a continually increasing number of magnetic observatories throughout the world. By 1840, about 50 of these were making coordinated measurements of the declination at hourly (and occasionally 5-minute) intervals. In recent years, over 250 stations have been operated on a continuous or intermittent basis. Of these, over 130 are permanent formal observatories, the majority of which publish data on a routine and regular basis. Others are repeat stations, that is, locations which are carefully marked and used periodically for standard measurements with portable instruments. Still others are special stations set up for research on some particular problem. The geographical distribution of magnetic observatories is shown in Figure 11-10. In Section 11.8.1 are listed, in order of geomagnetic latitude the name and location of most of the magnetic stations in operation during recent years.

The data provided by almost all observatories include, as a minimum, (1) photographic recordings (magnetograms) of three quantities to specify the vector field (for example, D, H, and Z) at a chart speed sufficient for time resolution of about one minute; (2) periodic absolute measurements of the same (and other) quantities for accurate calibration of the magnetograms; and (3) hourly mean values of these quantities, derived from the magnetograms. Field-component values are

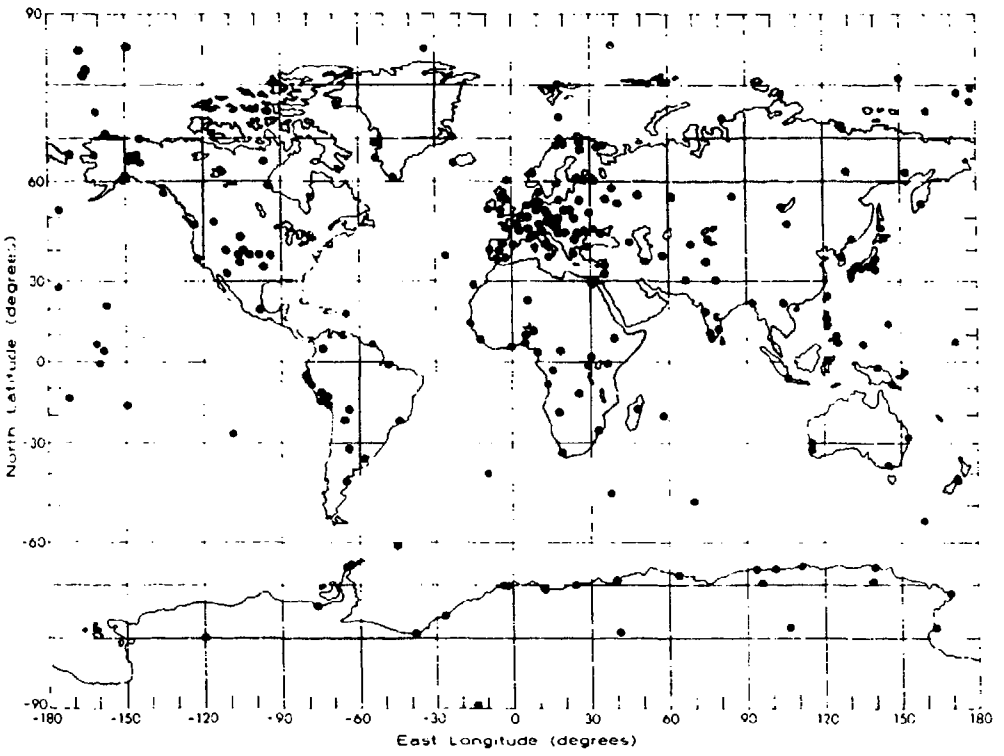

Figure 11-10. Geographical Distribution of Magnetic Observatories

typically accurate to about one gamma, and angles (D and I) to about 10 or 20 seconds of arc. Most observatories also derive K indices (see Section 11.6.6), and many make so-called rapid-run magnetograms, which are recorded with a higher chart speed for better time resolution. A smaller number make more extensive and specialized measurements; some are highly competent research centers which measure a variety of geomagnetic and related geophysical parameters.

At present, the principal sources of data from magnetic stations are the World Data Centers established for the IGY, as listed in Section 11.8.2.

11.3.3 Other Surface Measurements

Surface measurements have also been made aboard ships, aircraft, and anchored or towed buoys. While these have been limited in accuracy by the difficulties of achieving magnetic cleanness and establishing spatial location and orientation, they have been necessary and important, particularly before satellite surveys were possible. The nonmagnetic United States ship Carnegie was operated for many

years before it was destroyed by fire more than forty years ago. In 1957, the nonmagnetic Russian ship Zarya, fitted with a gyro-stabilized platform, began a program of vector and total-intensity measurements for the IGY. Some sea and air measurements are being continued and improved, for both general worldwide and special-purpose magnetic surveys. Measurements by nonmagnetic ships and aircraft have been particularly important in the derivation of quantitative models of the main field; survey routes covered in the past quarter century are shown in Figure 11-11.

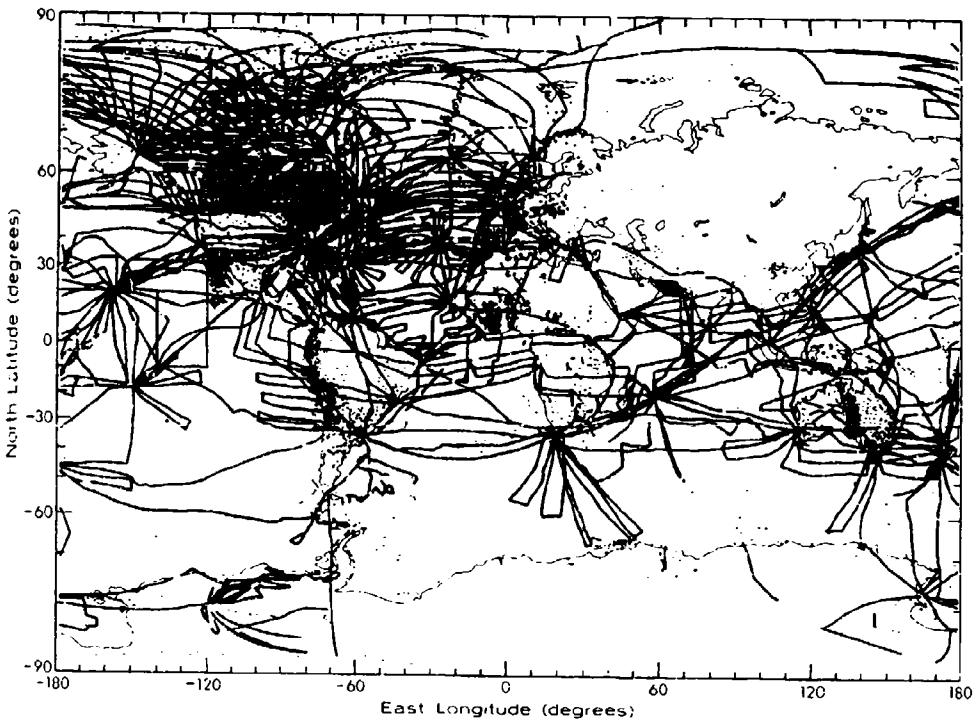

Figure 11-11. Magnetic-Survey Coverage During the Years 1945-1964 [after Cain, 1971]

11.3.4 Satellite and Rocket Measurements

The altitude range accessible to small rockets has permitted direct measurement of magnetic fields at the location of ionospheric current systems. Rocket-borne magnetometers have been particularly useful in studying the equatorial

and auroral electrojet currents and the magnetic fields associated with auroral events.

Magnetic measurements by satellite were begun in 1959 by the Sputnik 3 and Vanguard 3 spacecraft. It was soon appreciated that for magnetic-survey purposes a polar-orbiting satellite could accomplish in several weeks what had earlier required many years. Furthermore, it would largely eliminate the unequal distribution of data points, the large unexplored areas, the inaccuracies due to secular change during the survey, and the errors due to differences in technique when many investigators contribute. Since that time the seven other low-altitude satellites listed in Table 11-1 have contributed to magnetic surveys. Despite several limitations (for example, precise vector measurements have not been attempted), expectations have proved well founded. Current models derived from satellite data appear to be as good as those based on surface data for predicting the surface field and are superior for predicting the field in space; crustal anomalies are mostly not observable in satellite data, but they are not reproduced in surface-data models either. The current status has been summarized by Cain [1971]. Results of the recent World Magnetic Survey are summarized in IAGA Bulletin No. 28 [Zmuda, 1971].

Table 11-1. Geomagnetic Measurements by Low-Altitude Satellites [after Cain, 1971]

Spacecraft	Orbital Inclination	Altitude Range (km)	Operational Time Interval	Type of Magnetometer	Est. Total Error
Sputnik 3	65°	440 - 600	May 58 - Jun 58	Fluxgates	100γ
Vanguard 3	33°	510 - 3750	Sep 59 - Dec 59	P-precession	10γ
Cosmos 26	49°	270 - 403	Mar 64	P-precession	*
Cosmos 49	50°	261 - 488	Oct 64 - Nov 64	P-precession	22γ
1964-83C	90°	1040 - 1089	Dec 64 - Jun 65	Rb-vapor	22γ
OGO 2	87°	413 - 1510	Nov 65 - Sep 67	Rb-vapor	10γ
OGO 4	86°	412 - 908	Jul 67 - Jan 69	Rb-vapor	10γ
OGO 6	82°	397 - 1098	Jun 69 - Aug 70	Rb-vapor	10γ
Cosmos 321	71°	270 - 403	Jan 70 - Mar 70	Cs-vapor	*

The configuration and dynamic processes of the magnetosphere have been studied with many satellites, notably those of the Explorer, OGO, and Pioneer series. Frequencies from dc to VLF and spatial locations from ionospheric

altitudes to 1000 R_e down the tail have been explored, with major emphasis on mapping the magnetosphere and studying its interaction with the solar wind.

Raw data and analyses resulting from satellite experiments are disseminated mostly through the open literature and several data centers. The following sources of data are provided in Section 11.8: (1) a list of pertinent active and planned spacecraft with reference to a detailed catalog of all experiments carried (Section 11.8.3), (2) a list of satellite ELF and VLF experiments with references (Section 11.8.4), (3) a list of the journals in which most experimental results are published (Section 11.8.5), (4) references to major data centers and their data catalogs (Section 11.8.2), and (5) references to other source listings (Section 11.8.6).

11.4 THE MAIN FIELD

As noted above, the steady field consists of the main field, of terrestrial origin, plus the nonvarying components of extraterrestrial current systems. The latter are described in the subsequent discussion of variation fields, since their importance arises from their dynamic behavior. While they are omitted here, it should be remembered that they contribute to the surface field an amount which exceeds the uncertainty of present satellite survey measurements.

11.4.1 Basic Description

The detailed characteristics of the main field are most easily shown in world charts of the elements. Historically, such charts have been prepared by fitting curves by hand to observatory and survey data. Recently, however, experimental measurements and mathematical models (see Section 11.4.2) have both attained sufficient accuracy that differences between them are not detectable on world charts of moderate scale, and current charts are plotted from the models. Such charts are presented in the following section.

An explanation of the source of the main field must be consistent with seismic and other geophysical data, which indicate the interior of the earth to be roughly as shown in Figure 11-12. The crust of granite and basaltic rock is only 5 to 30 km thick. Under it is the mantle, which extends to a depth of about 2900 km, constituting the major bulk of the earth. Interior to that is the core, mainly iron; the outer core is molten, while the inner core (below a depth of about 5100 km) is thought to be solid. Of the limited number of explanations which have been proposed, most have been discarded on the basis of convincing arguments. Permanent magnetism cannot be sufficient because of the temperatures and material properties known to exist in the interior of the earth. An electromagnet without a driving source would

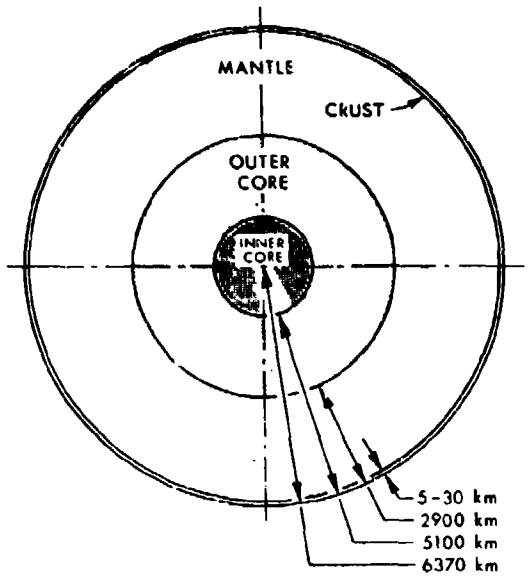

Figure 11-12. The Interior Structure of the Earth

decay in less than a million years. The existence of a net charge rotating with the earth could be detected by its electric field and other effects. The induction of a terrestrial current system by magnetic storms seems inconsistent with what is known about storm phenomena. Several other suggestions are similarly unpromising. The so-called "Hall-effect" and "twisted-kink" theories proposed, respectively by Vestine [1954] and Alfven [1950] have not yet been proved untenable but are not widely favored. At present the most satisfactory theory is that first developed by Elsasser [1946a, 1946b, 1947] and Bullard [1948, 1949a, 1949b], in which the field is generated by some sort of self-exciting dynamo system, that is, a configuration in which an emf generated by the motion of a conductor (molten iron) in a magnetic (excitation) field produces a current in a circuit so oriented as to produce the excitation field. The simplest such dynamo is shown in Figure 11-13. The conducting disc rotating in the axial field B generates a radially directed emf which is picked up by the brushes of the nonrotating coil; the emf produces the current i which generates the field B. It is easily found that there is an angular velocity for which the dynamo is self-sustaining, and the field can be developed in either direction. The dynamo of the earth cannot, of course, be visualized as an assembly of discrete parts, but must consist of bulk current densities in the molten core. The theory of such a homogeneous dynamo has been developed for several simplified configurations, and it is now widely believed that such a system must be the source of the main field. Present knowledge is still insufficient to provide a detailed picture of core circulations. It is believed that the dipole part of the field

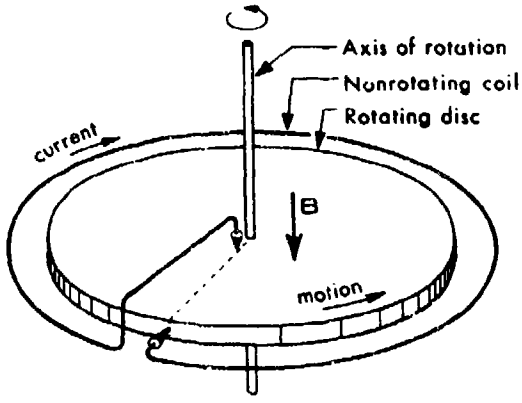

Figure 11-13. The Simple Disc Dynamo

must result from a major two-dimensional circulation, which is probably constrained to remain perpendicular to the geographic axis by the Coriolis force. The nondipole regional anomalies are believed to arise from eddy circulations in the outer layer of the core; the nondipole field obtained in the mathematical models discussed below can be extrapolated to the depth of the core surface, with a result such as that shown in Figure 11-14. The distribution of electrical current density required in the core surface to produce this field has a similar pattern, and it is found that the field can be fitted fairly well by assuming about nine radial dipoles of various strengths (equivalent to circulation vortices) within the core [Alldredge and Hurwitz, 1964]; their locations are also indicated in Figure 11-14. Local anomalies, of limited extent, arise from permanent magnetism in the crust; because the source is so close to the surface, these fields sometimes exceed that arising from the core. The Kursk anomaly, largest in the world, located 400 km south of Moscow, is shown in Figure 11-15.

11.4.2 Precise Quantitative Descriptions

A first approximation to the geomagnetic field near the surface of the earth is an earth-centered dipole with its axis tilted to intersect the earth at 78.5° N, 291.0° E, the geomagnetic north pole; the other intersection at 78.5° S, 110.0° E is the geomagnetic south pole. (These values were adopted internationally to define the geomagnetic coordinate system; however, the dipole terms of the more recent International Geomagnetic Reference Field, also adopted internationally, place the pole at 78.56° N, 290.24° E, and at present this axis is also frequently used.) In spherical coordinates, r, θ, and φ, with r measured from the center of the earth and θ measured from the dipole axis (geomagnetic colatitude), the dipole field has the vector components

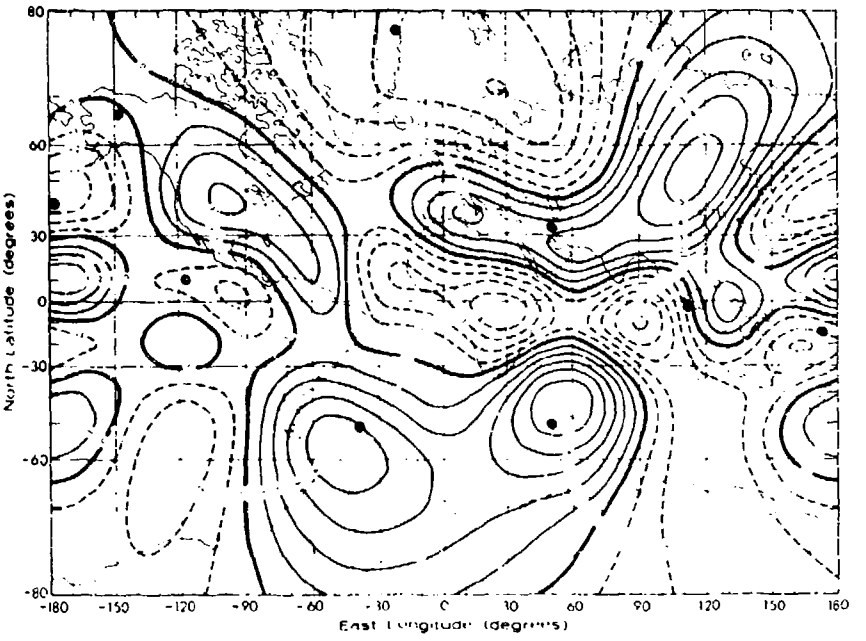

Figure 11-14. The Vertical Component (in Units of Oersteds) of the Nondipole Field, Extrapolated to the Surface of the Core. Solid circles indicate the locations of the nine interior radial dipoles found by Alldredge and Sterns [1969] to fit the field [redrawn after Vestine, 1967]

$$B_r = -\frac{M}{r^3} 2 \cos \theta$$

$$B_\theta = -\frac{M}{r^3} \sin \theta \qquad (11\text{-}1)$$

$$B_\varphi = 0$$

The total intensity is then

$$B = \frac{M}{r^3} [3 \cos^2 \theta + 1]^{1/2} \qquad (11\text{-}2)$$

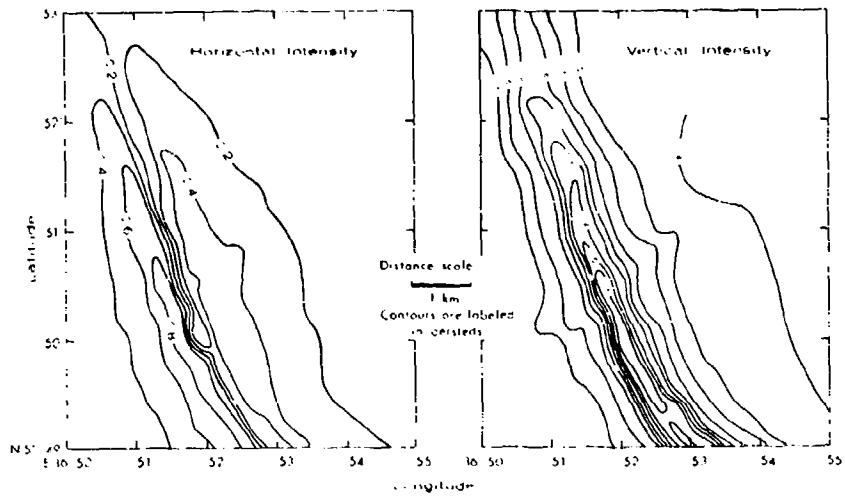

Figure 11-15. Isointensity Contours (in Units of Oersteds) of the Magnetic Field at the Kursk Anomaly (Northern Portion Only) [redrawn after Chapman and Bartels, 1940]

where M is the dipole moment of the earth (about 7.98×10^{25} gauss cm^3 in 1972). The equation of a field line is obtained by equating its slope to the slope of the field vector:

$$\frac{r\, d\theta}{dr} = \frac{B_\theta}{B_r} = \frac{1}{2} \tan \theta$$

Integration yields

$$r = r_0 \sin^2 \theta \qquad (11\text{-}3)$$

where the constant of integration r_0 is the geocentric distance at which the field line crosses the geomagnetic equator. A magnetic shell, which is the surface of revolution generated by rotating a field line about the dipole axis, is a useful concept in studying charged-particle motion. In the B-L coordinate system of

McIlwain, trapped particles which move adiabatically to conserve three invariants of the motion are confined to a shell of constant L. The B-L coordinate system is, roughly speaking, a transformation of the actual distorted field of the earth into an equivalent dipole field (employing a multipole expansion of the former, as discussed below), and the shells of constant L transform into the simple magnetic shells of the dipole field, with $L = r_0$. In considering trapped-particle populations, it is often useful to know roughly the volume within one or between two magnetic shells; Figure 11-16 shows the volume above the earth (in units of earth volumes, $V_e = 1.10 \times 10^{27}$ cm^3) enclosed by successively larger magnetic shells.

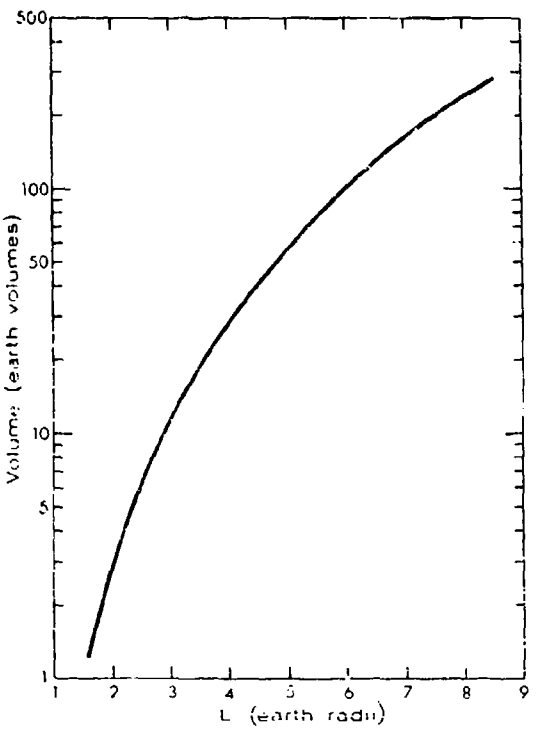

Figure 11-16. Volume (Above the Surface of the Earth) Enclosed by an L-Shell Plotted as a Function of L. Units are earth volumes [from data of Hess, 1968]

The centered dipole is a rather poor approximation to the actual field. Equation 11-2 yields an equatorial field intensity of 0.308 gauss, while the actual intensity ranges between values of 0.41 and 0.24 gauss, more than 25% above and below the calculated value. Much of this discrepancy can be removed by taking the dipole to be eccentric, a good fit (for epoch 1955) being obtained by displacing the center of the dipole 436 km toward 15.6° N, 150.9 °E and inclining the dipole axis to intersect the spherical earth at 81.0° N, 275.3° E and at 75.0° S, 120.4° E [Parkinson and

Cleary, 1958]. However, the improvement is not good enough for most purposes; discrepancies of about 10% remain. Further, the awkward transformation from the dipole to geographic coordinates makes the approximation unsuitable for hand calculation, and since much better models are readily available for machine computation, the eccentric dipole is seldom used.

Any field derivable from a potential function can be expressed in terms of a multipole expansion of the potential. The coefficients of the various terms may then be adjusted by a least-squares method to give the best fit to the measured field. The methodology for such analyses is well developed, and sets of coefficients, along with computer programs to calculate the field and a number of related parameters, are readily available. In simplest form, the analysis is as follows. The magnetic scalar potential may be written as a spherical-harmonic expansion:

$$V = a \sum_{n=1}^{\infty} \sum_{m=0}^{n} P_n^m (\cos\theta) \left[\left(\frac{a}{r}\right)^{n+1} (g_n^m \cos m\varphi + h_n^m \sin m\varphi) + \left(\frac{a}{r}\right)^{-n} (A_n^m \cos m\varphi + B_n^m \sin m\varphi) \right] \tag{11-4}$$

where r, θ, and φ are the geographical polar coordinates of radial distance, colatitude, and east longitude, and a is the radius of the earth ($a = R_e$). The functions $P_n^m(\cos\theta)$ are the Schmidt functions:

$$P_n^m(\cos\theta) = \left[\frac{\epsilon_m (n-m)!}{(n+m)!} \right]^{1/2} \left[\frac{(1-\cos^2\theta)^{m/2}}{2^n n!} \frac{d^{n+m}}{d(\cos\theta)^{n+m}} (\cos^2\theta - 1)^n \right]$$

$$\epsilon_m = 2 \text{ if } m > 0$$

$$\epsilon_m = 1 \text{ if } m = 0 \tag{11-5}$$

The second quantity in brackets is the associated Legendre function $P_{n,m}(\cos\theta)$. Its numerical multiplier makes the Schmidt function partially normalized. (Its mean-square value integrated over the sphere is not unity, but $(2n+1)^{-1/2}$.) The

coefficients g_n^m, h_n^m, A_n^m, and B_n^m appropriate to this function, referred to as "Schmidt coefficients", are now quite universally used in quoting results of analyses, although earlier analyses have used other normalizations, particularly the Gaussian. For Gaussian normalization, the numerical multiplier is replaced by $[2^n\, n!\, (n-m)!\,/(2n)!]$. Therefore, to obtain the corresponding Schmidt coefficients, Gaussian coefficients must be multiplied by $q = [2^n\, n!\,/(2n)!]\,[(n-m)!\,(n+m)!\,/\,\epsilon_m]^{1/2}$; values of q through n=m=10 are listed in Section 11.8.7.

In the potential, those terms containing g_n^m and h_n^m arise from sources internal to the earth, while those containing A_n^m and B_n^m arise from external currents; the potential function is valid in the space above the surface and below the external current system. The field is given by

$$\overline{B} = -\nabla V \,. \tag{11-6}$$

The northward, eastward, and downward components of the field are thus

$$X = (1/r)\,(\partial V/\partial\theta)$$

$$Y = -(1/r \sin\theta)\,(\partial V/\partial\varphi)$$

$$Z = \partial V/\partial r \,. \tag{11-7}$$

Until very recently, analyses have been unable to identify contributions from external sources, and the coefficients A_n^m and B_n^m are ordinarily assumed to be zero. The coefficients g_n^m and h_n^m are adjusted by the least-squares procedure to minimize some quantity such as the weighted sum of the squares of the differences between X, Y, and Z values calculated from the model and measured X, Y, and Z values; the sum is taken over a network of measurements covering the entire earth. As the degree of the multipole terms increases, the magnitude of their effect decreases, and it is pointless to retain more terms than are warranted by the accuracy of the experimental measurements; most recent analyses retain terms through n=m=6 to 10, depending on the accuracy of the data, though some have retained more.

While the method is mathematically quite straightforward, the process of selecting, reducing, and weighting the data is not. Measurements must be corrected for disturbance and quiet-day variations, instrumental error, seasonal variation, and

secular change, and uncertainties in these corrections lead to a noise level in the final values used. Other sources of noise also contribute, such as the effect of surface anomalies too localized to be resolved by the multipole terms retained. The weighting of surface data is most complicated by their uneven geographic distribution and varying precision. The usual procedure has been first to chart the data and then to take an evenly spaced network of values from the chart, assigning higher weight where the measurements are dense and precise; newer machine procedures permit using the original data directly, which eliminates much of the subjectivity inherent in charting by hand. In any case, the methodology chosen has a significant effect on the coefficient values obtained. While it is usually important to get the most accurate absolute values of the coefficients, it is also often important (for example, to study the secular variation) to assure that a comparison of models derived with different methodologies does not yield a spurious result.

Current analyses yield coefficients which predict the surface field to within about 200 gammas rms difference and the field at a low-altitude-satellite orbit to within about 10 gammas. The coefficients for three of the most useful recent models are listed in Table 11-2. The first is that of Jensen and Cain [1962] for epoch 1960.0, which was widely used as a reference field for many purposes prior to the availability of the later two. (Published coefficients for this model were Gaussian normalized; in the table they have been converted to Schmidt coefficients to facilitate comparison.) The second model is the International Geomagnetic Reference Field for epoch 1965.0 (IGRF 1965.0) [Zmuda, 1971]. This model resulted from a recognition, in connection with the World Magnetic Survey, that a standard reference field was required for international use; applicability over a fairly long period of time (1955 to 1972) was of greater importance than highest accuracy. It resulted from a weighted average of several recent models, retaining coefficients through $n=m=8$. It fits surface data from observatories, land and sea surveys, and most airplane surveys to within about 200 gammas; data from four satellites are fitted to within about 50 gammas. The third model is that of Cain and Sweeney [1970], designated POGO 8/69, for epoch 1960.0. It was derived from total-field measurements by three OGO satellites during the period 1965.7 - 1968.4; these data are fitted by the model to within 9 gammas rms difference. Terms to $n=m=10$ are retained. From comparing the qualities of fit obtained with the various models, it is clear that for some purposes the POGO 8/69 model yields substantially higher accuracy, particularly for the period after 1965.

In computing the field for a time different from the epoch quoted, the secular change must be taken into account. Both the IGRF and POGO models include the first time derivative of each coefficient; these values are also given in Table 11-2. Note that while the POGO coefficients are quoted for epoch 1960.0 the experimental data were for a much later time interval.

Table 11-2. Spherical-Harmonic Coefficients for Three Useful Models of the Geomagnetic Field

		JENSEN & CAIN epoch 1960.0		IGRF 1965.0 epoch 1965.0				POGO 8/69 epoch 1960.0					
		Main Field (gammas)		Main Field (gammas)		Secular Change (gammas/year)		Main Field (gammas)		Secular Change (gammas/year)			
n	m	g_n^m	h_n^m	g_n^m	h_n^m	$\dot{g}_n^m$	$\dot{h}_n^m$	g_n^m	h_n^m	$\dot{g}_n^m$	$\dot{h}_n^m$	n	m
1	0	-30411.2		-30339		15.3		-30479.8		26.62		1	0
1	1	-2147.4	5798.9	-2123	5758	8.7	-2.3	-2170.2	5757.1	10.03	2.25	1	1
2	0	-1602.3		-1654		-24.4		-1542.5		-23.66		2	0
2	1	2959.1	-1912.4	2994	-2006	0.3	-11.8	2989.3	-1979.3	1.50	-6.84	2	1
2	2	1545.1	182.3	1567	130	-1.6	-16.7	1555.9	266.1	7.92	-28.32	2	2
3	0	1260.7		1297		0.2		1333.4		-7.24		3	0
3	1	-2029.2	-485.7	-2036	-453	-10.8	4.2	-1982.6	-424.9	-11.42	4.49	3	1
3	2	1285.7	210.4	1289	242	0.7	0.7	1292.2	241.7	0.84	-0.96	3	2
3	3	821.7	-26.6	843	-176	-3.8	-7.7	833.6	-174.0	3.27	1.77	3	3
4	0	955.3		958		-0.7		964.7		-1.57		4	0
4	1	818.5	213.7	805	149	0.2	-0.1	810.8	134.4	-1.18	3.63	4	1
4	2	557.0	-235.7	492	-280	-3.0	1.6	506.8	-303.7	-5.36	5.64	4	2
4	3	-335.0	-20.6	-392	8	-0.1	2.9	-397.8	19.4	1.72	-1.09	4	3
4	4	276.4	-187.3	256	-265	-2.1	-4.2	224.7	-276.4	8.24	-2.05	4	4
5	0	-206.4		-223		1.9		-237.5		3.59		5	0
5	1	338.4	7.8	357	16	1.1	2.3	356.6	5.1	0.58	2.34	5	1
5	2	253.0	26.0	246	125	2.9	1.7	249.8	108.0	-0.27	4.01	5	2
5	3	12.9	-97.7	-26	-123	0.6	-2.4	-14.3	-107.3	-3.26	-4.24	5	3
5	4	-125.1	-109.1	-161	-107	0.0	0.8	-149.7	-106.3	-1.08	0.63	5	4
5	5	-99.3	173.6	-51	77	1.3	-0.3	-75.7	117.1	5.04	-5.03	5	5
6	0	135.2		47		-0.1		44.8		0.12		6	0
6	1	25.7	30.5	60	-14	-0.3	-0.9	59.4	-7.6	0.38	-0.65	6	1
6	2	-21.5	58.6	4	106	1.1	-0.4	-2.7	118.1	2.35	-2.38	6	2
6	3	-214.9	34.2	-229	68	1.5	2.0	-232.4	58.3	1.28	2.49	6	3
6	4	-19.3	2.2	3	-32	-0.4	-1.1	9.6	-18.1	-2.77	-1.70	6	4
6	5	-9.8	48.0	-4	-10	-0.4	0.1	7.7	-27.9	0.09	2.34	6	5
6	6	-166.0	48.4	-117	-13	-0.2	0.9	-83.1	8.1	-1.69	-2.59	6	6
7	0			71		-0.5		79.3		-1.69		7	0
7	1			-54	-57	-0.3	-1.1	-51.6	-59.4	-0.26	-1.68	7	1
7	2			0	-27	-0.7	0.1	-0.3	-2.2	0.72	-1.14	7	2
7	3			12	-6	-2.5	0.4	8.9	-8.7	0.86	0.58	7	3
7	4			-2	9	0.3	0.7	-23.5	1.4	0.85	1.22	7	4
7	5			-9	23	0.9	2.4	-3.3	14.3	-0.57	0.91	7	5
7	6			13	-19	-2.2	0.2	10.6	-21.6	1.01	0.40	7	6
7	7			-2	-17	-0.6	0.3	3.9	-27.8	-1.44	0.60	7	7
8	0			10		0.1		9.4		0.19		8	0
8	1			9	3	0.4	0.1	3.6	9.9	0.27	0.01	8	1
8	2			-3	-13	0.6	-0.2	-5.4	-16.2	0.33	0.39	8	2
8	3			-17	5	0.0	-0.3	-18.5	9.9	0.83	-1.26	8	3
8	4			-4	-17	0.0	-0.2	-3.3	-19.9	0.42	-0.09	8	4
8	5			7	4	-0.1	-0.3	5.8	10.6	-0.00	-0.49	8	5
8	6			-5	22	0.3	-0.4	-12.0	20.6	0.47	0.56	8	6
8	7			12	-3	-0.3	-0.3	10.2	-9.2	0.73	-0.67	8	7
8	8			6	-16	-0.5	-0.3	18.7	-20.7	-1.48	-0.08	8	8
9	0							9.6		0.17		9	0
9	1							9.3	-25.4	-0.08	0.48	9	1
9	2							3.1	12.8	-0.46	0.47	9	2
9	3							-12.0	3.1	-0.95	0.17	9	3
9	4							15.3	-2.5	-0.37	-0.41	9	4
9	5							0.7	-2.3	-0.03	-0.22	9	5
9	6							8.8	7.3	-0.48	0.21	9	6
9	7							0.6	12.7	0.54	0.01	9	7
9	8							6.2	4.7	-0.13	-0.13	9	8
9	9							-3.9	9.7	0.33	0.16	9	9
10	0							-1.7		-0.33		10	0
10	1							-2.2	2.9	-0.08	-0.16	10	1
10	2							1.3	3.5	0.17	-0.37	10	2
10	3							1.8	-2.7	-0.97	0.51	10	3
10	4							-2.1	4.4	-0.12	-0.09	10	4
10	5							9.4	-5.9	-0.33	0.04	10	5
10	6							0.7	1.0	-0.33	-0.19	10	
10	7							0.3	-2.8	-0.21	0.07	10	
10	8							-2.4	2.1	0.27	0.40	10	
10	9							-0.1	4.2	0.49	-0.53	10	9
10	10							5.3	-8.8	-0.75	0.31	10	10

Charts of all the magnetic elements, X, Y, Z, H, F, D, and I as computed from the model IGRF 1965.0, are presented as Figures 11-17 through 11-23, respectively. In the following section are presented corresponding charts of the secular variation of the elements. Charts were drawn at AFCRL, based on charts produced with a computer contour program by J. C. Cain, Goddard Space Flight Center, U.S.A., and improved by B. R. Leaton and M. Fisher, Institute of Geological Sciences, U.K. [Leaton, B.R., IGRF Charts, pp 189-203 in Zmuda, 1971]. On plots to this scale, the actual and model fields are indistinguishable. On a much expanded scale the actual field would show crustal anomalies. Since these seldom exceed 100 km in extent, they are not reproduced by the spherical harmonic models, whose components have wavelengths for n=m=10 no shorter than about 4000 km.

Until recently, the quality of experimental data has not warranted such refinements as accounting for the oblateness of the earth, including contributions from magnetospheric current systems, and retaining terms beyond about n=m=6. Now, both the IGRF and POGO models refer surface values (approximately) to the international ellipsoid (equatorial radius 6378.160 km, flattening 1/298.25), and higher-degree terms have been included. The averaged quiet-time surface contributions of external currents are known to exceed the uncertainty of the fit but have not yet been separately identified.

To study the secular variation, analyses for earlier epochs are of interest. An analysis yielding coefficients to n=m=4 was made by Gauss in 1835, and analyses have been made for epochs spaced about 10 years apart throughout the present century.

For situations in which a model for only a limited region of the surface of the earth is required, an expansion in orthogonal polynomials, rather than spherical harmonics, can be made. The methodology for such analyses has been developed; a description has been given by Fougere [1964].

At some distance (several R_e) from the earth, the field is so distorted by the solar-wind interaction that the model field must account for the responsible external current systems. The first such models [Mead, 1964; Midgley, 1964; Williams and Mead, 1965] included magnetopause and neutral-sheet currents for a variable-strength solar wind blowing perpendicular to the geomagnetic axis. In a current model [Olson, 1970], the dipole field is tilted at an adjustable angle, the geomagnetic tail is cylindrical, the neutral sheet is hinged to the dipole equatorial plane (that is, intersects it) at a geocentric distance of 10 R_e, and the neutral-sheet current varies with geocentric distance and closes along the two halves of the cylinder. The coefficients A_n^m and B_n^m in Eq. 11-4 are adjusted to yield agreement with measurements in the geomagnetic tail, where the field is very unlike the main field. Since the equations are linear, contributions from internal sources,

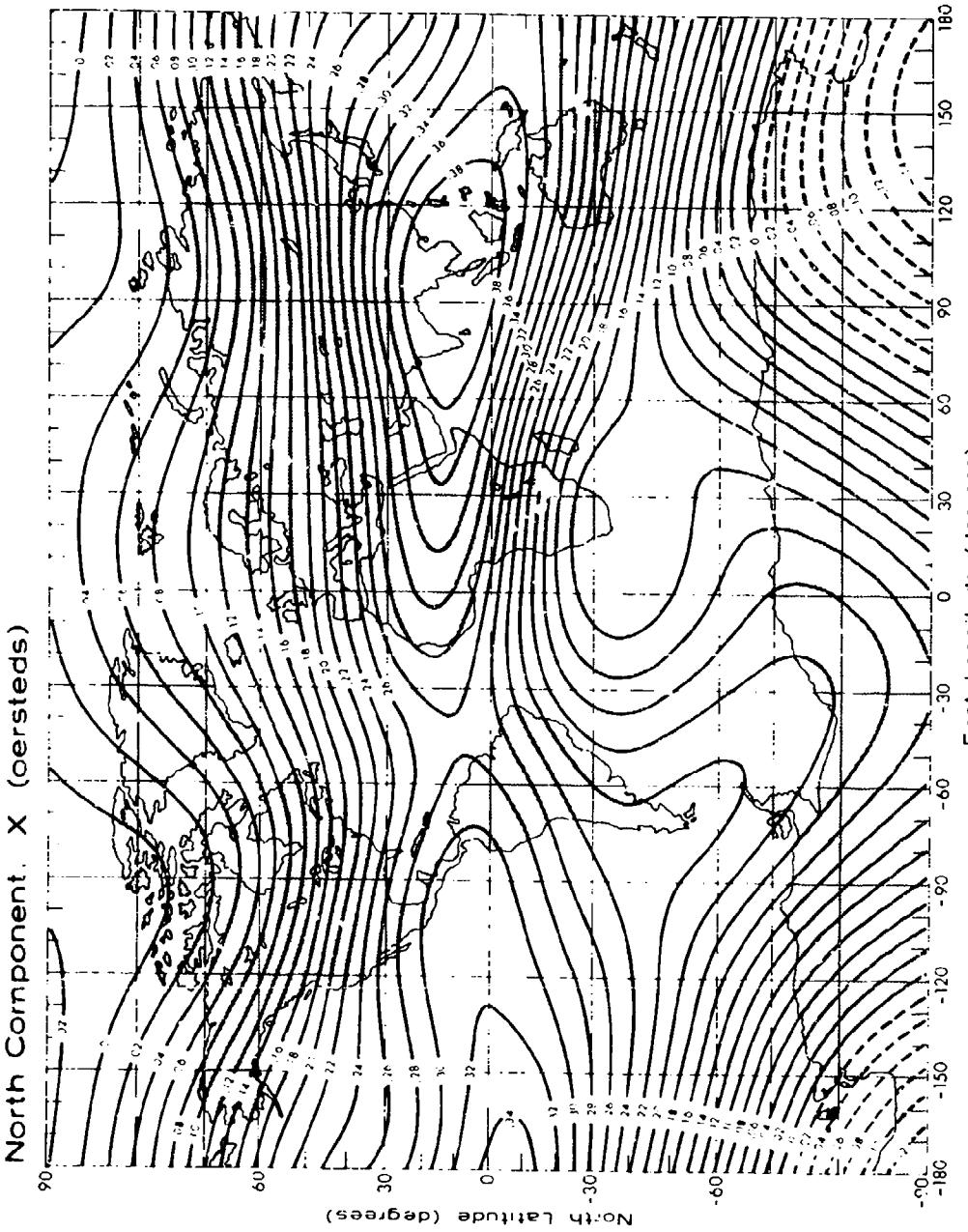

Figure 11-17. Contours of Constant X (Northward Component) for IGRF 1965.0 [see text]

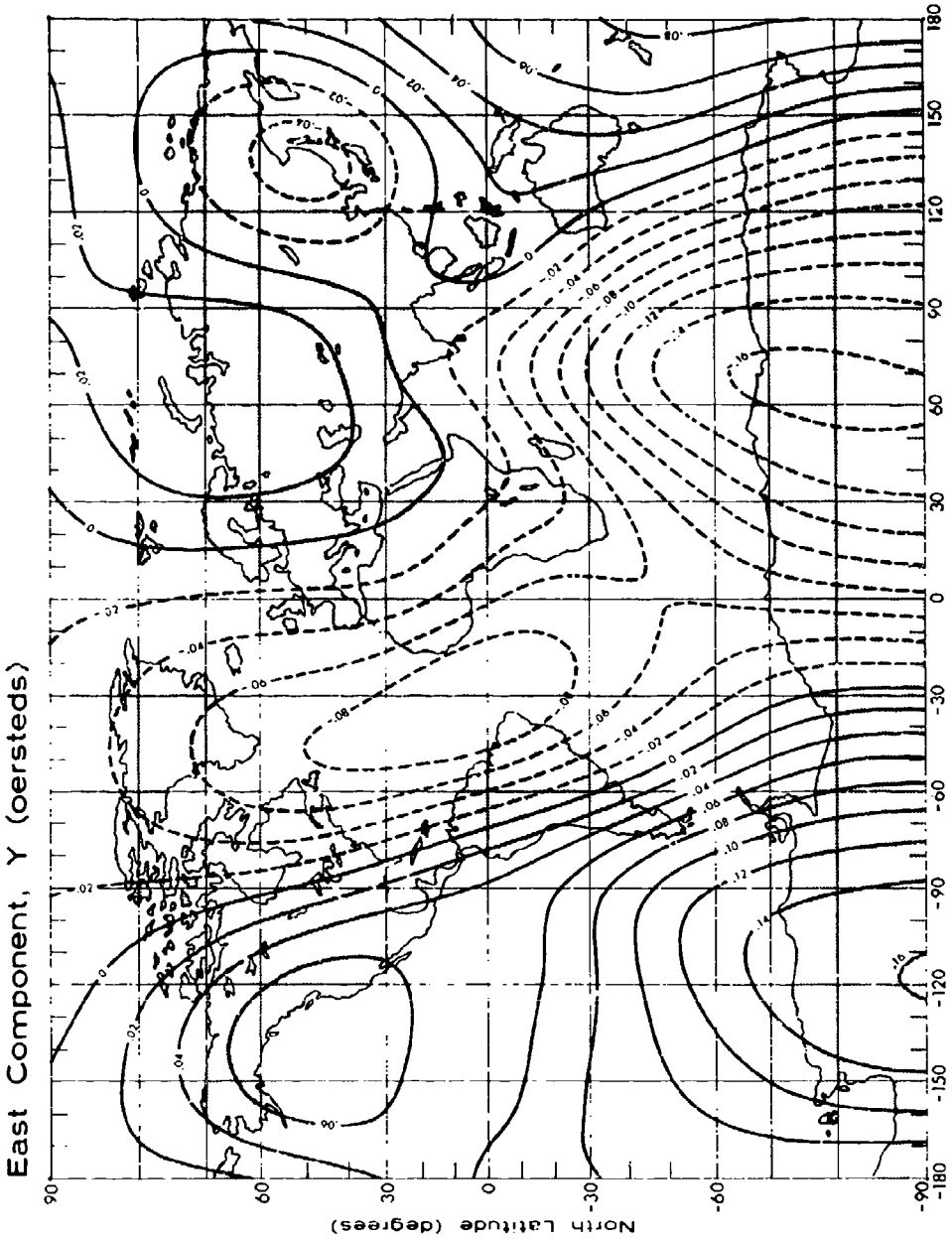

Figure 11-18. Contours of Constant Y (Eastward Component) for IGRF 1965.0 [see text]

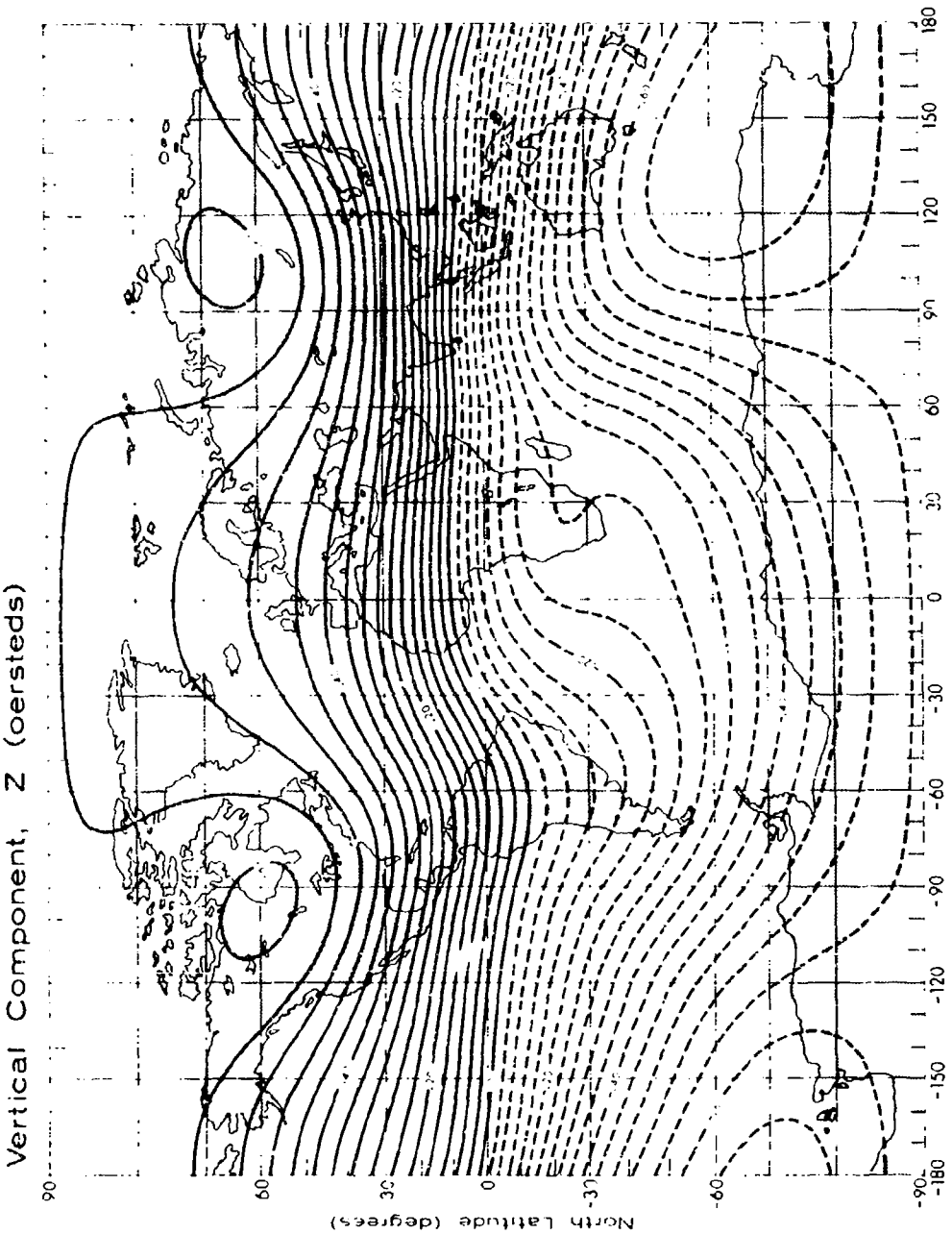

Figure 11-10. Contours of Constant Z (Vertical Component) for IGRF 1965.0 [see text]

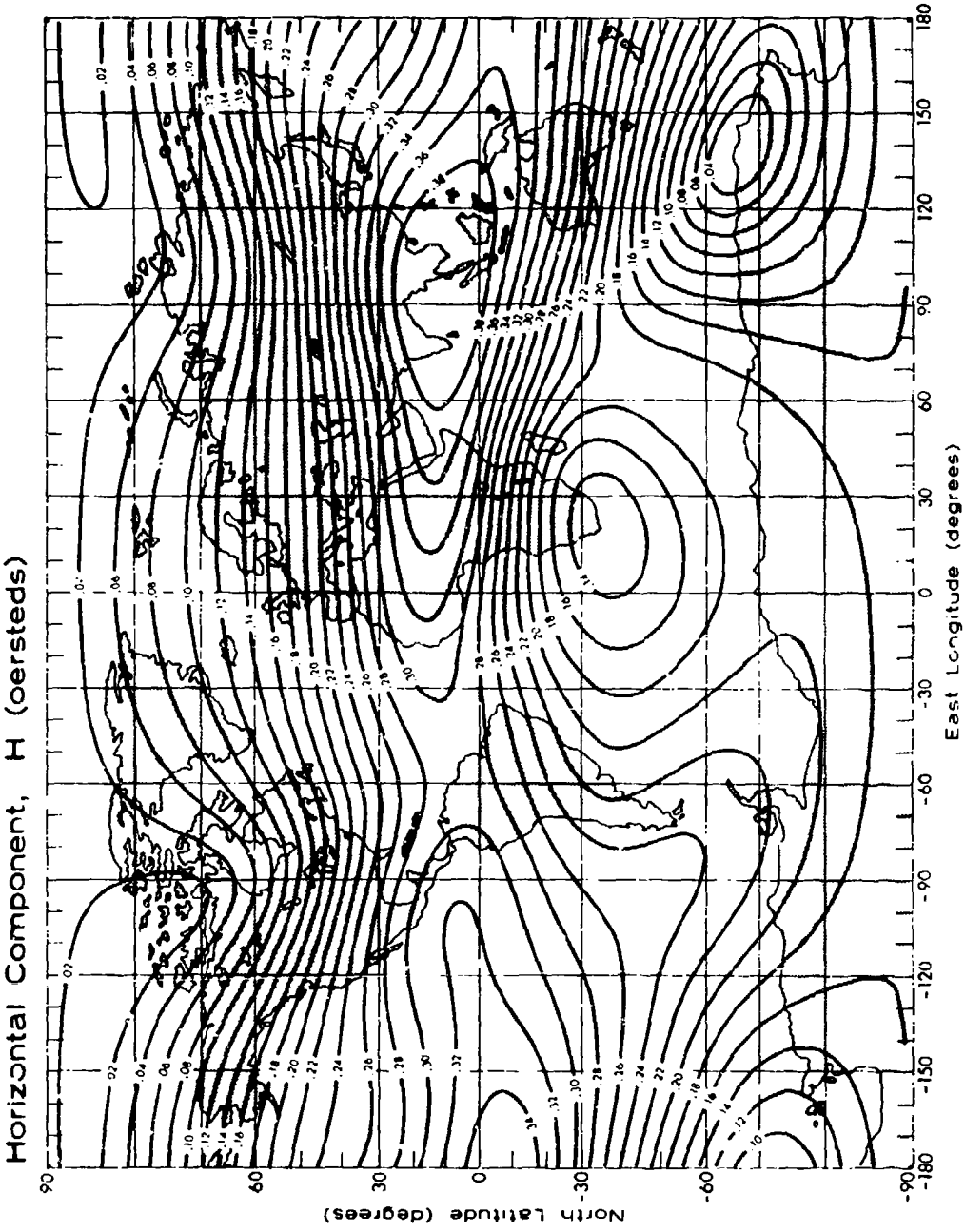

Figure 11-20. Contours of Constant H (Horizontal Component) for IGRF 1965.0 [see text]

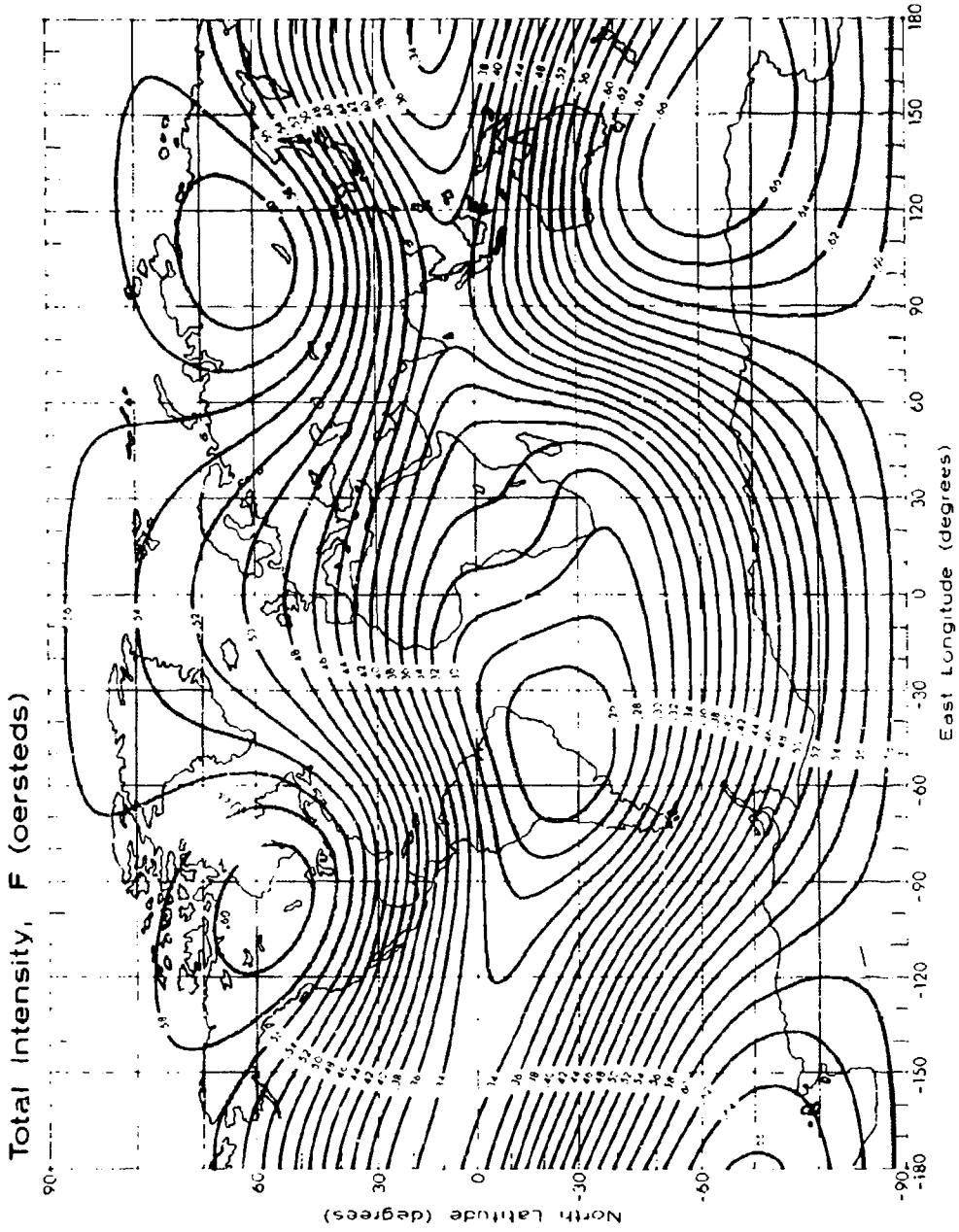

Figure 11-21. Contours of Constant F (Total Field) for IGRF 1965.0 [see text]

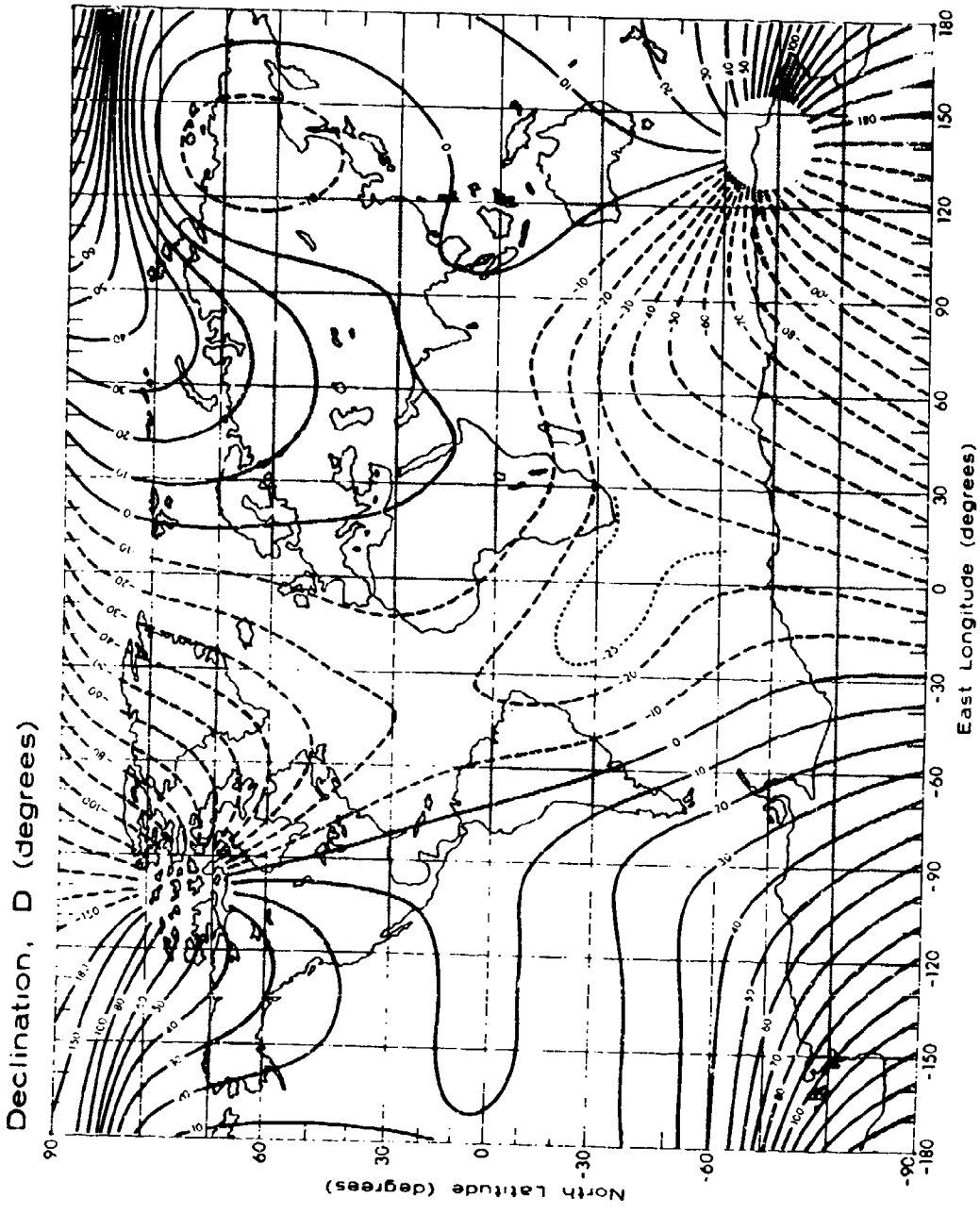

Figure 11-22. Contours of Constant D (Declination) for IGRF 1965.0 [see text]

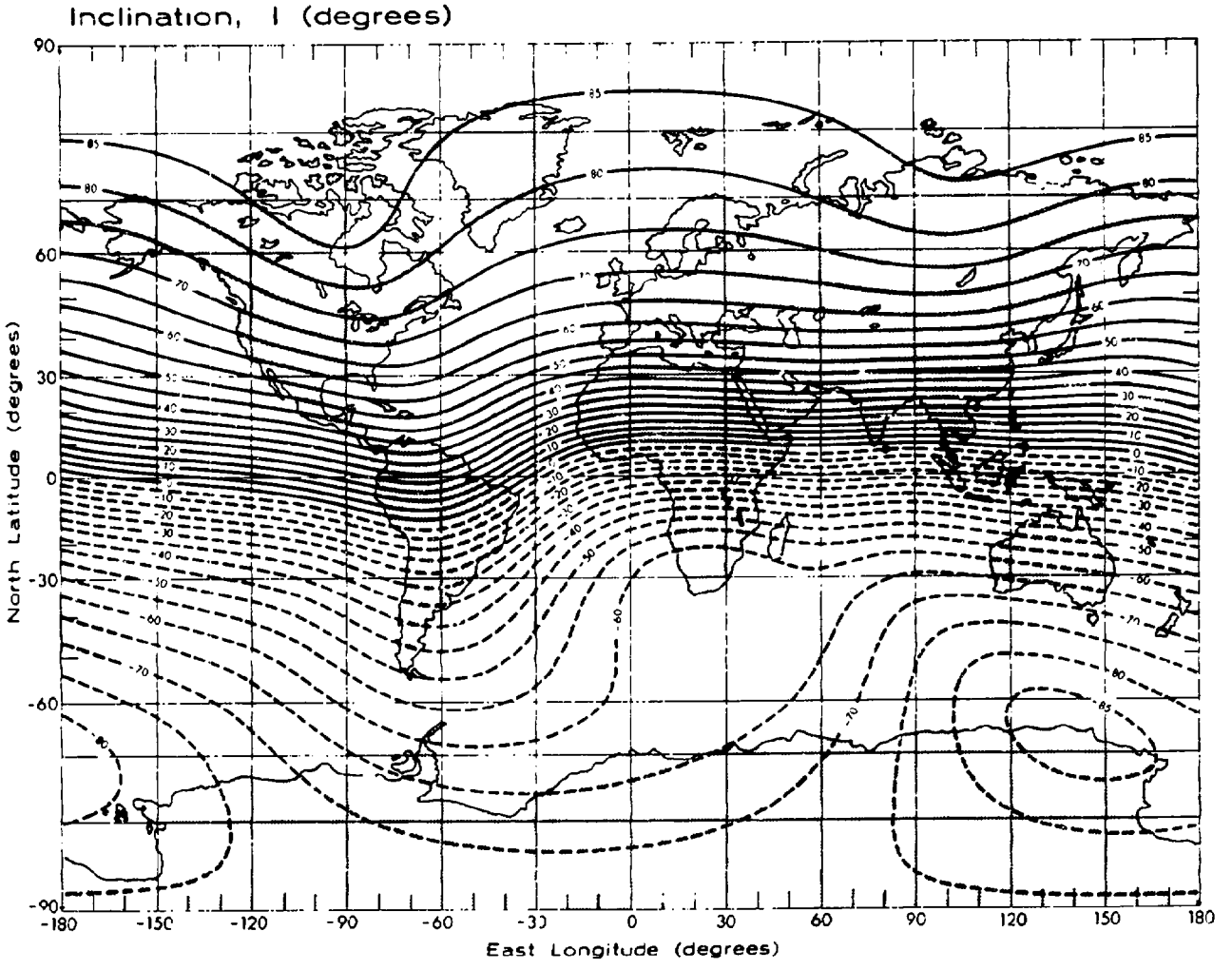

Figure 11-23. Contours of Constant I (Inclination) for IGRF 1965.0 [see text]

magnetopause currents, and neutral-sheet currents are additive; the model includes these separately, with a set of A_n^m for each of the two current systems. (The B_n^m are zero because of symmetry.) The model yields fairly good qualitative and quantitative agreement with measurements in the tail. It also predicts accurately the daily variations observed at a geostationary (synchronous) satellite at 6.6 R_e; these are dominated by magnetospheric effects since the satellite is both motionless relative to the main field and quite distant from ionospheric currents [Olson and Cummings, 1970]. The predicted contribution to the surface daily variation is at least 20% of the total observed and has qualitatively the same temporal and spatial form. Although the agreement with current data is good, the current systems of the model are certainly oversimplified. The model also fails to produce a vanishing field outside the cylindrical magnetopause. Coefficients for a number of models and computer programs for computing field values, tracing field lines, and calculating B-L coordinates are available as noted in Section 11.8.8.

11.4.3 The Secular Variation

The study of changes in the field which have occurred over the past 400 years or so is based on historical records. The precision of such data depends, of course, on their age; for most of this period, observations separated by many years have been required, but at present satellite surveys can measure changes occurring over intervals as short as a year or less. This section describes the secular variation during the period of recorded data; its earlier behavior is discussed in Section 11.4.4 below.

The secular variation is found by comparing world magnetic charts for successive epochs. As noted in the preceding section, this process is now incorporated into the computer programs which fit mathematical models to the data. A determination of the secular variation for all elements of the field has been included as part of the IGRF 1965.0 model. Charts of the results are presented in Figures 11-24 through 11-30.

The secular variation in recent decades and centuries may be considered to consist of four components: (1) a decrease in the strength of the centered-dipole part of the field, (2) a westward drift of regional anomalies (that is, the nondipole field), (3) a northward movement of the centered dipole and (4) residual nondrifting variations of regional or worldwide extent. These may be described individually as follows.

Over the entire period of recorded data, the dipole strength has been decreasing at an average rate of about .05% per year (16 gammas per year in the equatorial field strength); data for the past 150 years are plotted in Figure 11-31. Paleomagnetic studies described below indicate a decrease over a much longer

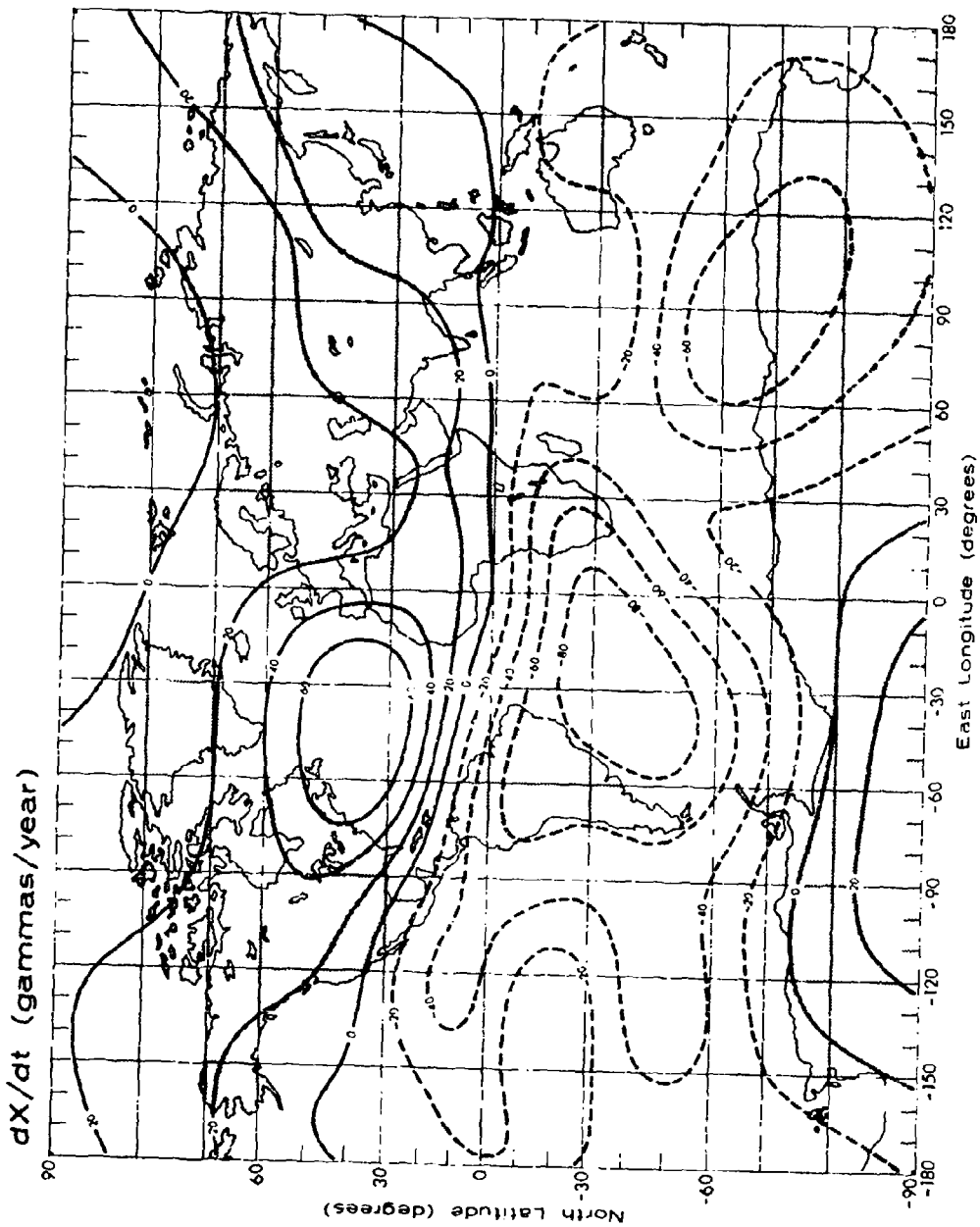

Figure 11-24. Contours of Constant Secular Change in X (Northward Component) for IGRF 1965.0 [see text]

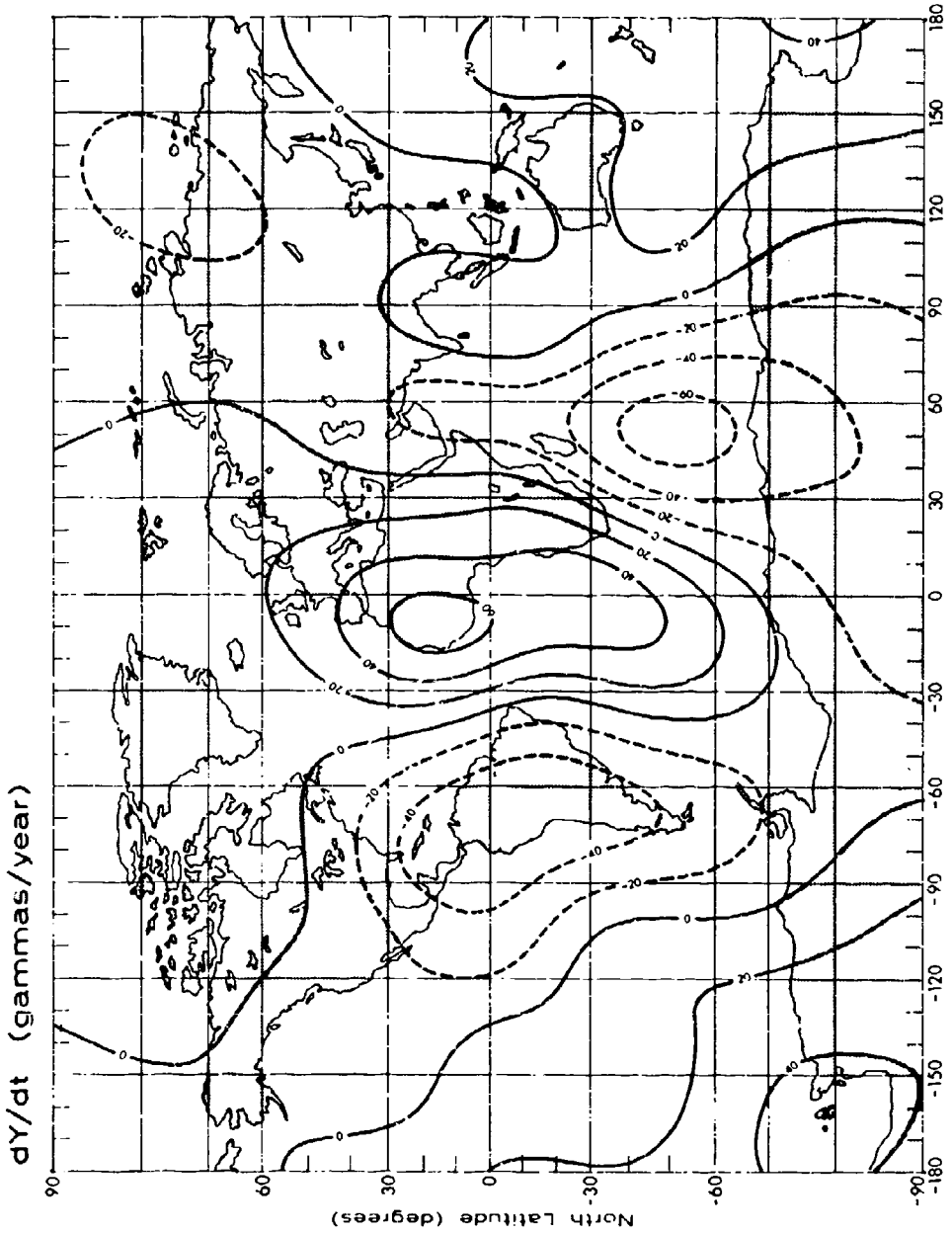

Figure 11-25. Contours of Constant Secular Change in Y (Eastward Component) for IGRF 1965.0 [see text]

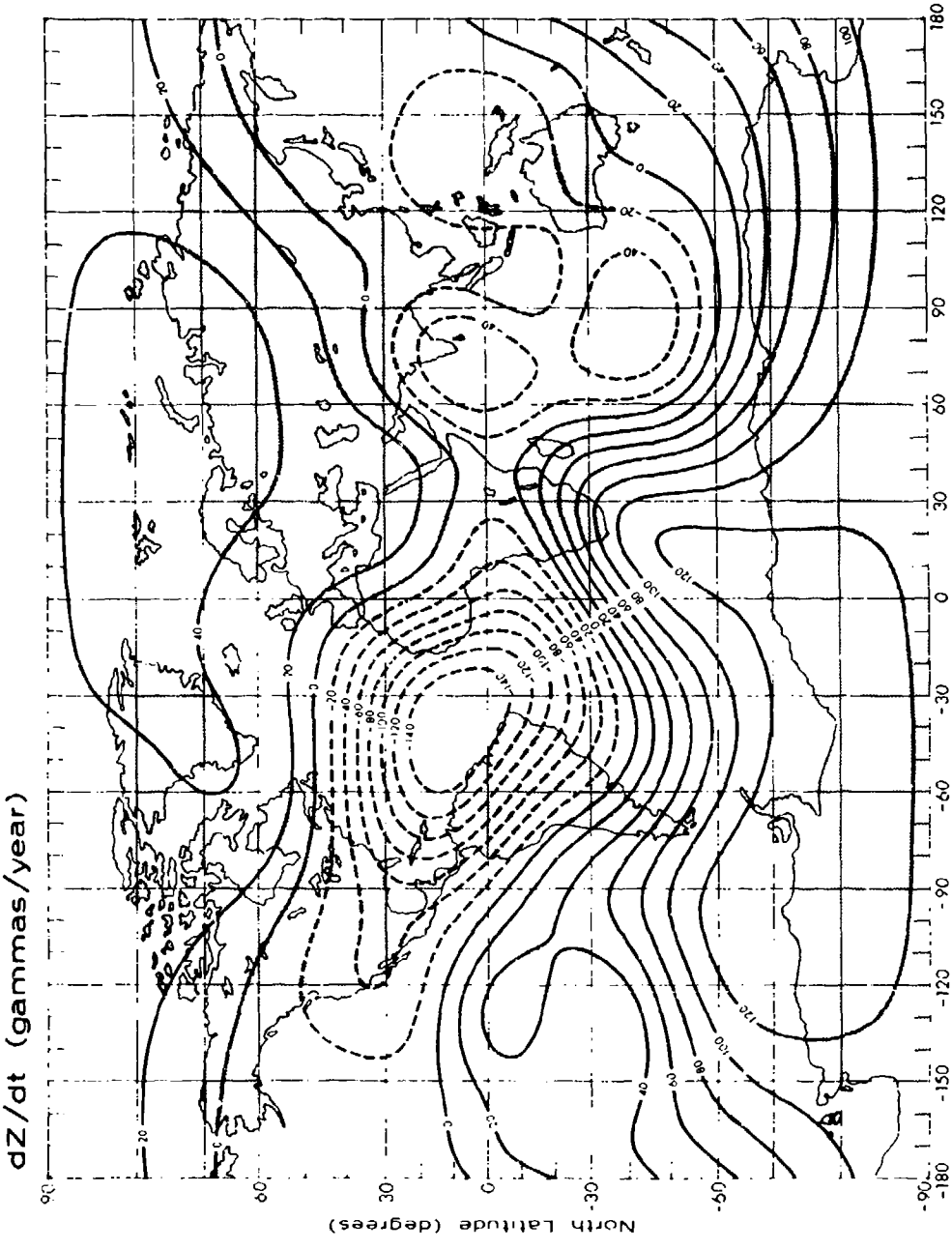

Figure 11-26. Contours of Constant Secular Change in Z (Vertical Component) for IGRF 1965.0 [see text]

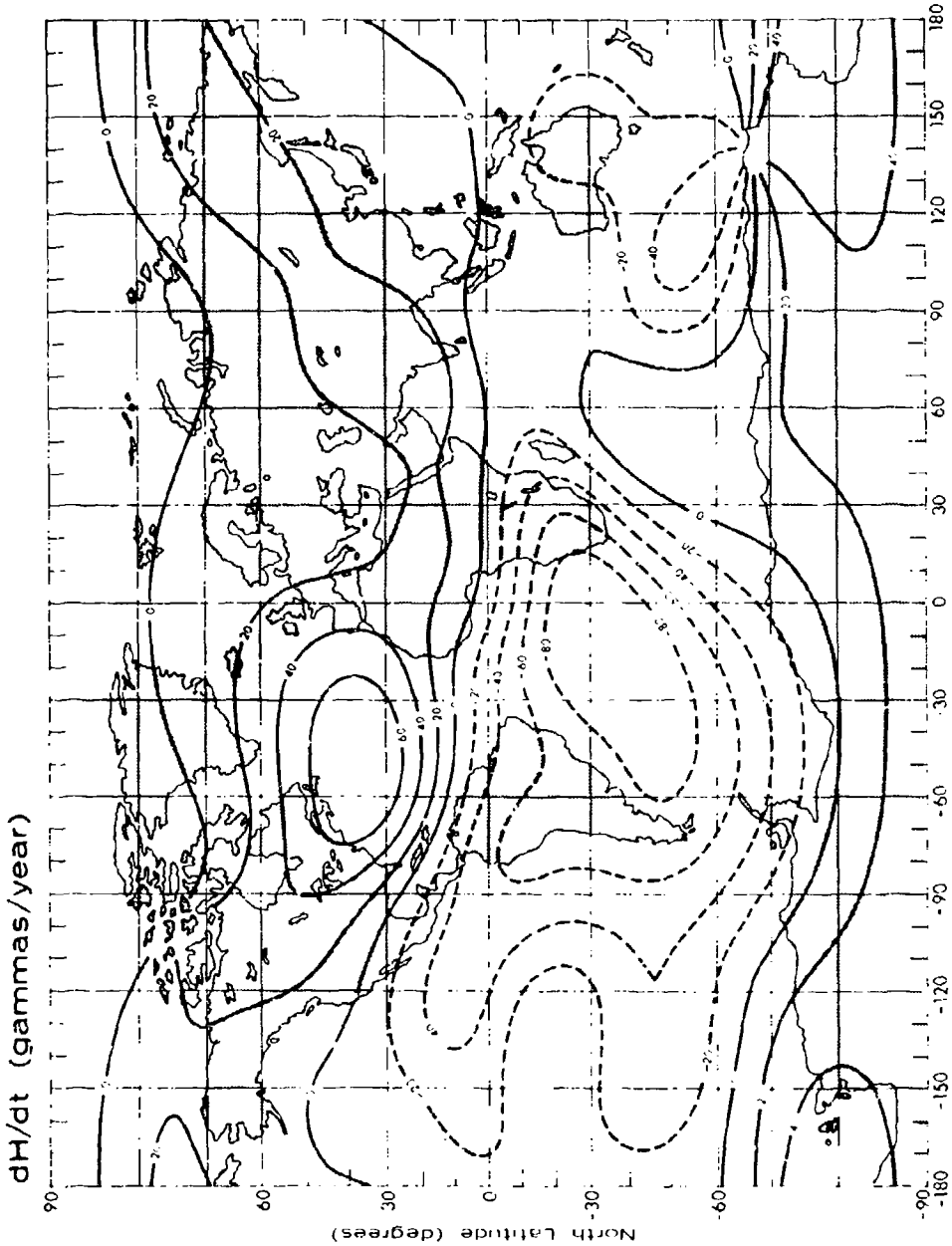

Figure 11-27. Contours of Constant Secular Change in H (Horizontal Component) for IGRF 1965.0 [see text]

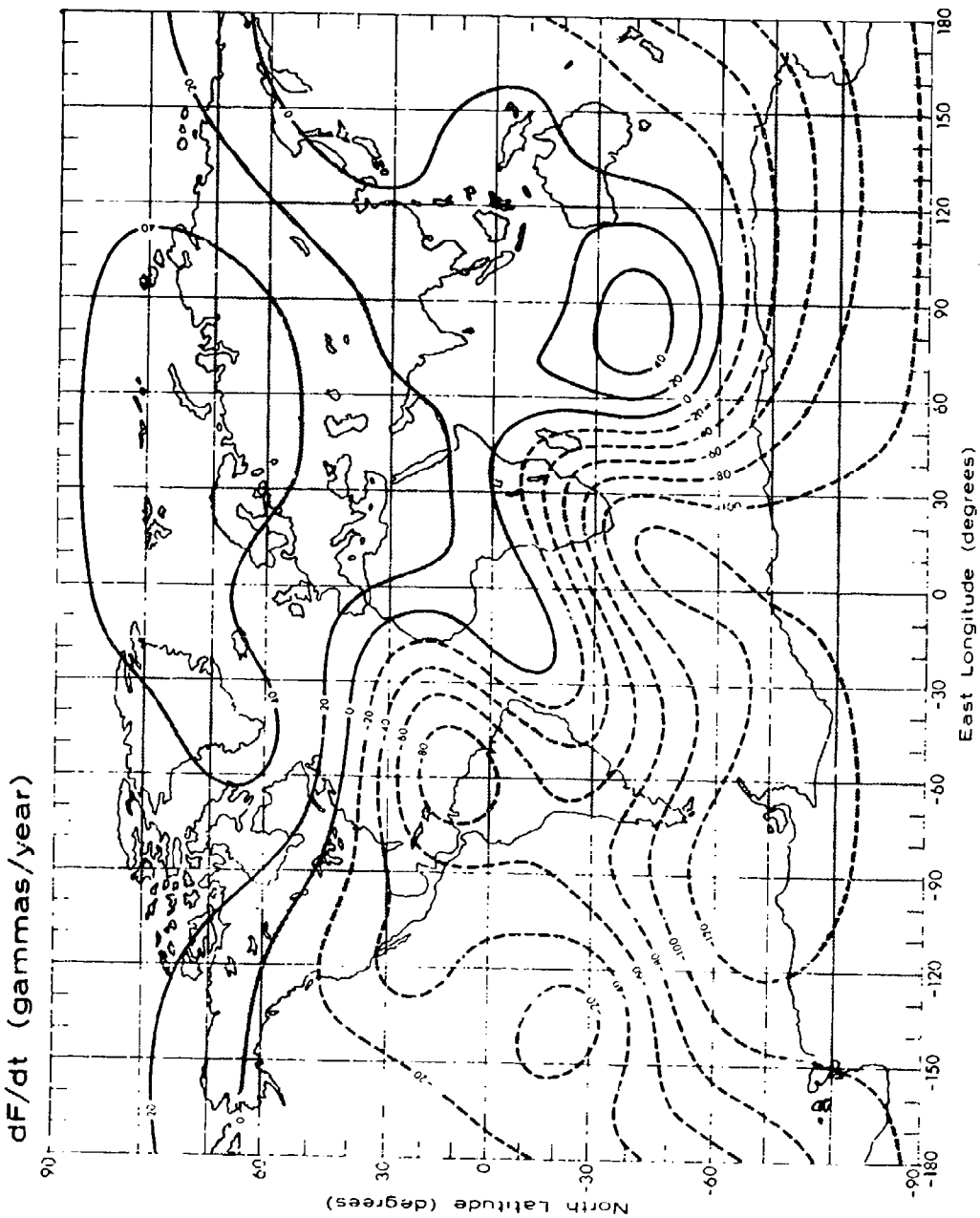

Figure 11-28. Contours of Constant Secular Change in F (Total Field) for IGRF 1965 [see text]

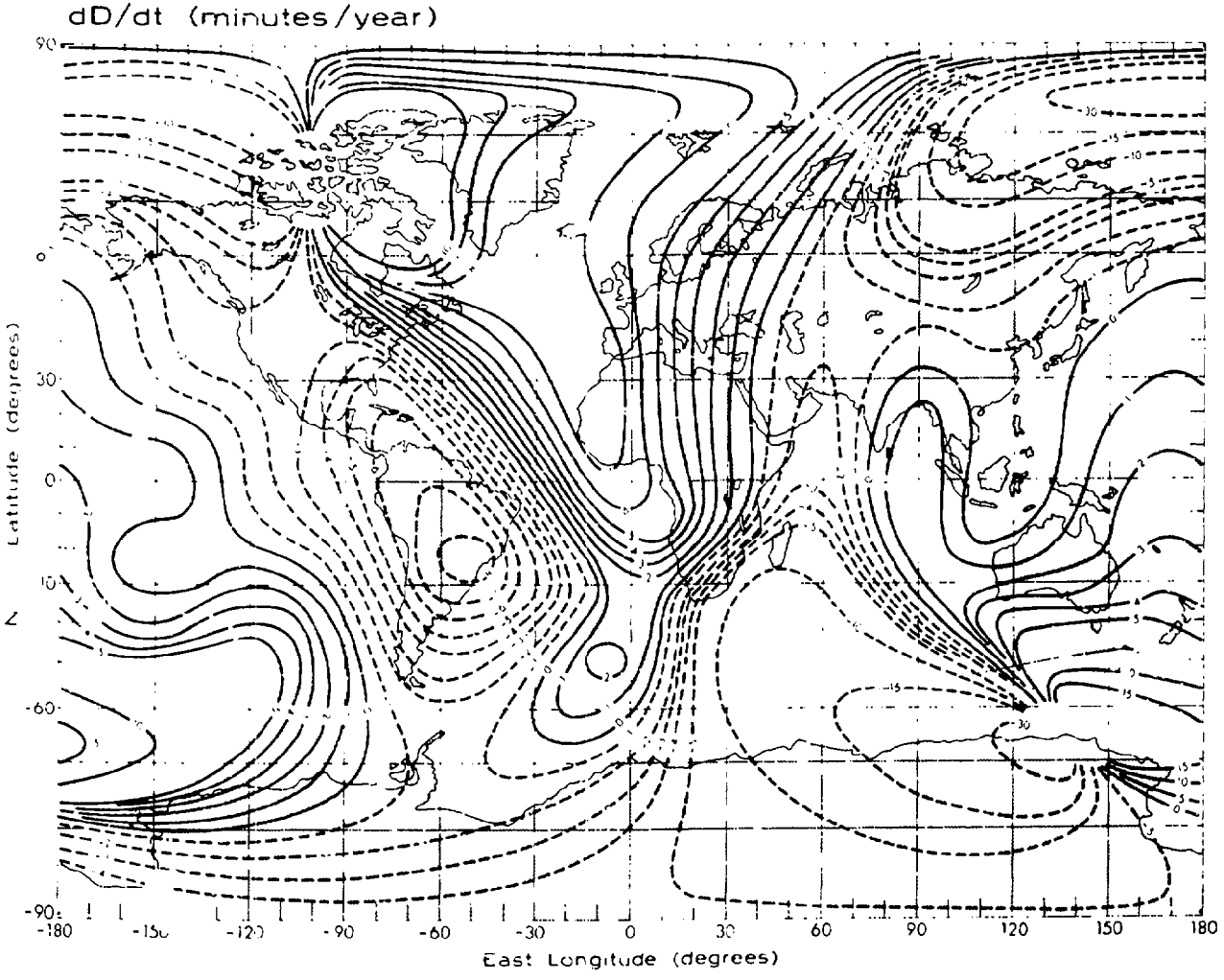

Figure 11-29. Contours of Constant Secular Change in D (Declination) for IGRF 1965.0 [see text]

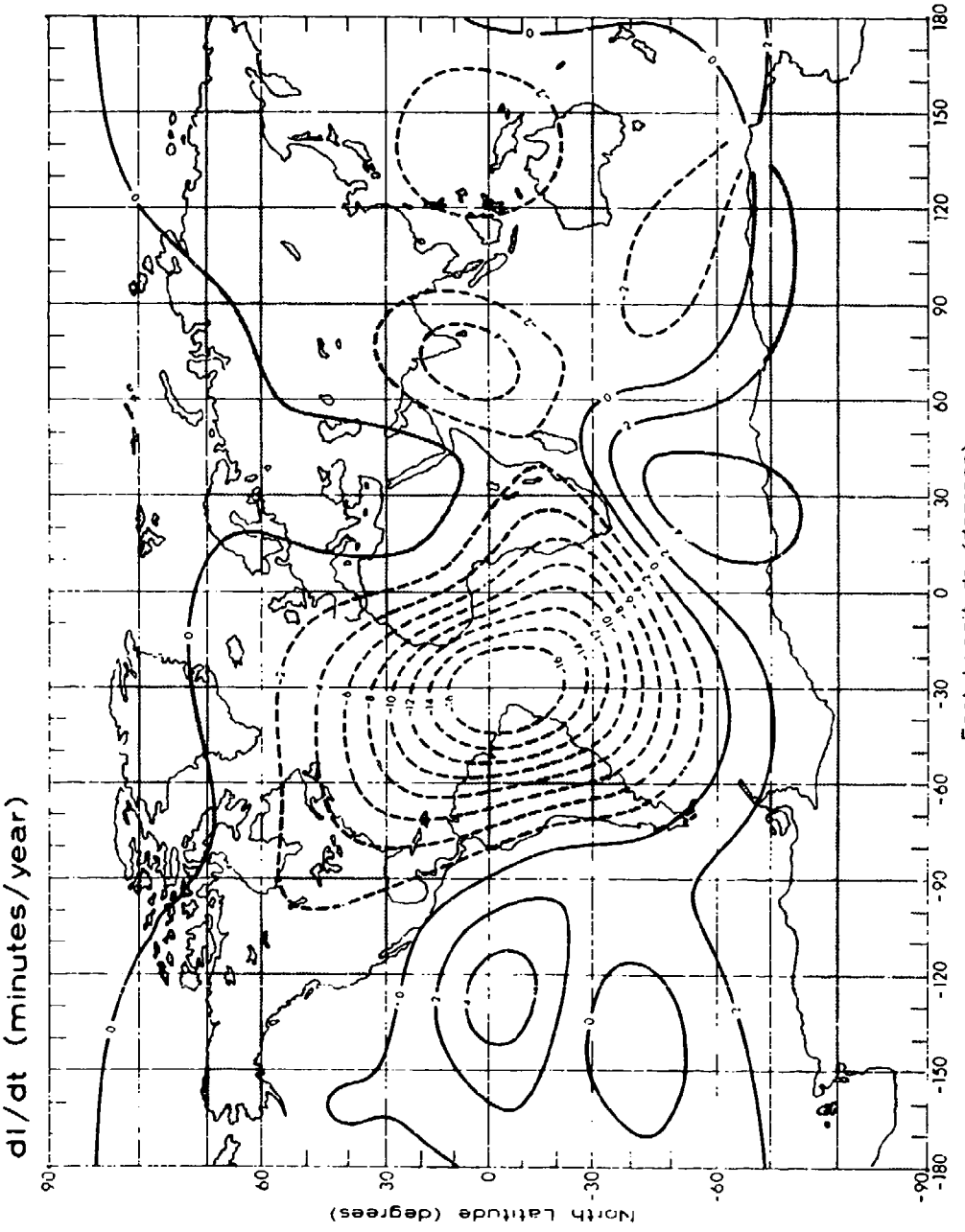

Figure 11-30. Contours of Constant Secular Change in I (Inclination) for IGRF 1965.0 [see text]

period. Were this rate to continue, the dipole field would vanish in another 2000 years. Only in recent decades has the rate over intervals as short as several years been measurable. As shown by the data of Figure 11-32, the decrease has become appreciably faster over the past two decades. This trend may indicate an oscillation about the mean rate with a period of about 40 years (dashed curve), or it could be nonperiodic (dotted curve), perhaps foreshadowing a total collapse of the field, as discussed below.

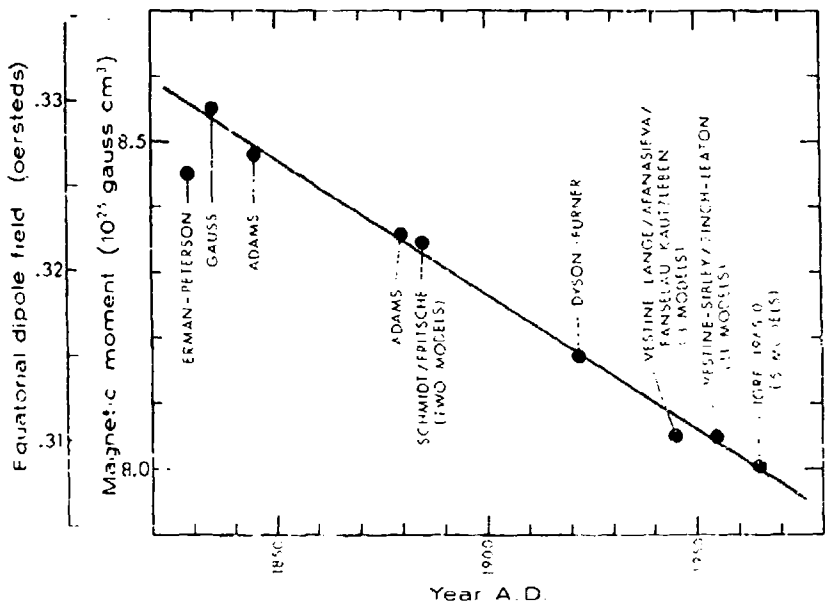

Figure 11-31. Equatorial Field Strength During the Past 150 Years [computed and plotted from data in Table 11-1 of Vestine, 1962]

The secular variation has the complex patterns shown in the charts of Figures 11-24 through 11-30. It has long been observed that the major regional anomalies in the field appear to be moving westward, and mathematical analysis [Nagata, 1962] confirms that, of the secular variation which is not attributable to dipole weakening, roughly 60% can be accounted for as a westward drift of the nondipole field by about 0.2 degree per year. This drift is easily observed in Figure 11-33 which shows the shift, over about 40 years, in the profile of the vertical equatorial field as a function of longitude. This is believed to indicate that the fluid core and solid mantle rotate at slightly different rates. The rate of drift is apparently not

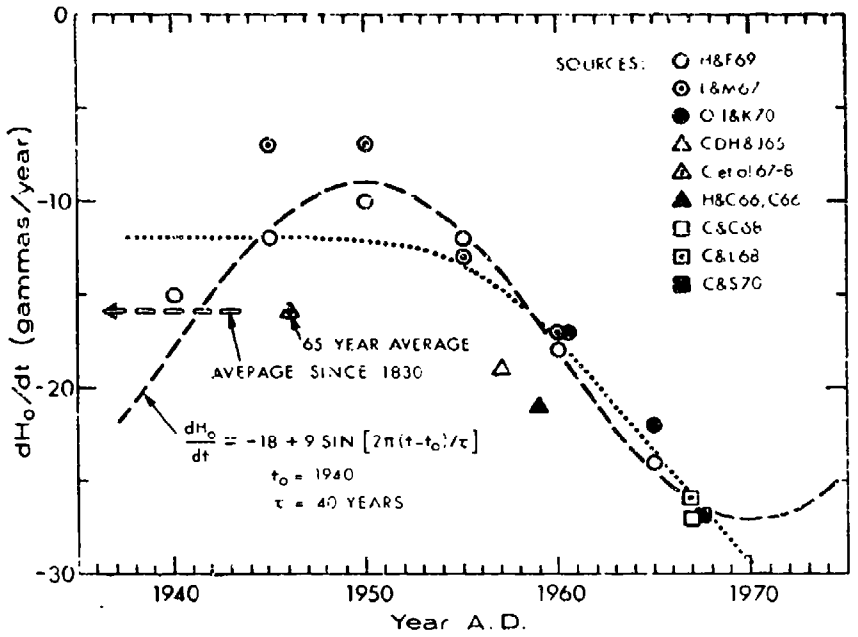

Figure 11-32. Rate of Change in the Equatorial Field Strength Over the Past 30 Years. The dashed curve is a sinusoidal oscillation of 40-year period which fits the data; the dotted curve is a nonoscillatory trend suggested by the data [data compiled by Cain, 1971]

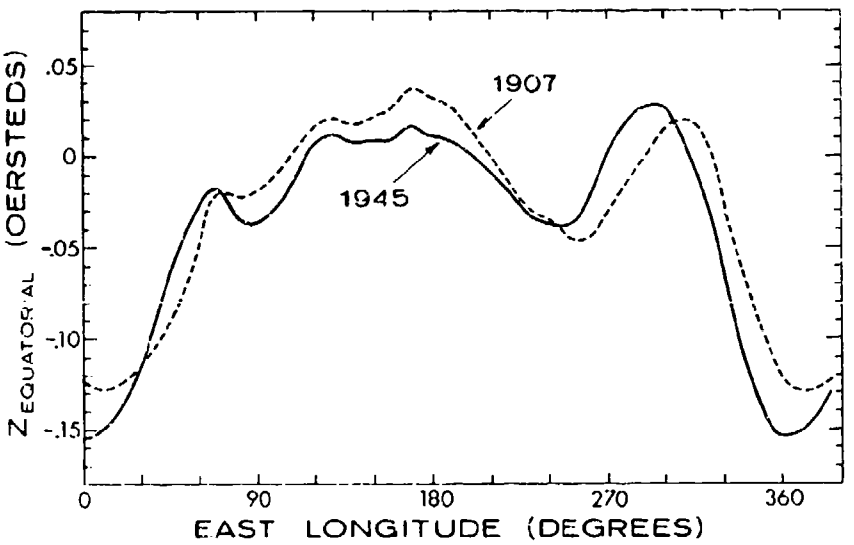

Figure 11-33. Longitudinal Profile of the Vertical Equatorial Field in the Years 1945 and 1907, Showing the Cumulative Westward Drift of the Nondipole Field in 38 Years [after Bullard et al, 1950]

constant. Since the core and mantle are coupled by electromagnetic as well as viscous forces, and since angular momentum must be conserved for the earth as a whole, changes in convective motion which alter the angular momentum of the core can produce rotational accelerations of the mantle. Changes in the rotation rates are indeed observed and appear to correlate well with secular variation changes [Vestine, 1962].

A smaller part of the present secular variation may be described as a northward movement of the center of the dipole with a velocity somewhat greater than 2 km per year. Since at this rate the dipole center would reach the surface of the core (about 3470 km geocentric distance) in about 1500 years, it is likely that the northward movement is a transient state of an axial oscillation of the current system which generates the dipole.

The remainder of the secular variation is nondrifting, is of relatively small magnitude (except in Antarctica), is not accurately determined, and seems to have about a dozen regional foci. Several hypotheses involving core convection have been proposed in explanation, but none has yet been generally accepted.

11.4.4 Paleomagnetism

Paleomagnetism is the study of the geomagnetic field in times earlier than those for which recorded data exist. It is based on the fact, discovered more than 100 years ago, that the natural remanent magnetism (NRM) of some rocks and archaeological samples is a measure of the geomagnetic field which existed at the time of their production. Providing the NRM is stable, its direction is the same as and its intensity is proportional to the field in which the rocks or samples were formed. However, NRM can be produced by several physical processes, under various conditions, in many types of material, and only certain combinations result in NRM which is stable enough for reliable results. To date, the most reliable data depend on thermoremanent magnetization, that is, magnetization which has been "locked into" the sample by cooling after formation at a higher temperature; the best archaeological samples are baked earths from previous civilizations (for example, kilns, hearths, and furnaces), and the best geological samples include materials formed at high temperature (for example, lava). Although great care and special experimental techniques are required, the validity of a great many paleomagnetic data and conclusions is well established.

Measurements of the secular change of the geomagnetic-field intensity have been extended backward in time about 5000 years by measurements on baked earths obtained in Japan, Russia, and France. [Nagata et al, 1963; Nagata and Ozima, 1967]. The equatorial field strength deduced from these data is plotted in Figure 11-34. The intensity has tended to decrease over the most recent 2000 years at an

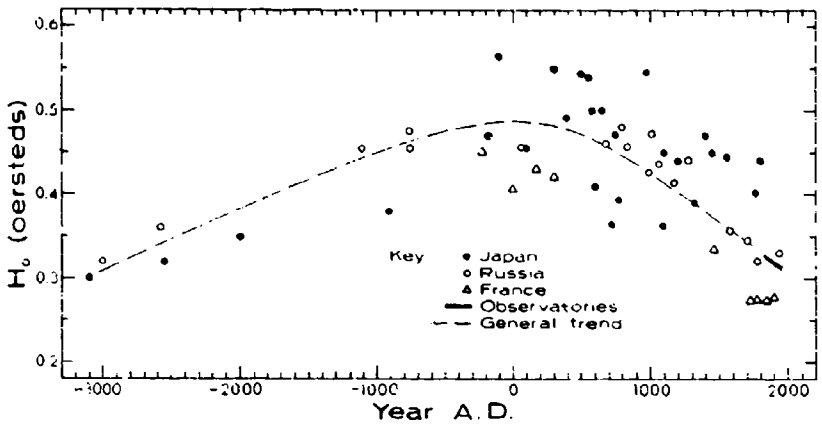

Figure 11-34. Equatorial Field Intensity in Recent Millenia as Deduced From Measurements on Archaeological Samples and Observatory Data [redrawn after Nagata and Ozima, 1967]

average rate of about 10 gamma/yr, while an increase of similar magnitude is observed for the preceding 2000 years. The data suggests a cyclic variation with a period of about 10,000 years.

Knowledge of the direction of the magnetic field has been extended backward over both archaeological and geological time scales on the basis of data from rock samples. The direction during the past several tens of thousands of years shows quasiperiodic oscillations ranging over several tens of degrees. A spectral analysis shows peaks at a number of periodicities between 400 and 7000 years, some of which have been ascribed tentatively to various components (dipole and nondipole) of the main field. However, data are not yet sufficient to describe completely the secular variation in recent millenia.

Measurements covering the past few millions of years have yielded the important discovery that, at least during this time period, the dipole axis has not wandered over the entire earth but has remained quite closely aligned with the axis of rotation. Measurements covering hundreds of millions of years have yielded the second important discovery that there exist reversely magnetized rocks; in the absence of an alternative explanation this implies that the field has periodically undergone complete reversals. Although it has been shown to be possible for some rocks to acquire a remanent magnetism opposite to the field in which they were formed, other evidence [Irving, 1964, Chapter 7] is now very convincing that field reversals have actually occurred a number of times between at least 500 million years ago and the present. The two most recent reversals occurred about 1.0 and 2.4 million years ago, as shown in Figure 11-35. There is some evidence that

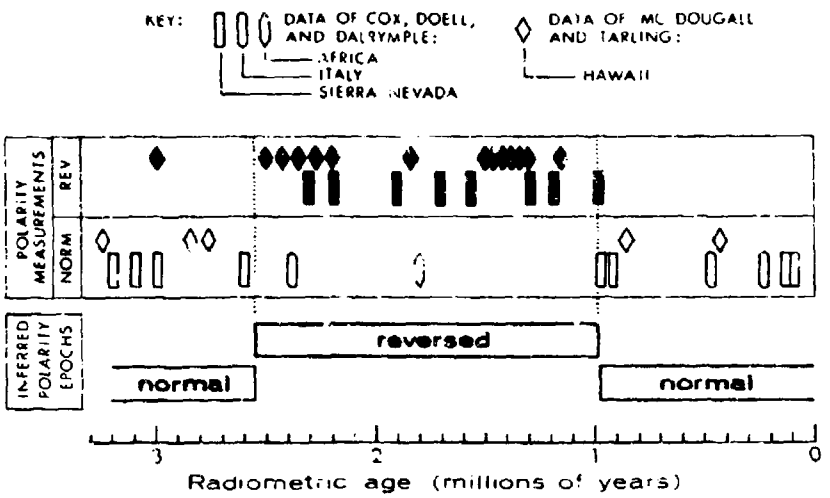

Figure 11-35. Polarity Epochs of the Geomagnetic Field During the Past Few Million Years (Lower Half of Figure) as Deduced From Paleomagnetic Measurements (Upper Half). Subsequent work has confirmed this picture, but has established the age of the earlier reversal to be 2.41 ± .05 million years [from the data of Cox et al, 1963a, 1964, and McDougall and Tarling, 1963, 1964]

during the reversal (that is, the period of transition from one direction to the other) the field strength drops to a small fraction of the present-day strength, suggesting that the dipole contribution first diminishes to zero, leaving only the nondipole terms, and then grows again in the opposite direction. However, it has also been suggested that the undiminished dipole contribution may swing abruptly from one stable position to another, and this question is not yet resolved. The duration of the transition is estimated to be at least a thousand years, while the duration of each polarity epoch seems always to be much longer (several thousands to many millions of years); so far there is no evidence that reversals occur with a regular periodicity or that either polarity persists longer than the other.

Large variations in the strength of the geomagnetic field in the past may have consequences in other fields of study, for example, influencing biological evolution through modulation of the cosmic radiation and causing a difficulty in the radiometric dating of geological samples, in which a constant upper-atmosphere cosmic-ray intensity has been assumed.

When data from recent epochs (for example, those of Figure 11-34) are viewed in the light of more ancient data, it is certainly not clear whether the present weakening of the dipole field represents the beginning of another field reversal or a less drastic oscillation.

Apart from the phenomenon of field reversal, paleomagnetic data indicate an apparent motion of the geomagnetic poles. As already noted, data for the last 10 million years or so show the dipole axis fairly close to the geographic axis. There seems generally to be a clockwise motion of the dipole axis about its mean position with a period estimated to be roughly 10,000 years, suggesting a precession about the axis of rotation. For earlier geological ages the behavior is not as clear. Paleomagnetic and paleoclimatological data obtained on any one continent (even at widely separated locations) tend to be consistent and yield a time history of the apparent location of the magnetic poles [Nagata and Ozima, 1967]; over hundreds of millions of years, such virtual poles appear to have moved systematically by many tens of degrees towards the present pole positions. However, as shown in Figure 11-36, there is a large disagreement between the traces measured for different continents. The implication is that the continents themselves have been in motion, having evolved from primeval land masses bearing little resemblance to the present continents. Several concepts have been proposed; one that is widely favored assumes two primitive continents, Laurasia (North America, Europe, and northern Asia) and Gondwanaland (South America, Africa, Australia, Antarctica, Arabia, and India). Figure 11-37 shows one reconstruction of Gondwanaland which brings the virtual poles of about 150 million years ago into fairly good agreement; it suggests that India (5000 miles from its present location) and Australia had already broken off and drifted away by that time. At present there are insufficient data to locate unambiguously either the poles or the land masses, nor is there a satisfactory physical theory to explain the continental drift; it is also not clear how the axis of rotation has moved relative to the surface as a whole.

11.5 QUIET VARIATION FIELDS

The fact that the surface magnetic field has a daily variation was first discovered in 1722. That the variation is caused by electric currents in a conducting layer of the atmosphere was predicted in 1882, though the existence of the ionosphere was not discovered until 1902. Subsequent study has shown that the quiet variation consists of a large effect of solar origin, a smaller effect of lunar origin, and a still smaller remainder due to magnetospheric processes.

11.5.1 The Solar Quiet Daily Variation

The solar quiet daily variation (the Sq field) results from currents flowing in the E layer of the ionosphere. Both the conductivity which permits the current to flow and the electric field which powers the currents are produced by solar electromagnetic radiation, though some contribution to the electric field may be the result

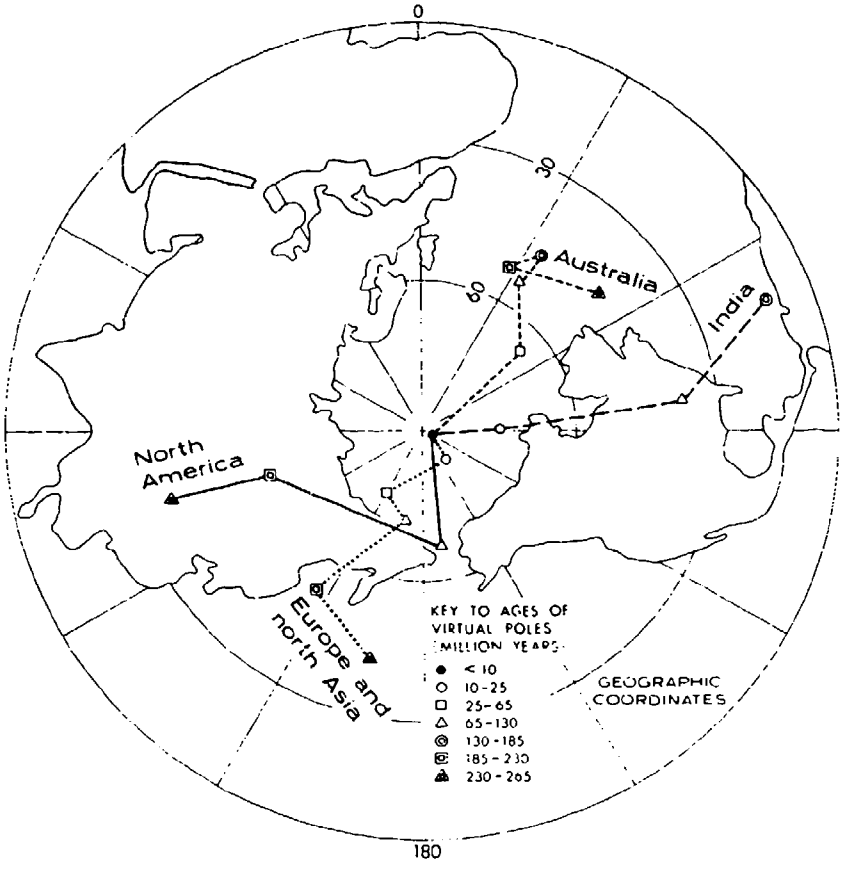

Figure 11-36. Comparison of the Apparent Paths of the North Magnetic Pole Over the Past 250 Million Years as Determined From Paleomagnetic Measurements on Four Different Land Masses [redrawn after Irving, 1964]

of a continuous convection of the outer magnetosphere (see Section 11.7.2). The major part of the electric field is generated in the manner of a dynamo by high-speed tidal winds which are produced by solar heating of the atmosphere. The pattern of winds at ionospheric altitudes is still poorly known, but the pattern of Sq is less dependent on this factor than on ionospheric conductivities. A fraction (about 30%) of the Sq field is produced by earth currents induced by the primary

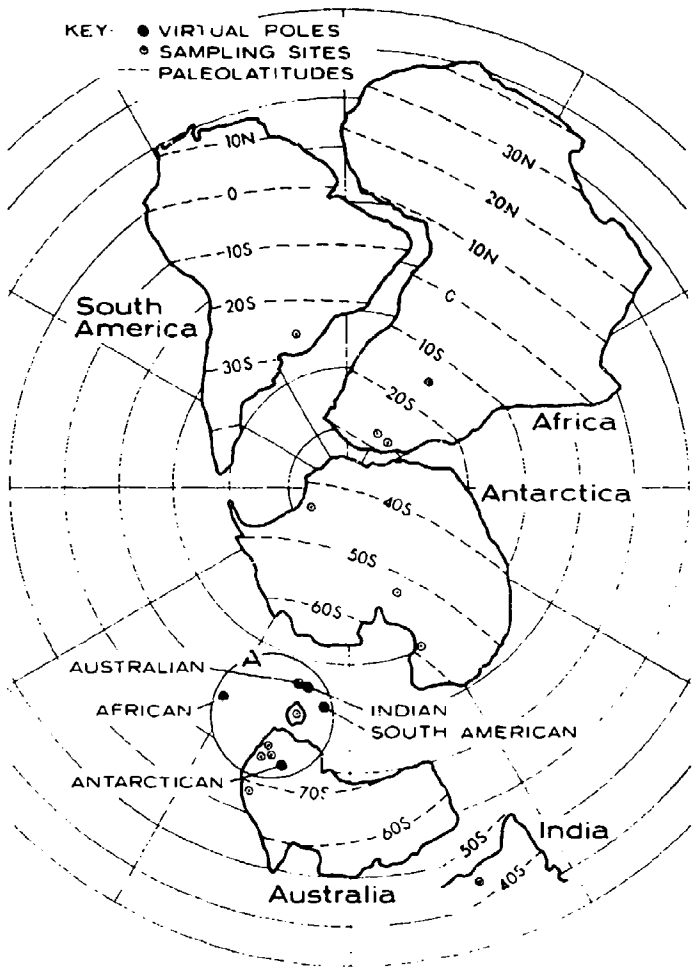

Figure 11-37. A Reconstruction of Gondwanaland for the Jurassic Period (130 to 185 Million Years Ago) Which Yields Agreement Between Paleomagnetic Data; Poles Determined From the Five Continental Masses Fall Within a 10-Degree Circle (A), Which is the Limit of Accuracy of the Data. Also shown are the paleolatitudes deduced from paleoclimatic data [redrawn after Irving, 1964]

ionospheric currents. To a first approximation, the Sq current is stationary in nonrotating coordinates, and the field variation is observed on the ground as a function of local time because the earth rotates under the currents; it is therefore similar for all observers at the same latitude. This is a poor approximation, since

the conductivities which determine the current pattern are controlled by the magnetic field, which is tilted, and the Sq variation is much more nearly the same along contours of constant dip latitude φ than it is at constant geographic latitude. (Dip latitude is defined by the relation $\varphi = \arctan [\tan I)/2]$, where I is inclination.) Also contributing to a longitudinal dependence are other effects, such as the influence of ocean areas upon the strength of induced internal currents.

Figure 11-38 shows the worldwide average Sq variation in the elements H, Z, and D near the time of an equinox. Figure 11-39 shows the inferred ionospheric and induced earth currents. The most notable feature is a concentration of current,

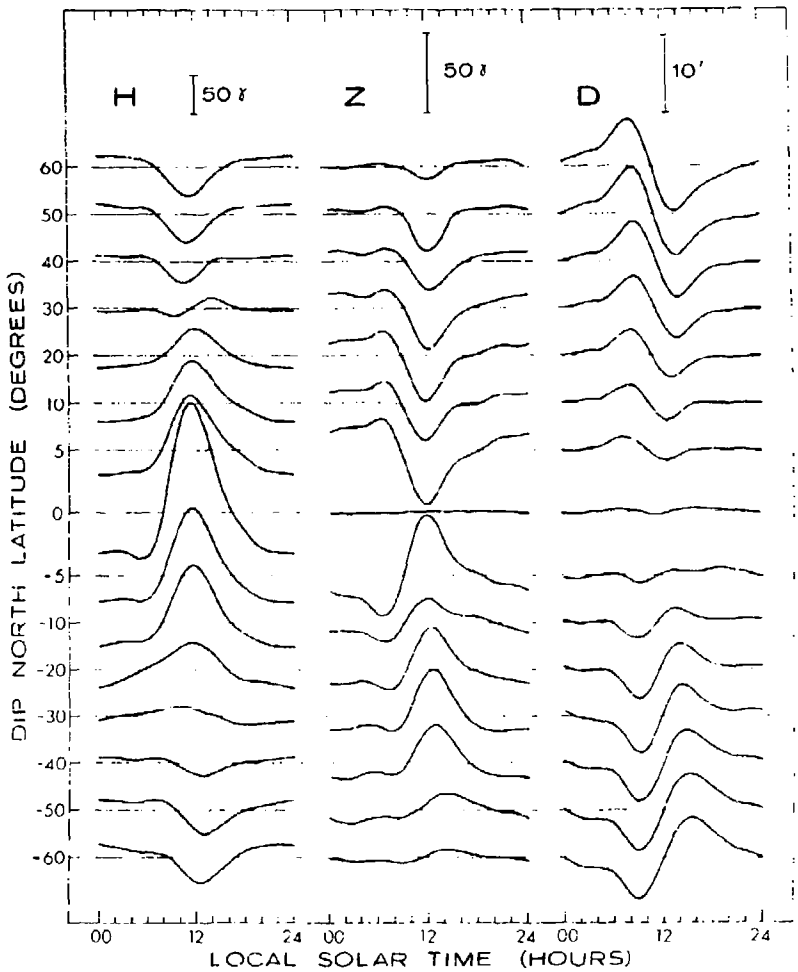

Figure 11-38. Worldwide Average of the Solar Quiet Daily Variation for the Months March, April, September, and October, 1958 (Solar Maximum) [combined and redrawn after Matsushita, 1967]

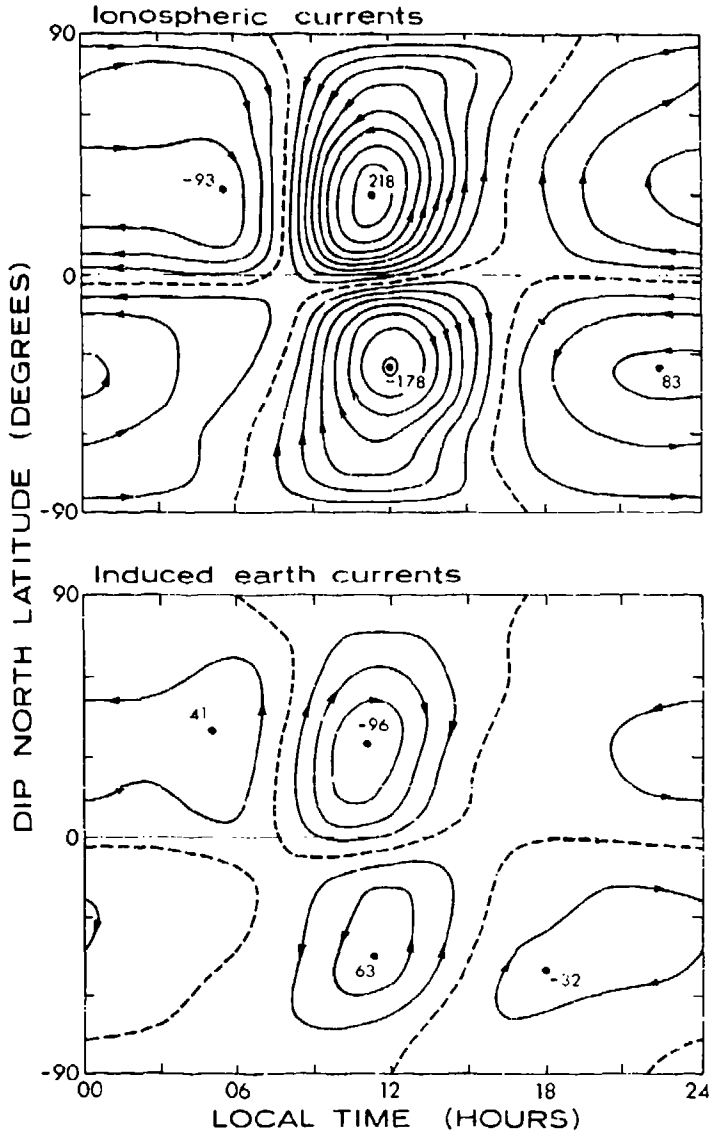

Figure 11-39. Ionospheric and Induced Earth Currents Inferred From the Worldwide Sq Variation Shown in Figure 11-38. Current between adjacent contours is 25 x 10^3 amperes. In each vortex, the dot indicates the center and the number gives the total current in units of 103 amperes. Dashed curves are zero-intensity contours [redrawn after Matsushita and Maeda, 1965a]

the equatorial electrojet, at the magnetic dip equator. The electrojet is, in fact, only a few hundred kilometers wide, being more concentrated than shown. (The spherical-harmonic analysis used to compute the currents cannot reproduce such sharp features.) The electrojet exists because of a special circumstance. The fact that the field at the dip equator is exactly horizontal creates a narrow belt of high conductivity in the following way. An electric field impressed perpendicular to a magnetic field (here eastward and northward, respectively) would normally produce a Hall current flowing perpendicular to both (here vertically). However, in this case, the conductive medium is bounded in the vertical direction, the Hall current is inhibited, and a polarization results. It is found, experimentally and theoretically, that the polarization enhances the effective conductivity in the direction of the electric field (Cowling conductivity). At all other points, even slightly off the dip equator, the conductivity along the slightly tilted field lines is sufficient to allow the polarization to leak off partially, and the Cowling conductivity is much less enhanced.

Longitudinal, seasonal, and yearly dependences are not shown here; they have been summarized quantitatively by Matsushita and Maeda [1965a]. The seasonal dependence is strong, with the current vortex in a given hemisphere becoming more intense during its local summer. There is also a strong dependence on solar cycle; while E-layer ionization is 50% greater at solar maximum than at solar minimum, the Sq variation is about 100% greater, presumably because the wind speed also increases. When the intensity of solar radiation is increased for brief intervals by solar-flare activity, the Sq variation appears to be enhanced. In fact, however, this so-called solar flare effect is not a simple enhancement, since the additional current is generated mainly in the D (rather than the E) region, where the wind system is likely to be different; it is discussed in Section 11.6.5. During solar eclipse, on the other hand, a diminution of the Sq field by about 12 gammas has been observed.

In recent years it was thought, for a time, that an additional independent solar contribution to the quiet variation field had been discovered. It was observed only in the polar regions, being obscured by the main Sq field elsewhere, and was termed Sq^P. Currently, however, it appears that Sq^P is really a disturbance (not a quiet-variation) field, being the same as the DP2 field discussed in Section 11.6.3.

11.5.2 The Lunar Daily Variation

The lunar daily variation (the L field) is generated in the same manner as the Sq field, except that the responsible winds are produced by luni-solar gravitational tides. The dominant behavior is a semidiurnal variation; the amplitude is about an order of magnitude smaller than the Sq amplitude. As in the case of Sq, about

50% of the L field is produced by induced earth currents. Figure 11-40 shows the average L variation in the elements H, Z, and D near the time of an equinox and for a mean lunar age. Figure 11-41 shows the inferred ionospheric and induced earth currents. A lunar equatorial electrojet is a principal feature, existing (as I being more intense than shown) for the same reasons as in the case of the S_q variation.

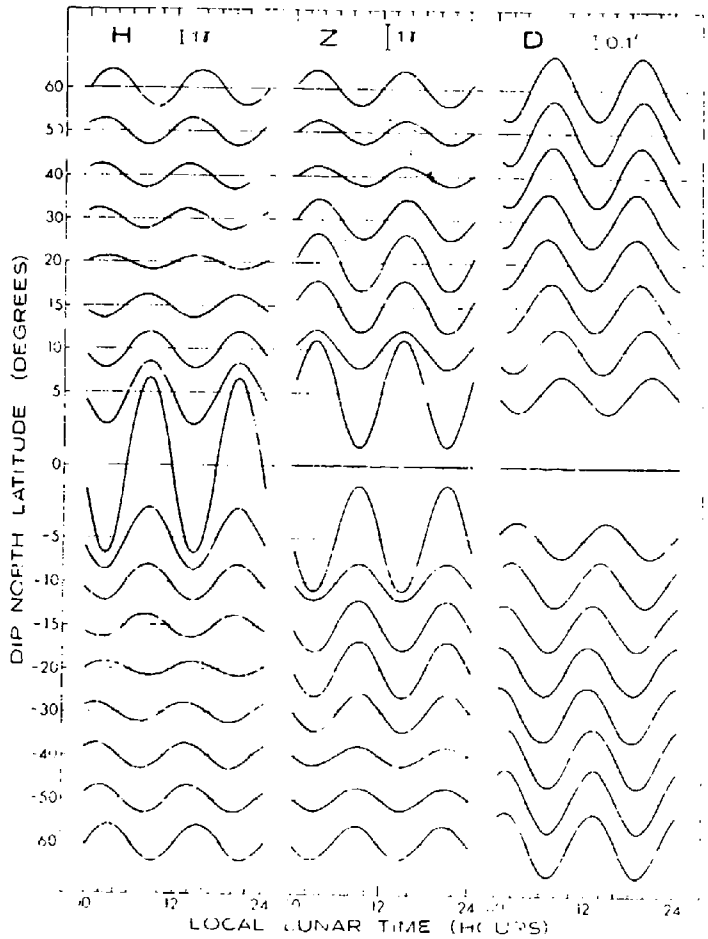

Figure 11-40. Lunar Semidiurnal Variation Near Time of an Equinox. Curves are derived from data covering period 1941-1962 (redrawn after Matsushita and Maeda, 1965b)

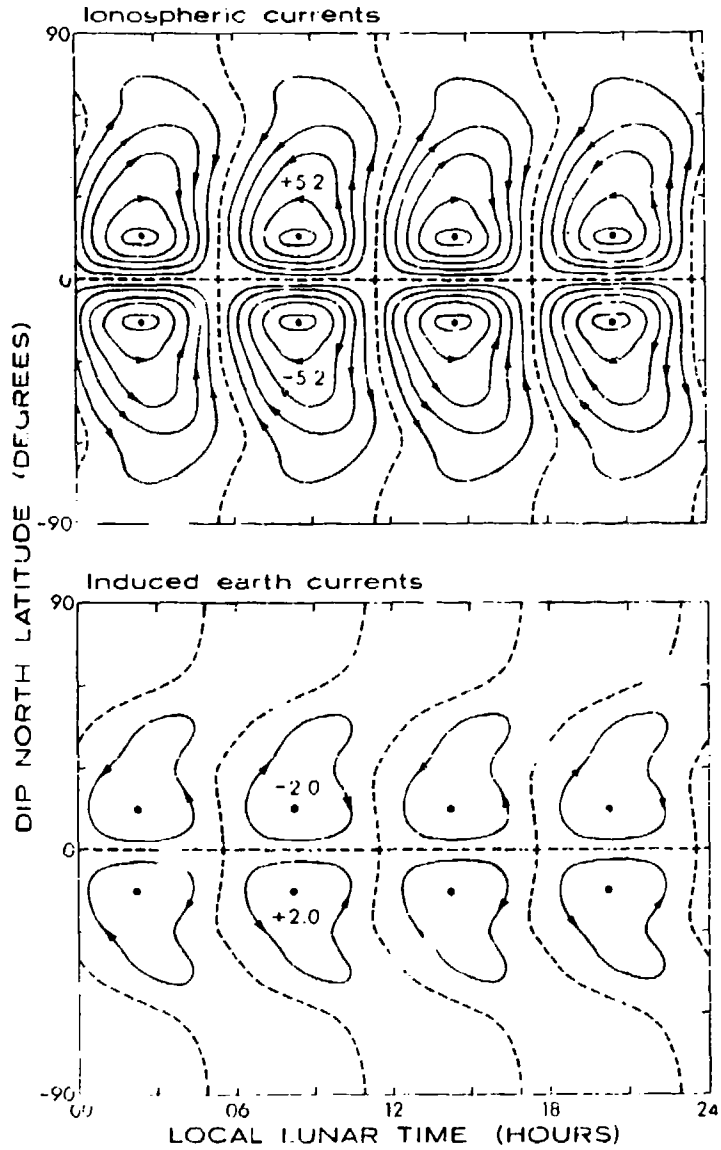

Figure 11-41. Ionospheric and Induced Earth Currents Inferred From the L Variation Shown in Figure 11-40. Current between adjacent contours is 1×10^3 amperes. In each vortex, the dot indicates the center and the number gives the total current in units of 10^3 amperes. Dashed curves are zero-intensity contours [redrawn after Matsushita and Maeda, 1965b]

The dependence of L on several parameters is consistent with expectations. There is a seasonal dependence, as for Sq, and also a dependence on lunar age. The solar-cycle dependence of L is smaller than that of Sq, the variation being about 30% (instead of 100%) greater at solar maximum than at solar minimum, because the increased activity increases only the conductivities and not the tidal wind speeds. The longitudinal dependence, if it exists, is too small to have been established to date. A quantitative summary of such dependences has been given by Matsushita and Maeda [1965b].

11.5.3 Daily Variation of Magnetospheric Origin

On the ground, the daily variation which results from magnetospheric effects has not yet been identified experimentally since it is certainly smaller than (and has characteristics confusable with) the Sq and L variations. The dayside-nightside difference in compression of the field by a quiet solar wind results in a surface diurnal variation computed to be only about 3 gammas; the strengths of quiet-time magnetospheric convection and of its associated diurnal variation have not been estimated; and the surface diurnal components of other magnetospheric fields (for example, a quiet-time ring-current field), which in principle might arise from the asymmetric geometries involved, are probably of negligible magnitude.

In the outer magnetosphere, such diurnal effects, are, of course, large; however, measurements are usually referred to solar-magnetospheric coordinates to remove most of the diurnal dependence. The remaining diurnal effect is usually of little interest, but may be an annoying complication in analyzing data for other purposes.

11.6 DISTURBED VARIATION FIELDS

The summary description of geomagnetic disturbance which follows presents a somewhat simplified view which is consistent with most current theoretical results and available data. However, in many areas there exist viable alternative theories and considerable controversy. Since it would be impossibly cumbersome to qualify each statement of this description, it must be remembered that parts of the description are not yet generally accepted, and some will surely, in the future, require revision or even be proved quite wrong.

11.6.1 Geomagnetic Storms

A geomagnetic storm is the magnetic manifestation of a magnetospheric [illegible]. As noted above, the classical [illegible] consists of two energizing parts (first, the

sudden commencement and initial phase; second, the main phase) followed by a recovery. The first part is a compression and correlates well with the pressure exerted by the bulk flow of the solar wind. The second is an inflation and appears most highly correlated with the direction of the interplanetary field. Since a feature such as a shock front or other discontinuity propagating with the solar wind is likely to involve changes in both pressure and field direction, it is reasonable that storms typically show both compression and inflation effects. On the other hand, either pressure or field direction may remain constant across a propagating discontinuity, and it is not uncommon to observe a storm without a sudden commencement or a storm which fails to develop a main phase.

The compression part of a storm, though not simple, is not nearly as complex as the inflation part and is not discussed further. The inflation part appears to be the cumulative effect of a number (often about 10) of magnetospheric substorms, each of which contributes a quantity of protons to form the main-phase ring current. If the substorms are few and widely separated in time, each fresh supply of protons can decay before the next batch is produced, and the main phase will be negligible or small, but if there occur a number of substorms within a short time interval, the protons accumulate to form a strong ring current and a large main phase. The intermittent and impulsive nature of the substorms accounts for the characteristic noise of the main phase. With a view of the classic storm as the sum of several substorms, the next step is to examine the features of a substorm.

A magnetospheric substorm comprises a number of features which, while generally intimately related, are often examined separately. These features themselves are also commonly (and confusingly) termed "substorms" and include (at least) the auroral, magnetic, ionospheric, micropulsation, proton-auroral, and VLF-emission substorms, some of these are discussed below. The term "polar" is often prefixed in referring to a substorm to indicate those manifestations which are observed in the polar and auroral regions.

11.6.2 Auroral Substorms

It has only recently been recognized that at any given time, auroral arcs tend to lie within a narrow, roughly oval belt which encircles the geomagnetic pole, its center displaced about 3 degrees toward local midnight. This belt, shown in Figure 11-4, is called the auroral oval. (See also Figure 11-4.) It is (roughly) the projection of the neutral sheet within and the magnetopause surrounding the geomagnetic tail; it is therefore most reasonable to define the polar cap, whence originate all the field lines drawn out to form the tail; as the area enclosed by the auroral oval. As the earth rotates, the auroral oval sweeps over a large geographic area, as shown in Figure 12; the oval approaches to within 2 degrees of the geographic pole

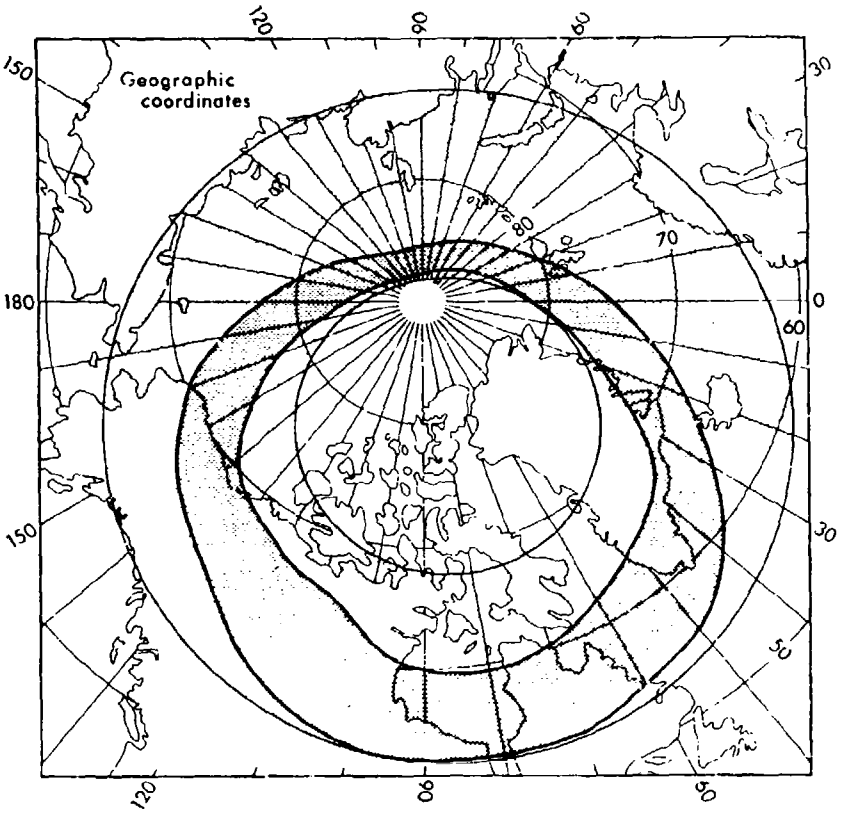

Figure 11-42. Location During Moderate Activity (Q = 4) of the Auroral Oval. Dark shading indicates the oval at 0800 UT, while light shading indicates the area swept over by the oval during the day [based on data of Feldstein, as plotted by Feldstein and Starkov, 1967, and Akasofu, 1968]

and dips as far south as 54° geographic latitude. Because of the elliptical shape and the displacement of the oval relative to the geomagnetic pole, a magnetic observatory may fall above, on, or below the oval during the course of the day, even if the oval retains a constant size. Apart from this diurnal motion, the size of the oval does vary with changing magnetic activity, contracting poleward in quiet periods and expanding equatorward during increased activity. The so-called auroral zone, a circular belt centered on 67° geomagnetic latitude, which earlier was incorrectly thought to be the instantaneous location of maximum auroral activity, is simply the average location of the midnight sector of the oval (where, statistically, auroras are most frequently observed). In the oval near local midnight, the aurora is always present, even on the quietest days, the quiet form being the steady "homogeneous arc". The more intense and active forms occur with

geomagnetic disturbance. Particles are precipitated into the atmosphere, down field lines which pass near the inner edge of the neutral sheet, and create the familiar visible forms as well as a greatly enhanced ionization. Where it has been possible to establish that auroras in the northern and southern hemispheres lie at opposite ends of the same field line, they have been observed to be strikingly similar and well correlated in time.

The auroral activity accompanying a magnetospheric substorm follows roughly the same time schedule for growth and decay as the substorm as a whole, reaching a peak within about 30 minutes of its commencement. It begins near local midnight and spreads explosively toward both earlier and later local times and also poleward and equatorward. Auroral substorms are especially important to geomagnetic phenomena because the enhanced ionization along the oval determines the configuration of the auroral electrojet discussed below.

11.6.3 Magnetic Substorms

The most common magnetic disturbance which indicates the occurrence of a magnetic substorm has been termed a "bay" because of its appearance on magnetograms. Figure 11-43 shows an example in which two substorms occur with a separation of about 7 hours. The four stations for which magnetograms are shown were all located on the auroral oval, and the substorms appear as negative bays. (Magnetograms, not shown, for other stations above and below the oval exhibit very different behavior.) The disturbance field is caused by ionospheric-magnetospheric currents; it can be explained by an equivalent current system (that is, one allowing ionospheric currents only) resembling that shown in Figure 11-44. Although current patterns derived by various investigators differ, partly because definitions of the disturbance field differ, a common feature is a sharp concentration of current along the auroral oval, usually with four vortices in the polar and subauroral regions. This current, the auroral electrojet, is intense, impulsive, and concentrated during substorms, weak and diffuse on quiet days. It is most intense in the post-midnight sector where it flows westward; its character in the afternoon sector, where Figure 11-44 shows an eastward flow, is still poorly established and controversial.

It is now clear that magnetic substorms are driven rather directly by the interaction of the solar wind and magnetosphere; data from synchronous and low polar-orbiting satellites confirm that the currents flow in and out of the oval through the magnetosphere, so the equivalent ionospheric system bears a limited resemblance to the real case. The actual electrojet system probably resembles the simplified configuration sketched in Figure 11-45, which is somewhat similar to several proposed much earlier (for example, Birkeland [1913] and Alfven [1939]). Currents flow

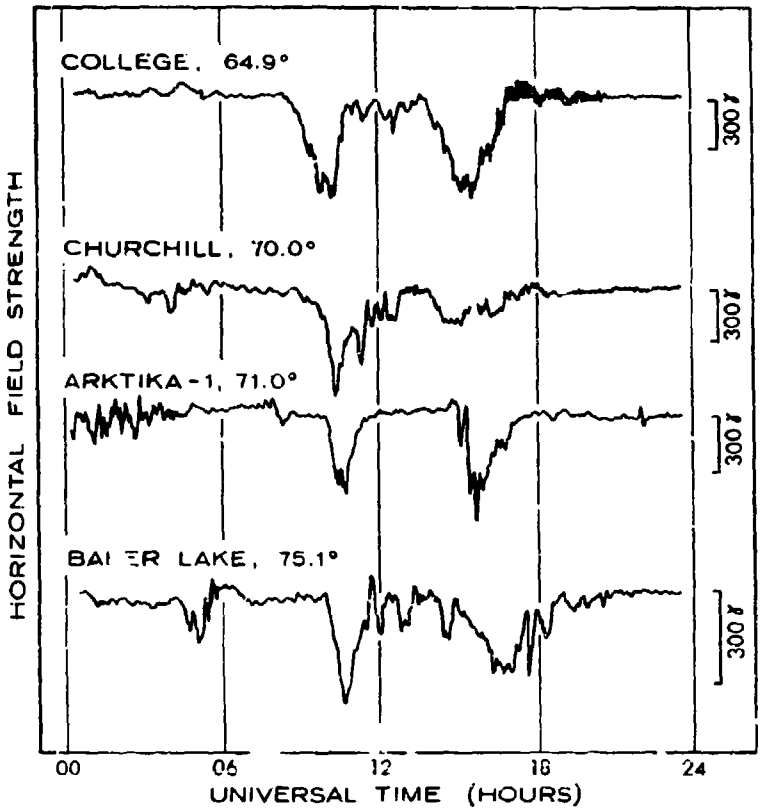

Figure 11-13. Magnetograms From Four Stations on 13th December 1957, Showing the Occurrence of Two Magnetic Substorms [selected and redrawn from 25 records collected by Zaytsev and Feldstein, 1967]

down into the late-morning and up out of the afternoon-evening auroral oval along closed field lines which lie near the trapping boundary. The concentratration of current in the oval, particularly in active auroras, results from enhanced conductivity; however, since conductivities are not negligible elsewhere, the current probably spreads over a rather broad belt, and currents across the polar cap are present.

The source of the electrojet current is now widely believed to be the assymetric component of the ring current responsible for the main phase. The ring current has been observed directly and appears to extend from below 3 R_e outward to the trapping boundary and the neutral sheet, the inner portion consisting of protons with energies above 100 keV and the outer portion consisting mainly of protons with energies of 50 keV or less. The growth and decay of the latter population during a

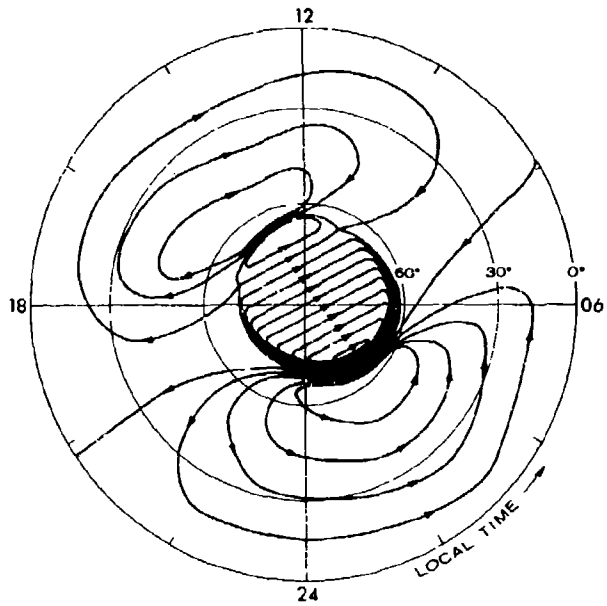

Figure 11-44. An Equivalent Current System Derived for an Average Polar Magnetic Substorm [redrawn after Silsbee ar ' Vestine, 1942]

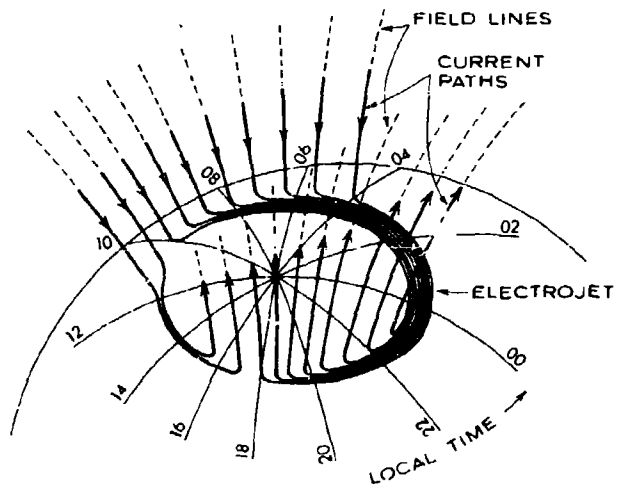

Figure 11-45. Sketch of a Simplified Probable Configuration for the Auroral-Electrojet Current System [drawn to be roughly consistent with Figure 11-44 and a description by Akasofu, 1968]

moderate storm is shown in Figure 11-46. The current develops asymmetrically, with an initial excess of protons within the afternoon-evening sector of the magnetosphere. It is likely that the electrojet system of Figure 11-45 is completed in a way resembling that shown in Figure 11-47; with each substorm, the electrojet closes the ring-current circuit for the excess particles until the ring current again becomes symmetrical with all current encircling the earth.

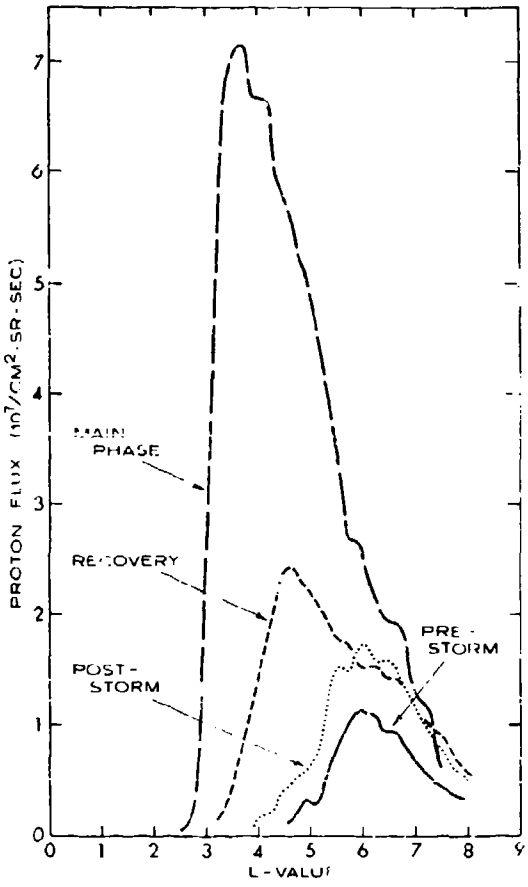

Figure 11-46. Directional Intensities of Ring-Current Protons (Energies Between and 49 keV) as a Function of Magnetic-Shell Parameter L During Several Phases of a Magnetic Storm in July 1966 [redrawn after Frank, 1967]

The origin of the ring-current protons and the mechanism by which energy from the solar plasma enters the magnetosphere are not yet understood. Direct rapid entry of solar plasma into the region of the ring current is prevented by the magnetic field. Moreover, the fast and explosive nature of substorms implies that energy must somehow be stored up within the magnetosphere and released abruptly;

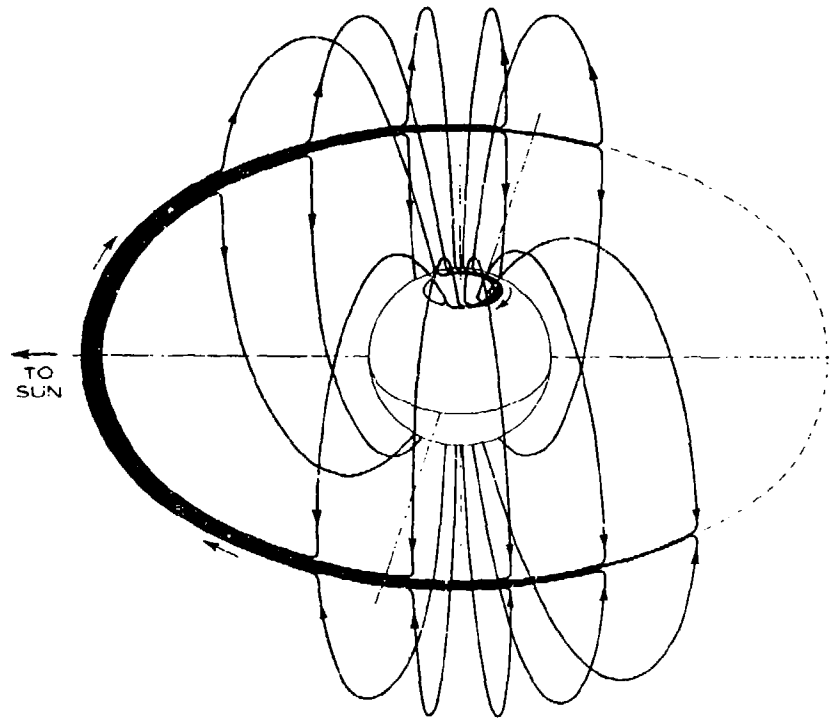

Figure 11-47. A Three-Dimensional Model of the Asymmetric-Ring-Current System During a Magnetospheric Substorm [redrawn after Akasofu and Meng, 1969]

therefore, the substorm is fundamentally a process internal to the magnetosphere. Too many (about a dozen) theories are under consideration to permit a useful comparison here. It may be noted, however, that they generally fall into two categories relative to the origin of the electric field which drives the currents; in the first it is thought to arise from the space charge associated with the asymmetry of the ring-current particles, while in the second it is thought to result from the convective motion of magnetospheric plasma.

Prior to the last decade it was commonly believed that all polar magnetic disturbance was of the type associated with the auroral electrojet. More recently, however, a second type has been discovered, distinguished from the first by its independence of the electrojet [Nishida and Kokubun, 1971]. An example is shown in Figure 11-48. The disturbance is not confined to the polar cap but is worldwide, coherent from polar to equatorial regions, as can be seen in the magnetograms at 83° and −1° latitude. (On the magnetogram from College, in the auroral zone, it is obscured by the larger electrojet disturbance.) Its time scale is typically an

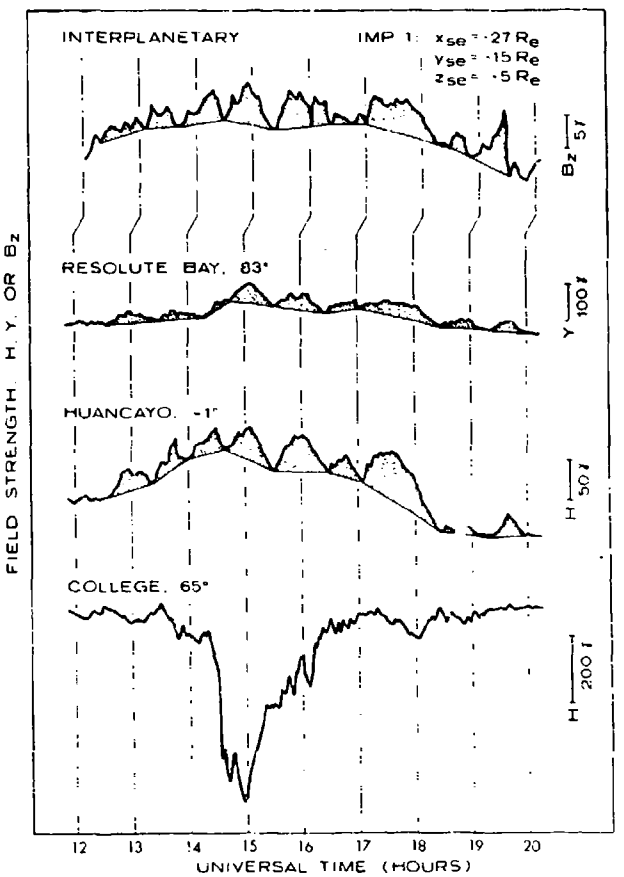

Figure 11-48. Example of DP2 Magnetic Disturbance, as Shown in Polar, Equatorial, and Auroral-Zone Magnetograms (2nd, 3rd, and 4th Traces, Respectively). The DP2 component is shaded where distinguishable. The first trace shows the southward (z_{se}) component of the interplanetary field, plotted with a time lag of 10 minutes [redrawn after Nishida, 1968]

hour or more, slower fluctuations being difficult to distinguish from the Sq variation. The general configuration of its equivalent current system is shown in Figure 11-49. Again, various investigators have defined the disturbance field in different ways and have obtained somewhat differing configurations; currently, these fields bear a variety of names (for example, DPC, DP2, D_p^e, Sq^p, SD^p, and SP), but they clearly all have much in common and cannot result from independent physical processes. It has been proposed [Obayashi, 1967], but not yet generally agreed, to call the disturbance field arising from the electrojet DP1 and to call

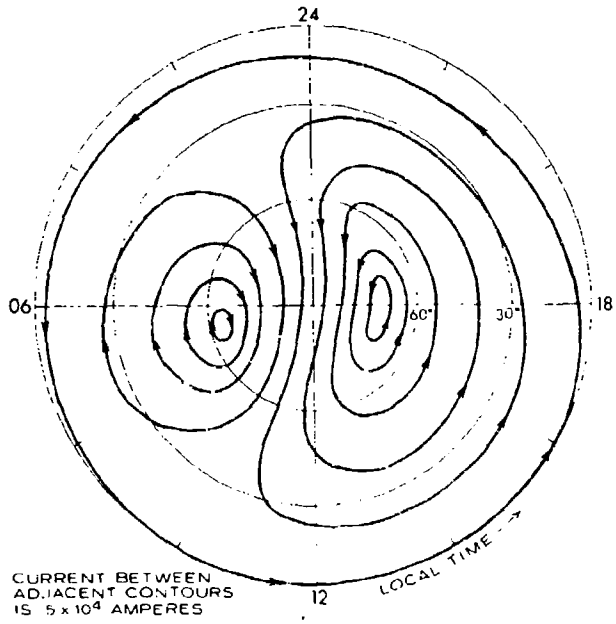

Figure 11-49. The Equivalent Current System Derived for DP2 Magnetic Disturbance [redrawn after Nishida, 1968]

the second type DP2. While it is possible that more independent modes may be found to exist, it appears that polar disturbances observed to date can be explaine ' by superposing DP1 and DP2 on the polar extension of known lower-attitude (particularly the Sq) current systems.

I P2 correlates strongly (a 10-minute delay, bow shock to ground) with the southward component of the interplanetary field but not with other parameters. The DP2 electric field is dawn-to-dusk in the ionosphere, consistent with a dawn-to-dusk field across the magnetosphere. These observations suggest that DP2, like DP1, results from a large-scale magnetospheric process, for example, field-line reconnection and magnetospheric convection (see Section 11.7.2). Although DP1 and DP2 can occur together, a correlation with the general level of activity is found. Both DP1 and DP2 are absent during quietest periods, DP2 is detected during slightly disturbed periods, and DP1 dominates during more disturbed periods. While the two types are clearly independent, in the sense that DP2 currents flow directly across the auroral oval to subauroral latitudes, both are similarly dependent on the condition of the interplanetary magnetic field, and it is very improbable that they have wholly independent causes. DP2 should probably be considered to be one more manifestation of the magnetic substorm.

11.6.4 Rapid Fluct ion

Micropulsations are rapid variatio..s of the surface magne ic field (periods from less than one to several hundred seconds) which are observed by ground-based magnetometers as a typ f geomagnetic disturbance. Similar variations are observed in the magnetosphere by satellite instruments. They are ultra-low-frequency (ULF) electromagnetic waves, and since their frequency is below the ion-gyro frequency of the magnetospheric plasma, they propagate as hydromagnetic waves. They are generated in the magnetosphere (and also the ionosphere) and travel to the surface of the earth through the plasma. Earlier classifications and common names for particular types of pulsations have largely been replaced by the new scheme given in Table 11-3. A rough indication of the natural micropulsation spectrum (averaged over spatial and temporal variations) is given in Figure 11-50, which shows a natural separation into several bands.

Table 11-3. Classification of Micropul ations

Type Sine	Description and range of period (in seconds)	Earlier classifications and common names included
Pc	Continuous 0.2 - 5	"Pearl" "pp" (Troitskaya) "Type A" (Benioff) "Type B" (Benioff)(part 1 - 2) "Hydromagnetic emission" (Tepley & Wentworth) "Sweeper" or "IPDP" (part Pc 1)
Pc 2	Continuous 5 - 10	"Type B" (Benioff)(part Pc 1)
Pc 3	Continuous 10 - 45	"Pc" "Pc-i" (Saito)
Pc 4	Continuous 45 - 150	"pc" or "giant" (but mostly Pc 5) "Pc" "Pc-ii" (Saito)
Pc 5	Continuous 150 - 600	"pc" or "giant" "I..." (Jacobs and Sinno) "Pc-iii" (Saito) "Pi" (Parouchev)
Pi 1	Irregular 1 - 40	"Si..." (Troitskaya) "Pulsation bursts" (Jacobs and Sinno) "Sweeper" or "IPDP" (intervals of pulsations diminishing by period)(Troitskaya)(part Pc 1)
Pi 2	Irregular 40 - 150	"Pi" (pulsation trains)

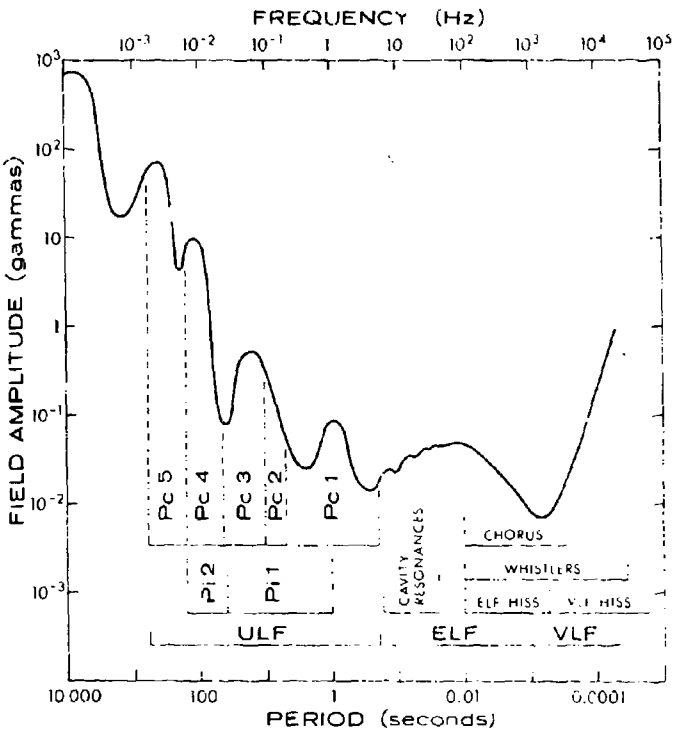

Figure 11-50. A Rough Indication of the Spatial-Temporal Average Spectrum of Observed Micropulsations [re drawn after Campbell, 1967]

At middle latitudes, Pi-2 pulsations predominate; however, these have their maximum amplitude in the auroral zone and are observed most frequently at about 2200 hours local time. They occur during the early phase of polar magnetic substorms, and their period becomes shorter as the general level of the disturbance increases. At high latitudes, pulsations have more complicated characteristics. Various types are observed in association with auroral substorms, electron precipitation, X-ray bursts, and other disturbance phenomena, often being seen mainly within certain ranges of local time. Most Pc-1 pulsations appear to originate at the plasmapause in association with an observed spatial fine structure in the proton density distribution [Kikuchi and Taylor, 1972]. Most Pc-3 pulsations are probably generated by oscillations of the dayside magnetopause [Heppner et al, 1970]. Pc-4 and Pc-5 pulsations may result from particle injection into (or instabilities of) the main-phase ring current of magnetic storms [Barfield et al, 1972]. Explanations

for some other types have also been advanced. In general, however, the origin of micropulsations is still poorly understood, and a detailed discussion is beyond the scope of this review. Useful reviews have been given by Campbell [1967] and Akasofu [1968]. Magnetic-field oscillations at higher frequencies (ELF and VLF) are also observed on the ground and (more recently) in the magnetosphere, as noted in Figure 11-50. Cavity resonances result from lightning discharges which resonate in the spherical waveguide formed by the ionosphere; therefore, they are not observed throughout the magnetosphere. A whistler is a noise burst from a lightning stroke which does propagate through the magnetosphere. VLF hiss (also called "auroral hiss") is unstructured noise believed to result from plasma oscillations or Cerenkov radiation from patricle precipitation. Chorus and ELF hiss are structured and unstructured noise, respectively, which appear to result from local instabilities of the magnetospheric plasma near the equator. Satellite measurements of ELF and VLF fields have been reviewed by Russell, et al [1972] part of whose tabulation is reproduced in Table 11-14 of Section 11.8.4.

11.6.5 Ionospheric Disturbance

Ionospheric disturbance is a departure of the ionosphere from its normal condition; an ionospheric substorm is the ionospheric manifestation of a magnetosperic substorm. Enhanced ionization is usually detected by the riometer (for relative ionospheric opacity meter), a standard ground-based instrument which monitors the ionospheric absorption of galactic radio noise.

The involvement of the ionosphere in some types of magnetic disturbance has already been noted in the foregoing discussion. The disturbance produced in auroral-magnetic substorms is called auroral absorption and occurs in the D region. Auroras also cause the so-called auroral sporadic E, an enhanced E-region ionization which is concentrated, probably by a wind-shear phenomenon, into very thin layers. Brief enhancements of the D region in the auroral zone at all local times are also produced by sudden commencements through the precipitation of energetic electrons. Decreases in F-region ionization called F-region storms accompany geomagnetic storms, displaying both storm-time and local-time variations corresponding to the Dst and DS magnetic fields; as possible explanations, atmospheric heating with redistribution of electrons, redistribution of oxygen to affect charge-exchange reaction rates, and redistribution of ionization by electric fields have been proposed.

Two types of ionospheric disturbance produce a measurable magnetic disturbance but are associated not with magnetospheric storms but with solar flares. Polar-cap absorption (PCA) results from an increased ionization produced by the bombardment of the polar-cap atmosphere by solar-flare protons which typically have energies between one and tens of MeV. The enhancement usually begins a few

hours after the flare and lasts for several days, the persistence apparently resulting from the storage of protons in interplanetary space after the flare is over. Sudden ionospheric disturbance (SID, also called short-wave fadeouts) and solar flare effects (SFE, also called crochets) are, respectively, the ionospheric and magnetic disturbances produced by solar-flare X rays of energy greater than 1 keV. The enhanced ionization is produced over all of the dayside (illuminated) ionosphere, predominantly in the D region. (Less energetic X rays produce a smaller E-region enhancement.) The disturbances are prompt, coincident in time with flares, and typically last for about an hour. As shown in Figure 11-51, the disturbance and its equivalent current system are confined to the sunlit region.

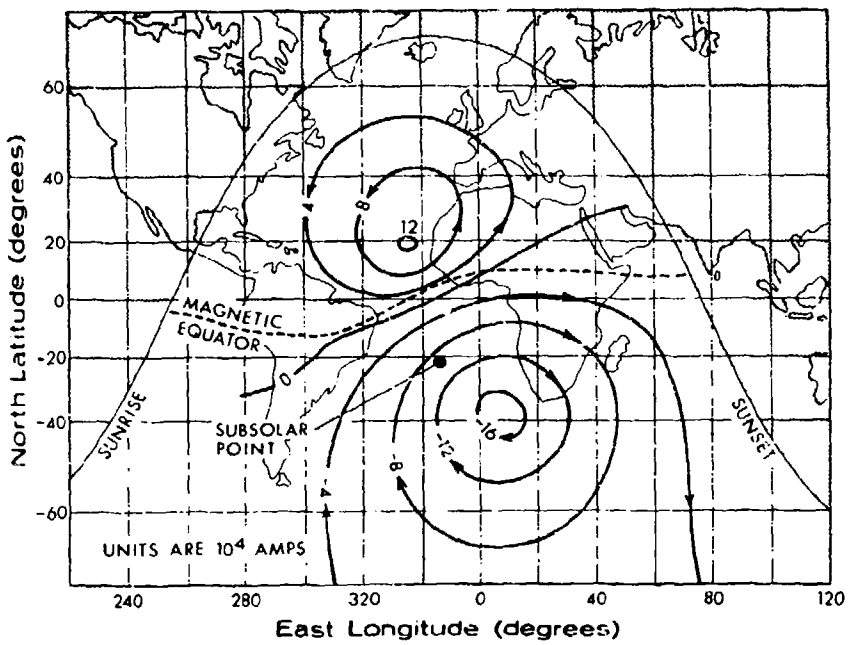

Figure 11-51. The Ionospheric Current System of a Solar-Flare Effect Occurring Near Winter Solstice (12th December 1958). For an SFE on 29th July 1958, the northern vortex was much more intense than the southern [redrawn after van Sabben, 1961]

11.6.6 Activity Indices and Charts

For correlating phenomena in related geophysical fields, the magnetograms and averaged data supplied by magnetic observatories are usually too detailed, and it has been found useful to compute some numerical parameters which indicate the level of general magnetic activity or specific types of disturbance. Various activity indices have been used; as understanding has increased and specific types of

activity have been distinguished, new indices designed to be a measure of these have been defined and adopted. A brief description follows for those ind ces which are currently in wide use or are important historically. Figure 11-52 helps illustrate the derivation of and relationships between a number of the indices. A more detailed review has been given by Lincoln [1967].

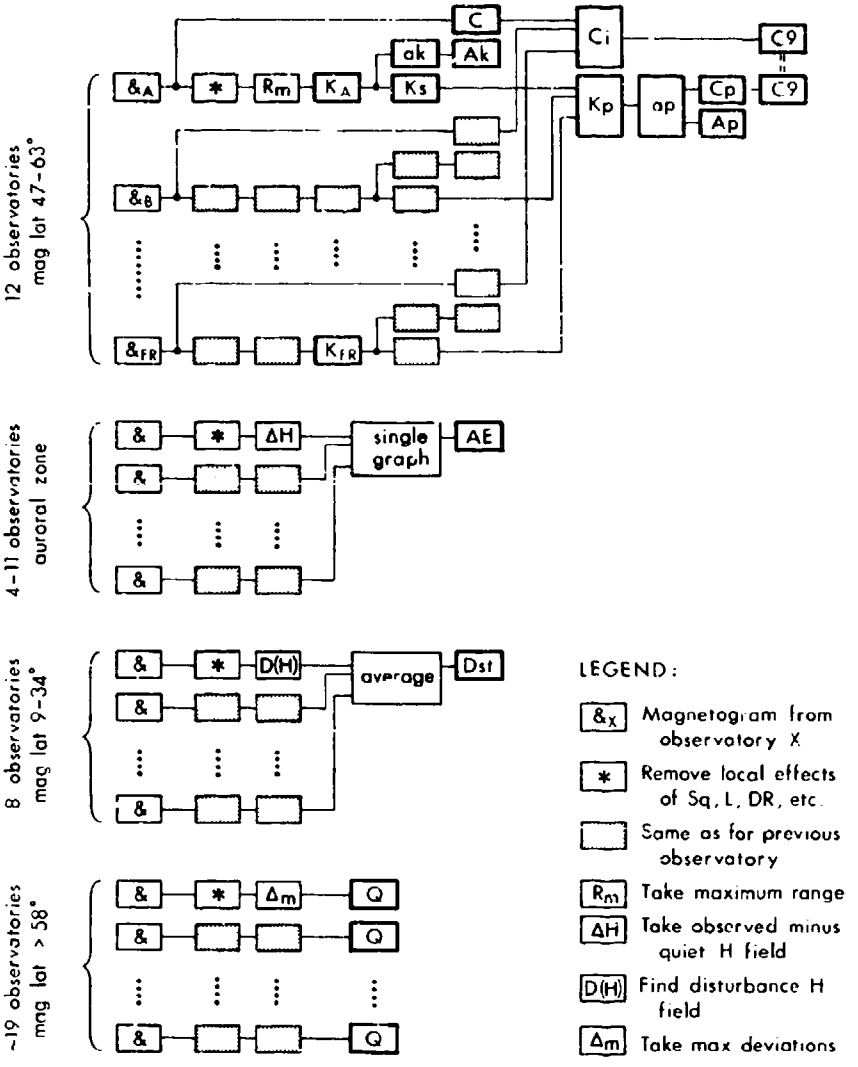

Figure 11-52. Summary of the Derivation of and Relationships Between a Number of Activity Indices

The K index (adopted 1939) is a measure of the irregular variations of standard magnetograms and is used as an indicator of the general level of magnetic activity caused by the solar wind. Each observatory computes a value of K for each 3-hour interval from the largest 3-hour range R in X, Y, D, or H, where R is the difference between the highest and lowest deviations from the regular daily variation. Since observatories in or near the auroral zone record much larger variations than others, the correspondence between K and R is adjusted for each observatory to permit comparison of K values from different stations. A two-letter subscript (for example, K_{SI} for Sitka) is used to identify the station. K values are integers ranging from 0 through 9; the calibration for six representative stations is given in Table 11-4; the K scale was originally based on data from Niemegk (52° 04'N, 12° 40'E) which has the same calibration as Fredericksburg. It may be noted that the K scale is quasi-logarithmic. The K index from Fredericksburg, Virginia, (K_{FR}) has been taken as a standard measure of geomagnetic activity for the United States.

Table 11-4. Definition of the K Scale for Several Representative Observatories

Name of Observatory	Geomagnetic Lat.	Long.	Lower limit of R (in gammas) for K value to be 0	1	2	3	4	5	6	7	8	9
Godhavn	79.9	32.5	0	15	30	60	120	210	360	600	1000	1500
Sitka	60.0	275.3	0	10	20	40	80	140	240	400	660	1000
Huancayo	-0.6	353.8	0	6	12	24	48	85	145	240	400	600
Fredericksburg	49.6	349.8	0	5	10	20	40	70	120	200	330	500
Tucson	40.4	312.2	0	4	8	16	30	50	85	140	230	350
Honolulu	21.1	266.5	0	3	6	12	24	40	70	120	200	300

The Kp index ("p" for "planetary") was intended to measure the worldwide average level of activity and is currently much used. In fact, however, its correlation with solar-wind parameters and specific types of magnetic activity vary widely; it is often a good measure of certain auroral-zone activity but a poorer measure of polar-cap disturbance. It is based on the K indices from twelve selected stations between geomagnetic latitudes 48° and 63°. Values of K are first used to compute the Ks index ("s" for "standardized"), from tables which reflect the characteristic seasonal behavior at the station and thereby remove local variations. The Ks index ranges continuously from 0.0 to 9.0 but is quoted in thirds of

an integer, using the three symbols, -, o, and +, as follows. The interval from 3.5 to 4.5 includes the Ks values 4−, 4o, and 4+, and other intervals are correspondingly defined, so Ks can assume 28 values: 0o, 0+, 1−, 1o, . . . 8+, 9−, and 9o. The Kp value for each 3-hour interval is the average of Ks from the 12 stations.

To compare activity in the northern and southern hemispheres, three additional indices, Kn (northern), Ks (southern; confusion with the standardized Ks must be avoided by context), and Km (mean; normally about equal to Kp) have been defined on the basis of separate data from the two hemispheres [Mayaud, 1968]. They are not widely used.

Because the 3-hour K, Ks, and Kp indices are defined with a quasi-logarithmic scale, they are not suitable for simple averaging to obtain a daily index. (Still, this is not uncommonly done, in spite of the illogic.) To convert to a roughly linear scale (that is, reconversion to an equivalent range), the ak index is defined from K and the ap index from Kp as indicated in Table 11-5. The average value of ak or ap over the eight 3-hour intervals in a day is then defined to be the daily Ak index or Ap index, respectively (single-station or planetary).

Table 11-5. Equivalent Ranges ak and ap for Given Values of K and Kp

If	K=	0	1	2	3	4	5	6	7	8	9				
then	ak=	0	3	7	15	27	48	80	140	240	400				
If	Kp=	0o	0+	1-	1o	1+	2-	2o	2+	3-	3o	3+	4-	4o	4+
then	ap=	0	2	3	4	5	6	7	9	12	15	18	22	27	32
If	Kp=	5-	5o	5+	6-	6o	6+	7-	7o	7+	8-	8o	8+	9-	9o
then	ap=	39	48	56	67	80	94	111	132	154	179	207	236	300	400

The ak and Ak indices are often quoted in units of gammas (range of field strength) by multiplying by a calibration factor f for the particular station, given by $f = R_9/250$, where R_9 is the lower limit of R for K=9. Thus, at Fredericksburg, f = (500 gammas)/250 = 2 gammas. As an example, if R = 27, then K = 3, and ak = 15, or ak = 15 × 2 gammas = 30 gammas. Begun in 1951, the indices ak, Ak, ap, and Ap are currently in wide use.

The Cp index, called the daily planetary character figure, is a number ranging continuously from 0.0 to 2.5, quoted to tenths of an integer. It is found, using Table 11-6, from the daily sum Σap (that is, the sum of the eight 3-hour values of

ap) used to compute Ap (Ap = Σap/8). It restores the quasi-logarithmic relationship originally introduced by the Kp scale and later removed by the ap scale. The peculiarity of its scale results from the intention that it replace, yet be equivalent to, a valuable older index, the Ci index, called the international daily character figure, which is available for all days since 1884; while Cp is more reliable and objective than Ci, they usually differ by less than 0.2. For each Greenwich day, the Ci index is the arithmetic mean of C index values from a number of observatories; at each observatory, the C index, called the daily magnetic character index, is reported as 0, 1, or 2 according to whether the UT day is quiet, moderately disturbed, or highly disturbed, respectively.

Table 11-6. Scale for Finding Cp From the Daily Sum of ap. For each Cp interval, the value listed is the upper limit of the daily-sum values included in the interval

If Σap<	22	34	44	55	66	78	90	104	120	139	164	190	228
then Cp=	0.0	0.1	0.2	0.3	0.4	0.5	0.6	0.7	0.8	0.9	1.0	1.1	1.2
If Σap<	273	320	379	453	561	729	1119	1399	1699	1999	2399	3199	---
then Cp=	1.3	1.4	1.5	1.6	1.7	1.8	1.9	2.0	2.1	2.2	2.3	2.4	2.5

The C9 index is sometimes used, especially for graphing, in place of Cp or Ci; it is found from either according to the scale given in Table 11-7, which converts from the 0.0-to-2.5 scale to the more familiar single-digit 0-to-9 scale.

Table 11-7. Scale for Finding C9 From Cp or Ci

If Cp or Ci=		0.0 0.1	0.2 0.3	0.4 0.5	0.6 0.7	0.8 0.9	1.0 1.1	1.2 1.3 1.4	1.5 1.6 1.7 1.8	1.9	2.0 2.1 2.2 2.3 2.4 2.5
then	C9=	0	1	2	3	4	5	6	7	8	9

Several newer indices now in use provide better time resolution than those based on the 3-hour K index, but their availability is more limited. The Q index is

a measure of high-latitude magnetic activity for each 15-minute interval; it is assigned by a number of observatories above 58° geomagnetic latitude. It is computed, from the more disturbed of the elements X and Y, as the sum S of the absolute values of the maximum positive and maximum negative deviations from the normal (quiet) curve, with the provision that if the "negative" (or "positive") deviation does not indeed become negative (or positive) it is considered to be zero. The conversion scale for obtaining Q from S, applicable to all stations, is given in Table 11-8.

Table 11-8. Scale for Finding Q From S. Listed values of S (in gammas) are the upper limits for the corresponding values of Q

If S<	10	20	40	80	140	240	400	660	1000	1500	2000	∞
then Q=	0	1	2	3	4	5	6	7	8	9	10	11

The AE index, called the auroral electrojet activity index, is derived from data of a number of auroral-zone stations distributed in longitude. It is intended to measure the strength of the auroral electrojet. It is tabulated for hourly and (to some extent) 2.5-minute intervals. Obtained graphically from a single combined plot of the deviations, at all stations, of the element H from its normal quiet-time value, AE is the height of the envelope (that is, the difference) between the curves AU and AL (for "upper" and "lower") drawn through the maximum and minimum excursions of the deviation, respectively. Another index, called A o is the mean deviation, defined by the curve midway between AU and AL.

The Dst index is the magnitude of the (normalized) horizontal component of the Dst field, as determined from the data obtained by a number of low-latitude observatories well distributed in longitude. The Dst index is designed as a measure of the magnetospheric ring current of magnetic storms; therefore, high-latitude and equatorial stations are avoided to minimize the effects of auroral and equatorial electrojets.

Several older indices are seldom used, either because newer indices are more useful or for other reasons. The indices U, u, u_1, and Δ are all derived from the difference between consecutive daily means of some element of the field. The U figure is the absolute magnitude of the difference between the daily means of the horizontal component for the given and preceding days. The u figure is a reduction of U to an equivalent equatorial value by the relation $u = U/(\sin \theta_m \cos \psi)$, where θ_m is geomagnetic colatitude and ψ is the angle between H and the magnetic

meridian. The u_1 figure is obtained from u by the nonlinear conversion given in Table 11-9; the scale is intended to reduce the influence of large disturbances. The indices U, u and u_1 have been useful historically for monthly and annual changes, but since they were intended to measure ring-current effects the Dst index has largely superseded them. The Λ indices described by Chernosky [1956] have not been widely used.

Table 11-9. Scale for Finding u_1 From u. Listed values are points on a continuous curve which may be plotted for interpolation

If u=	0.3	0.5	0.7	0.9	1.2	1.5	1.8	2.1	2.7	3.6
then u_1=	0	20	40	57	79	96	108	118	132	140

The W measure applies to quiet variation fields rather than disturbance phenomena, being derived from the amplitude of the Sq variation; it is a measure of solar radiation effects and the intensity of the equatorial electrojet (see Bartels [1946]).

Several graphical presentations of activity indices have been widely used. Figure 11-53 shows an example of the musical-note diagram originated by Bartels, which is a plot against time of the 3-hour Kp values, grouped by successive solar rotations to expose 27-day recurrences of activity. Figure 11-54 shows a similar plot of the C9 index (including also the sunspot number R9).

Recently, to encourage interdisciplinary analyses of solar-terrestrial activity, a project was commenced to produce a series of Solar-Terrestrial Activity Charts (STAC) of three types: yearly (STAC-A), 27-day (STAC-B), and special-event (STAC-C). Examples are shown in Figure 11-55, which is the preliminary yearly chart for 1968, and Figure 11-56, which is the 27-day chart for solar rotation 1839. For a detailed explanation of the quantities plotted, refer to STP Notes, Nos. 7, 8 and 9 as listed in Section 11.8.9.

As understanding of disturbance phenomena improves, new indices will no doubt prove useful; for example, Saito [1964] and others believe that an index of Pc-3 pulsations would serve as a good indicator of activity taking place on the dayside magnetopause.

A listing of principal sources for all of the indices and charts described above is provided in Section 11.8.9. Current availability and alternative sources may be determined by enquiry to those listed.

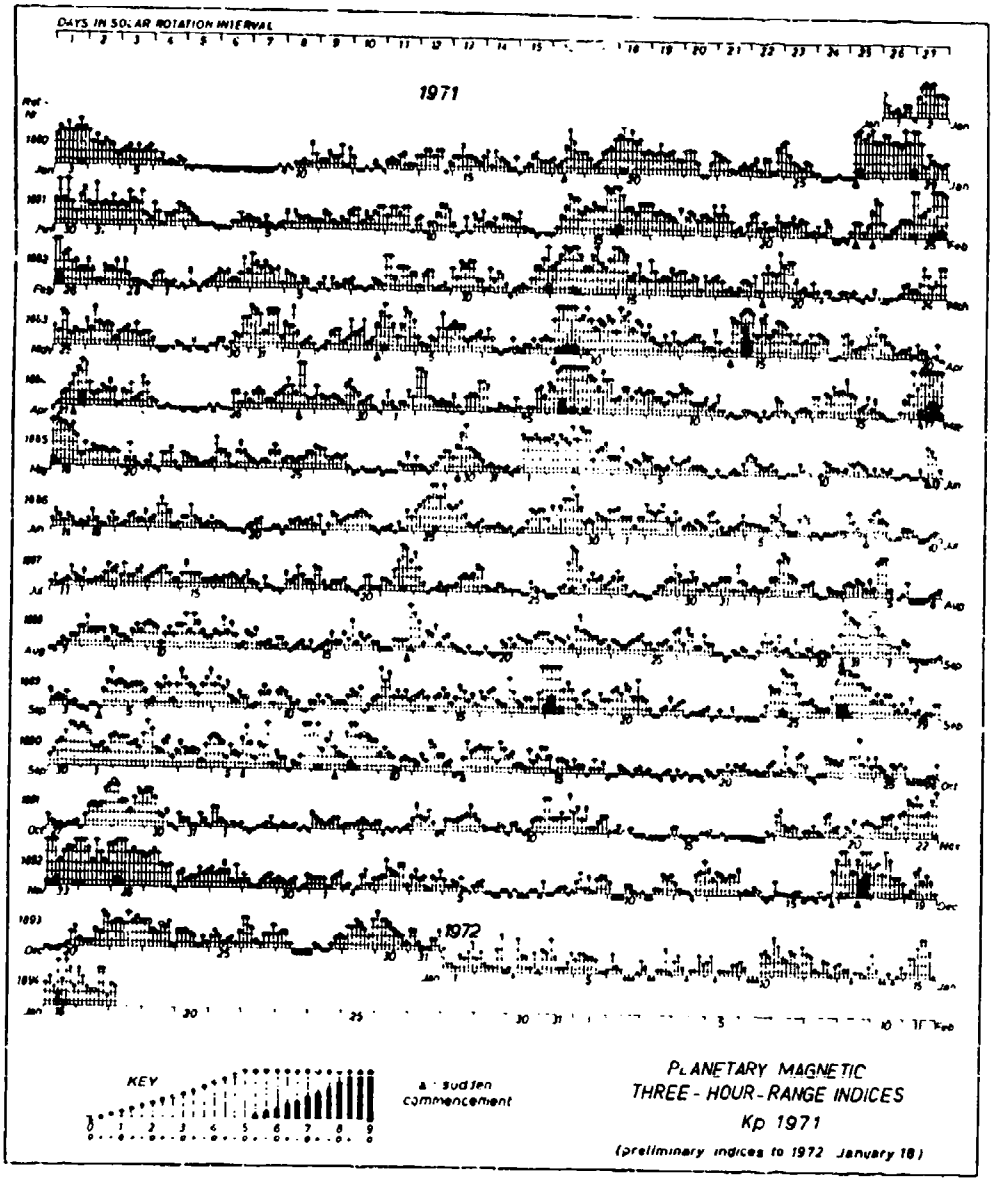

Figure 11-53. Musical-Note Diagram of Kp Values for the Year 1971 [provided by Prof. Manfred Siebert, International Service of Geomagnetic Indices, Göttingen]

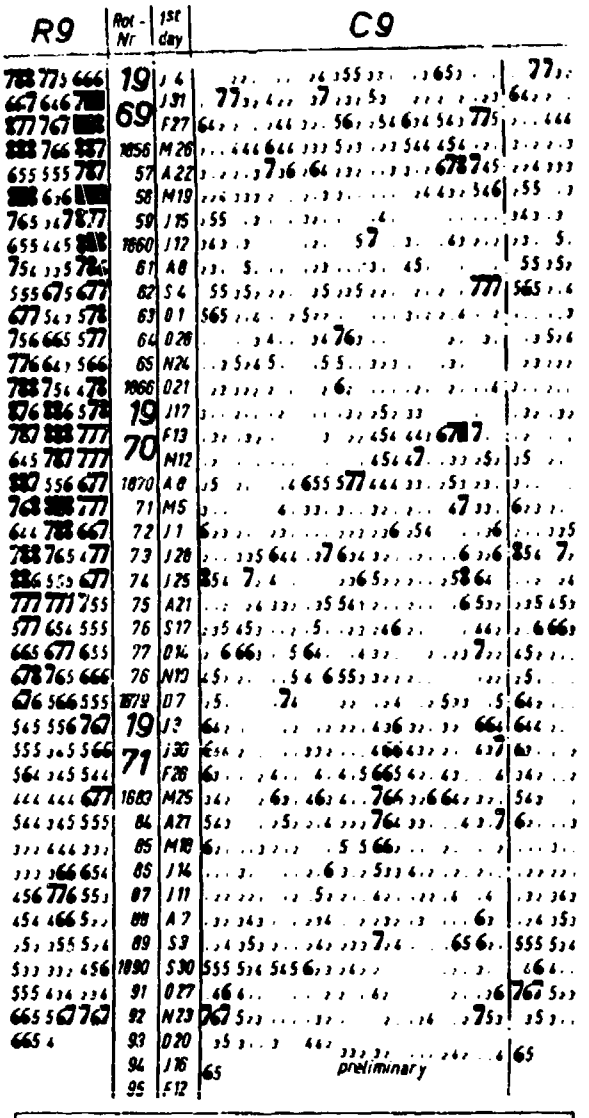

Figure 11-54. Plot of the C9 Index and Sunspot Number R9 for the Year 1971 [provided by Prof. Manfred Siebert, International Service of Geomagnetic Indices, Göttingen]

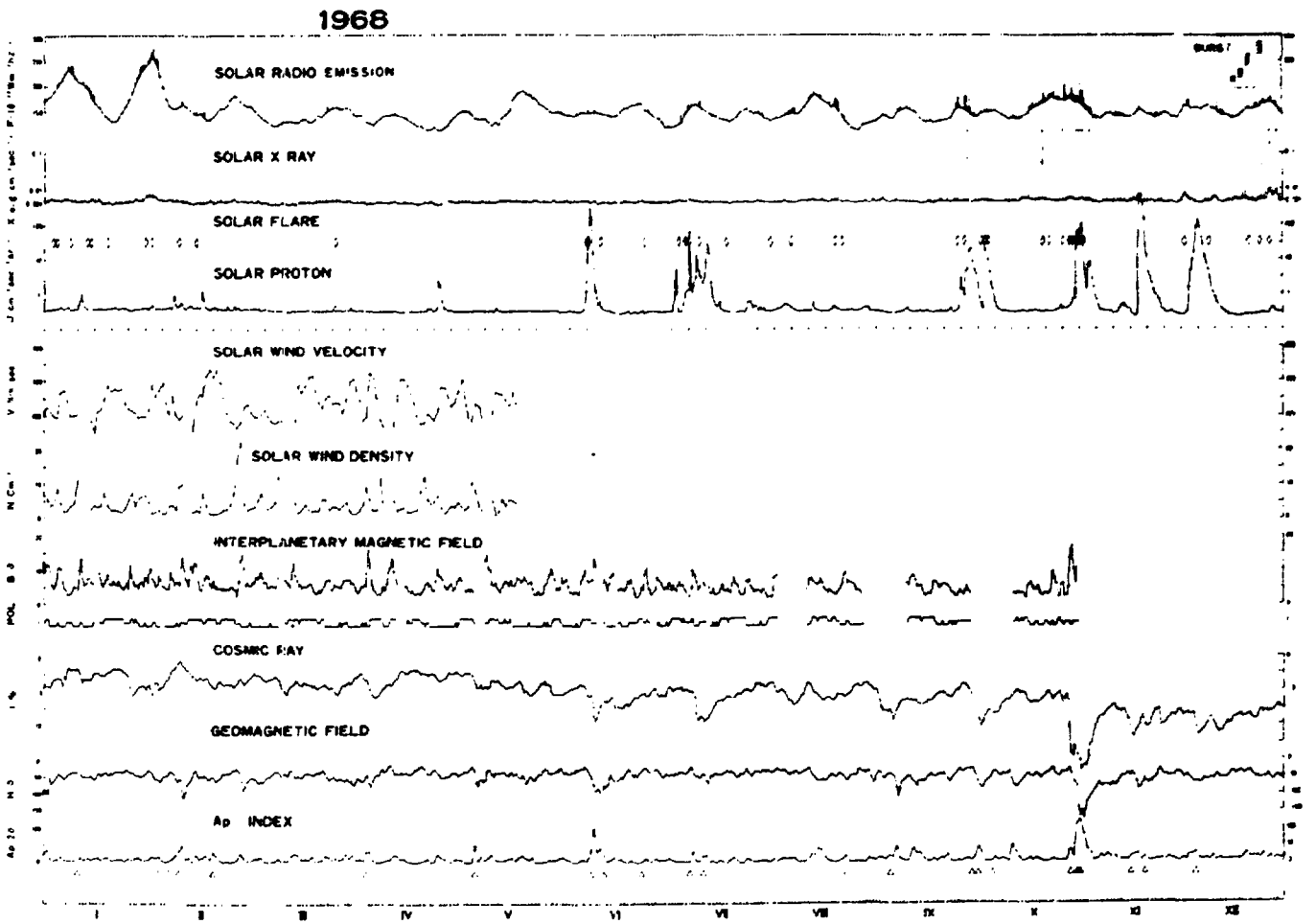

Figure 11-55. Solar-Terrestrial Activity Chart (STAC-A, Yearly) for the Year 1968 [prepared by the Interdisciplinary Analysis Center for Solar-Terrestrial Activity (Prof. T. Obayashi, Science Council of Japan, Tokyo)]

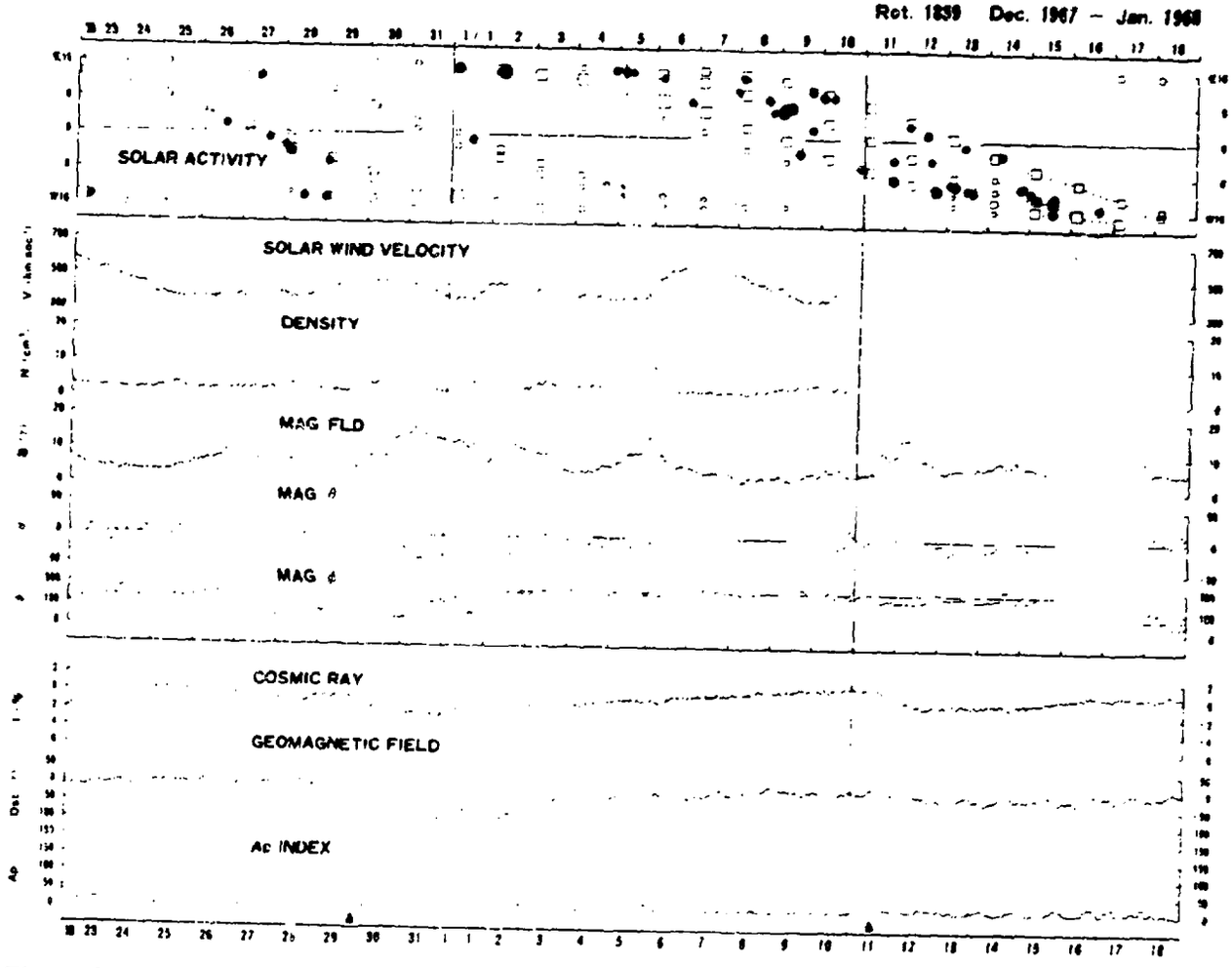

Figure 11-56. Solar-Terrestrial Activity Chart (STAC-B, 27-day) for Solar Rotation 1839 [prepared by the Interdisciplinary Analysis Center for Solar-Terrestrial Activity (Prof. T. Obayashi, Science Council of Japan, Tokyo)]

11.7 DYNAMICS OF THE OUTER MAGNETOSPHERE

An understanding of the configuration and dynamic processes of the outer magnetosphere is clearly essential to explaining the disturbance phenomena discussed above. In particular, the explosive onset of substorms with the rapid release of large amounts of energy implies a basically internal process with the storage of solar-wind energy within the magnetosphere, probably in the magnetic tail. Many processes have been explored theoretically, and some are believed, in fact, to occur, though at present no theory is satisfactorily consistent with all observations. The more important of these processes are noted here, along with a more detailed description of the magnetic field configuration.

11.7.1 Configuration of the Magnetosphere

The near-earth configuration of the magnetosphere is shown in Figure 11-4 and 11-57, the latter showing schematically (only roughly to scale) the separation of polar-cap field lines which form the geomagnetic tail from closed dipole-like field lines which enclose the trapping region. The neutral sheet in the tail (across which the field reverses) has a thickness of less than 1 R_e while the plasma sheet surrounding it is about 5 R_e thick at the center and about 10 R_e thick near the magnetopause. Beyond about 20 R_e, the size of the tail is roughly constant, the dimension in the plane of the neutral sheet (about 40 R_e) being less than the dimension perpendicular to it (about 60 R_e). It is now generally agreed that the tail has an "open" rather than a "closed" configuration; that is, most (or all) field lines in the tail are

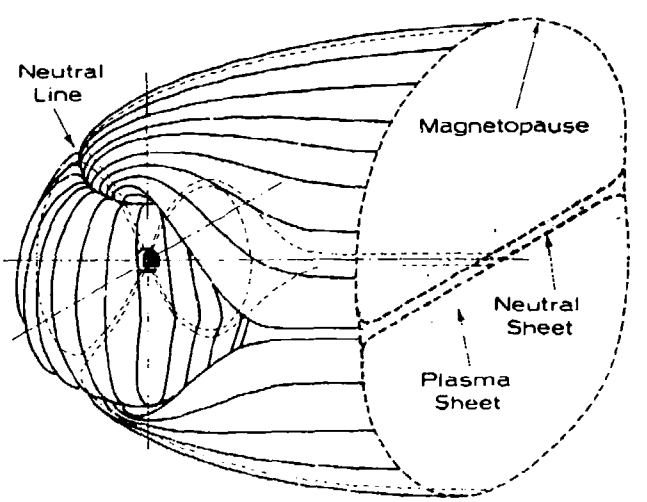

Figure 11-57. Sketch of the Configuration of Field Lines Near the Magnetopause and a Cross-Section of the Geomagnetic Tail

connected to the interplanetary field. The shape is well defined to a radial distance of at least 80 R_e, but it appears to break up into filaments before it reaches 500 R_e. The magnitude of the tail field is about 16 gammas at 20 R_e, but about half that at 80 R_e. During the main phase of a storm, the field may double, partly because equatorward expansion of the polar cap adds flux to the tail and partly because the tail is compressed. The tilt of the dipole axis causes the actual field-line configuration to be considerably skewed from the symmetric one shown in previous figures. Figure 11-58 shows the distortion inferred from satellite observations. Details of the field in the neutral sheet and magnetopause are discussed below.

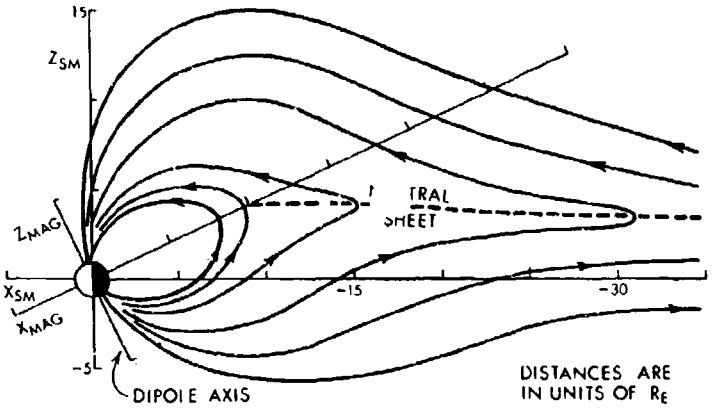

Figure 11-58. Distortion of the Geomagnetic Tail by the Tilt of the Dipole Axis Relative to the Solar Wind [adapted after Speiser and Ness, 1967]

11.7.2 Reconnection and Convection of Field Lines

By convection is meant the motion of field lines apart from that which they would have if they remained rooted to the surface of the earth. It is a useful concept both because it affords a convenient way to visualize the physical picture and because it reduces the number of variables in the magnetohydrodynamic equations which describe theoretical models. Of course, it is meaningless to speak of field lines moving if they are indistinguishable, as in a vacuum. However, in the magnetosphere, a field line may be identified by the particles associated with it, and the concept of convection essentially involves a transformation in which the field line is considered to move with the bulk flow of the plasma. The alternative mathematically equivalent viewpoint is that plasma drifts across a stationary mag-

netic field, driven by an electric field. The transformation, therefore, is to a moving coordinate system in which the electric field disappears. Field lines at the surface of the earth are frozen into the interior and remain stationary, while field lines in the conductive magnetosphere are frozen into the magnetospheric plasma and convect; surface and magnetospheric lines disconnect and slip (interchange) relative to each other in the atmosphere, which is a very good insulator. The electric field associated with the convection may be detected by a stationary observer in the atmosphere.

Convection occurs throughout all of the magnetosphere, with the exception of a small volume near the earth. The plasmapause, shown in Figure 11-59, is believed (at least approximately) to be the surface which separates the convecting and (except for the bulge) nonconvecting regions. It typically lies on subauroral field lines originating at about 60° geomagnetic latitude. Field lines within it remain closed and plasma is contained; field lines outside it are eventually convected into the tail, their feet within the polar cap, and plasma escapes. Current experimental results indicate, however, that it is a multilayered and variable boundary, and dynamic processes are not excluded from its interior. The convective motion must be

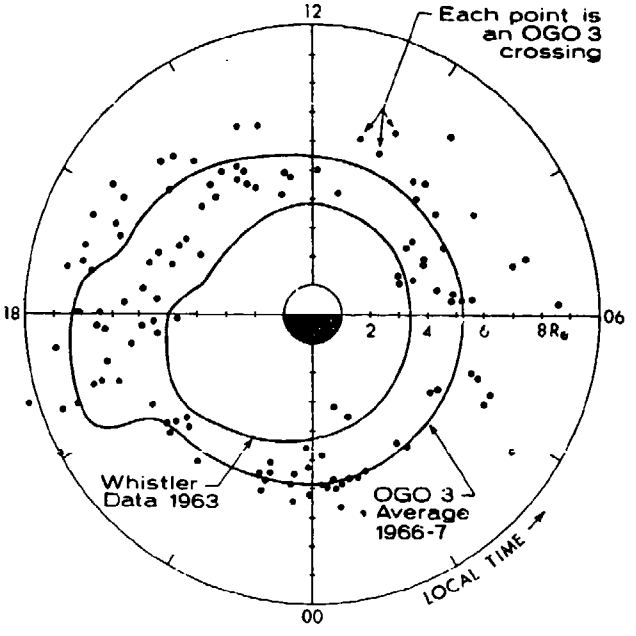

Figure 11-59. The Average Location of the Plasmapause in the Equatorial Plane, as Originally Determined From Whistler Data in July-August 1963 and as Observed by the OGO 3 Spacecraft in 1966-1967 [redrawn after Carpenter, 1966, and Kikuchi and Taylor, 1972]

driven by the solar wind through a tangential force on the magnetopause. It is now widely agreed that this force is magnetic and arises from field-line reconnection (also called merging or annihilation), that is, a process in which interplanetary field lines sweeping past the earth become connected to lines originating at the surface of the earth and pull them along with the solar wind. Thus, on the nose and equatorial flanks of the magnetosphere, closed field lines are pulled back into the tail, while over the poles field lines are drawn across the polar cap in a roughly antisolar direction. Superimposed on this motio. is that due to the rotation of the earth, since, in the atmosphere, field lines are not completely unconstrained but are, to some extent, tied to the surface. The strength and variation of such field-line tying may be a major controlling factor in the convection process. In a very rough schematic way, Figure 11-60 indicates a possible convection pattern; in successive panels are shown the field-line motion due to (a) rotation alone, (b) the tangential force of the solar wind, and (c) the composite of the two. The actual con-

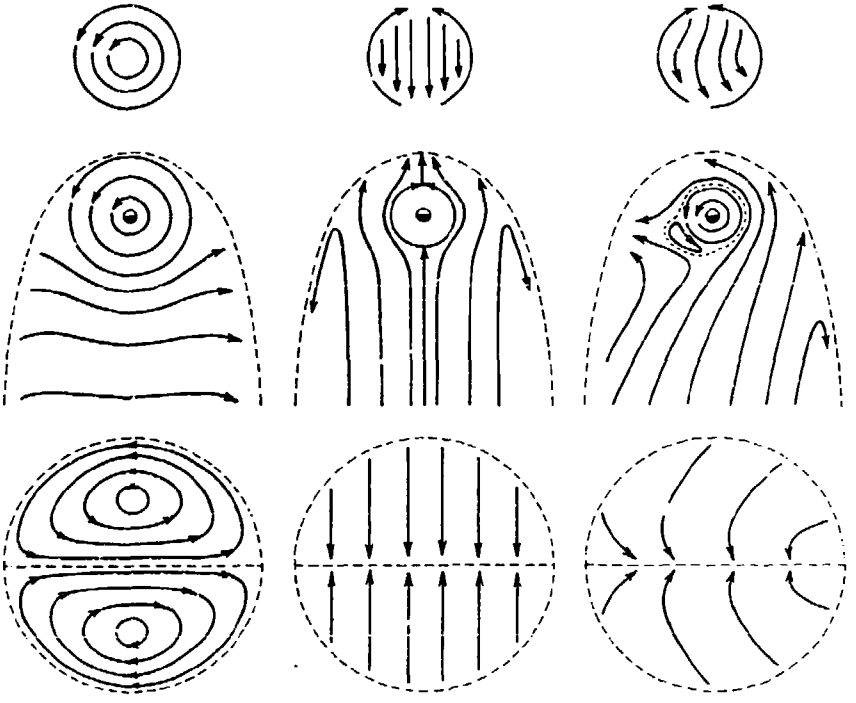

Figure 11-60. Convection Pattern in the Magnetosphere Expected From (Left to Right) Rotation of the Earth, Tangential Forces at the Magnetopause, and the Composite of These Two. Patterns are shown for (top to bottom) the polar cap (viewed from the north), the equatorial plane (viewed from the north), and a cross-section of the tail (viewed from the sun)

vection pattern is not yet known in detail and may prove to be considerably different, but it is likely to bear a general resemblance to that sketched. The occurrence of convection implies the existence of the electric fields, ionospheric currents, and contributions to the surface magnetic field which were discussed in preceding sections. Observations of these are roughly consistent with the postulated convection but are currently inadequate to yield a detailed and unambiguous picture of the convection process.

In the vicinity of the earth, the direction and magnitude of the interplanetary field are highly variable. The field in the ecliptic plane has a spiral configuration and is typically divided into sectors around the sun in which the field is alternately inward and outward; the component perpendicular to the ecliptic may be southward or northward. Therefore, the rate, location, and configuration of reconnection at the magnetopause is variable and asymmetric. In Figure 11-61, the earth is shown in a sector where the interplanetary field is outward with a southward component. Reconnection is occurring somewhere on the dayside part of the magnetopause. The field line labeled A may be thought to have reconnected near the subsolar point and been swept back to the configuration shown; field lines B and B' are about to reconnect and be swept around the magnetosphere. The direct entry of solar plasma and energetic particles into the tail is afforded by lines such as that labeled C; the curvature of such field lines becomes low enough for energetic particles to enter

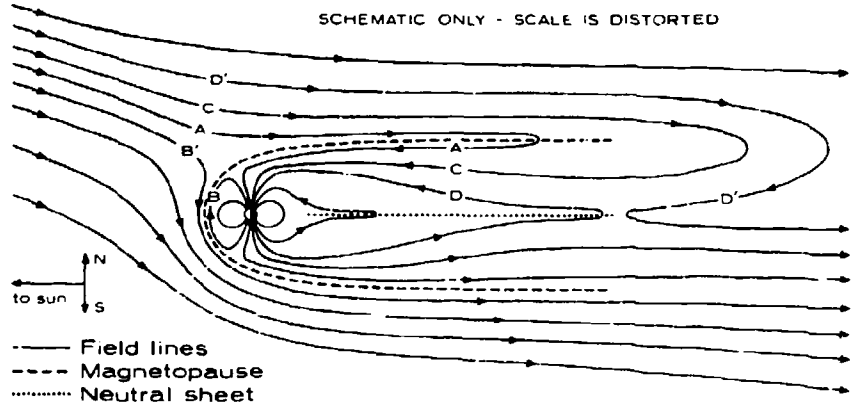

Figure 11-61. Reconnection of Magnetospheric and Interplanetary Field Lines, Shown Schematically (Not to Scale) for the Earth in a Sector of the Interplanetary Field Which is Outward With a Southward Component

without being scattered magnetically only after they have been swept well back into the tail (for example, more than 60 R_e for 20-keV electrons). Since the magnetic flux in the tail must, on the average, remain constant, reconnection at the magnetopause must be equaled by reconnection (disconnection) at the neutral sheet. That is, a closed field line (a line with both ends originating at the earth) which has become two open lines by reconnection to interplanetary lines at the magnetopause, must become closed again by reconnection of the two ends (disconnection from the interplanetary lines) at the neutral sheet. Field line D has just become closed, having disconnected from interplanetary line D'. The location at which this occurs is believed to be a neutral line in the neutral sheet; at other points in the neutral sheet the field should be very weak and directed northward or southward depending on whether it is earthward or more distant from the earth, respectively, than the neutral line. However, some observations conflict with the latter expectation, suggesting that other neutral lines may be generated by local concentrations of the neutral-sheet current into a series of filaments [Schindler and Ness, 1972]. The resulting field configuration internal to the neutral sheet may resemble that shown in Figure 11-62.

It is not known whether convection is more or less continuous or whether its rate fluctuates greatly. Moreover, over short periods of time, the rate at which flux is added to the tail by dayside reconnection may not be equaled by the rate of

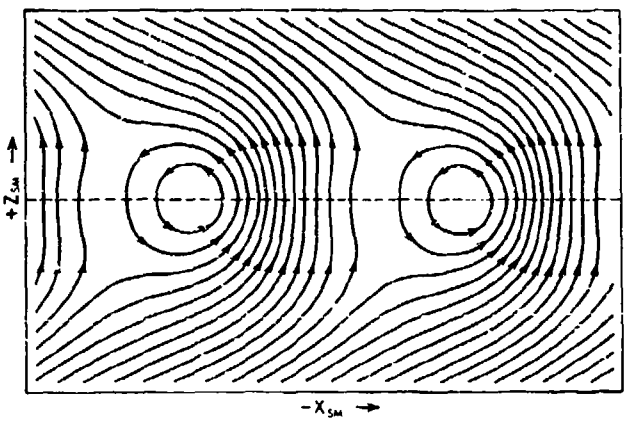

Figure 11-62. Configuration of the Weak Magnetic Field Interior to the Neutral Sheet for a Model in Which the Neutral-Sheet Current Has Periodic Local Concentrations. The model yields agreement with the observed statistical occurrence of southward values of B_Z near $x_{SM} = -30R_e$ [after Schindler and Ness, 1962]

annihilation at the neutral sheet; such an imbalance would exist, for example, if annihilation were inhibited by field-line tying in the nightside ionosphere, and energy would be stored up for a time in the enhanced tail field. Whether this is the energy source for substorms is not yet known, nor is it understood how the explosive release of such energy could be effected.

11.7.3 Hydromagnetic Waves and Discontinuities

As alluded to above, the conductive plasma of the magnetosphere and interplanetary medium constitutes a multi-fluid (one for each particle species) hydrodynamic medium in which waves and surfaces of discontinuity may propagate. The existence of hydromagnetic waves has been noted in discussing sudden commencements and micropulsations, while the existence of discontinuities has been noted in discussing the magnetospheric configuration and the features of the solar wind which cause disturbance. Theoretical treatments of such phenomena (particularly in the single-fluid approximation) have been considerably advanced in recent years. Hydromagnetic waves may be classified as shown in Table 11-10. The three basic modes are illustrated schematically in Figure 11-63.

Table 11-10. Classification of Hydromagnetic Waves

Type of Wave	$v_\parallel$	$v_\perp$	G	M
Basic Modes				
Ion acoustic wave	nonzero	zero	---	---
Alfven wave	zero	nonzero	zero	nonzero
Magnetoacoustic wave	zero	nonzero	nonzero	zero
Coupled Modes				
"Fast" wave (Alfven and magnetoacoustic modes coupled)	zero	nonzero	nonzero	nonzero
General case (all basic modes can exist with coupling)	nonzero	nonzero	---	---

$v_\parallel$ and $v_\perp$ are the parallel and perpendicular components of the center-of-mass perturbation velocity of the particles due to the wave, G is a parameter which specifies the pressure gradient, and M is a parameter which specifies the magnetic tension.

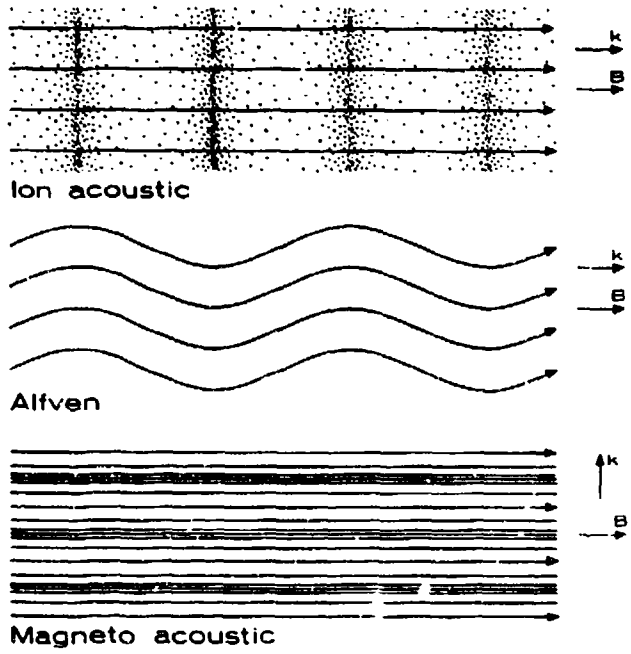

Figure 11-63. The Three Basic Modes for Hydromagnetic Waves, Represented Schematically. Solid lines are field lines; dots represent particle densities. Vectors B and k indicate field and wave-propagation directions, respectively [after Burlaga, 1971]

Discontinuities are classified as either shocks or stationary discontinuities, depending on whether they do or do not, respectively, move relative to the plasma. Shocks are classified as "parallel", "perpendicular", "fast", "slow", or "Alfvén", according to how they satisfy the condition for conservation of mass and momenta across the shock surface.

$$B_t \rho [v_\perp - U)^2 - V_A{}^2] = \text{constant}$$

where B_t = tangential field, ρ = density, $v_\perp$ = perpendicular component of particle velocity, U = shock speed, and V_A = Alfvén speed; Table 11-11 summarizes the classification. In the solar wind, shocks are additionally classified as "forward" or "reverse", depending on whether they move away from or toward the sun, respectively. Stationary discontinuities are either "tangential" or "contact" depending on whether the perpendicular component of the field is zero or nonzero respectively.

Most of these types of waves and discontinuities have been observed to occur in the solar wind and/or the magnetosphere; for example, the bow shock of the magnetosphere is a reverse fast shock moving in the plasma at a velocity just equal and opposite to that of the solar wind. However, a review of such observed phenomena and their theoretical treatment is beyond the scope of this discussion.

Table 11-11. Classification of Discontinuities

Classification	Criterion Satisfied (both sides of the discontinuity)
Stationary Discontinuities	
Tangential discontinuity	$B_\perp = 0$
Contact discontinuity	$B_\perp \neq 0$
Shocks	
Parallel shock	$B_t = 0$
Perpendicular shock	$V_A = 0$
Alfven shock	$(v_\perp - U)^2 = V_A^2$
Fast shock	$(v_\perp - U)^2 > V_A^2$
["n_1=n_2" shock]	[ρ = constant]
Slow shock	$(v_\perp - U)^2 < V_A^2$

11.8 MISCELLANEOUS INFORMATION

11.8.1 Geomagnetic Stations

Table 11-12 presents a list of geomagnetic stations in operation during recent years.

Table 11-12. List of Geomagnetic Observatories
[compiled by World Data Center A]

CSAGI No.	Observatory	Location	Sponsor	Geomagnetic Lat. (°)	Geomagnetic Long. (°)	Geographic Lat. (° ')	Geographic Long. (° ')
A001	North Pole 6	Arctic Ocean	USSR	70.6	197.4	80 56 N	150 02 E
				76.8	164.2	86 15 N	39 23 E
A003	North Pole 7	Arctic Ocean	USSR	78.5	198.4	86 21 N	149 38 W
				81.9	160.5	85 17 N	34 05 W
	North Pole 8	Arctic Ocean	USSR	71.0	230.0	75 32 N	162 47 W
				71.5	213.7	79 06 N	179 23 E
	North Pole 10	Arctic Ocean	USSR	66.1	208.9	75 11 N	160 52 E
				69.8	211.7	78 02 N	171 54 E
	North Pole 12	Arctic Ocean	USSR	69.7	217.8	76 50 N	179 59 E
				74.9	215.0	81 19 N	194 26 E
A019	Arctic Ice Floe A	Arctic Ocean	USA	75.2	214.5	81 38 N	164 34 W
				76.9	200.4	85 23 N	169 20 W
A021	Thule	Greenland	Denmark	89.0	358.0	77 29 N	69 10 W
A005	Alert	Canada	Canada	85.9	168.2	82 30 N	62 30 W
A030	Resolute Bay	Canada	Canada	83.0	289.3	74 42 N	94 54 W
A049	Godhavn	Greenland	Denmark	79.9	32.5	69 14 N	53 31 W
A028	Mould Bay	Canada	Canada	79.1	256.4	76 12 N	119 24 W
A070	Sukkertoppen	Greenland	Denmark	76.1	28.7	65 25 N	52 54 W
A044	Kap Tobin	Greenland	Denmark	75.6	81.6	70 25 N	21 58 W
A010	Murchison Bay	Norway	Sweden	75.2	137.5	80 03 N	18 15 E
A018	Barentsburg	Norway	USSR	74.6	132.5	78 38 N	16 23 E
A099	Baker Lake	Canada	Canada	73.8	315.2	64 20 N	96 02 W
A009	Tikhaya Bay	USSR	USSR	71.5	153.2	80 18 N	52 48 E
A009	Heiss Island	USSR	USSR	71.3	156.1	80 37 N	58 03 E
A031	Bear Island	Norway	Norway	71.1	124.5	74 30 N	19 12 E
A132	Julianehaab	Greenland	Denmark	70.8	35.5	60 43 N	46 02 W
A104	Leirvogur	Iceland	Iceland	70.2	71.0	64 11 N	21 42 W
A045	Barter Island	Alaska	USA	70.0	253.1	70 08 N	143 40 W
A122	Yellowknife	Canada	Canada	69.0	293.3	62 26 N	114 24 W
A145	Fort Churchill	Canada	Canada	68.7	322.8	58 48 N	94 05 W
A039	Barrow	Alaska	USA	68.5	241.1	71 18 N	156 45 W
A047	Tromso	Norway	Norway	67.1	116.7	69 40 N	18 57 E
A148	Great Whale River	Canada	Canada	66.6	347.4	55 16 N	77 47 W
A073	Fort Yukon	Alaska	USA	65.6	256.8	66 34 N	145 18 W
A020	Cape Chelyuskin	USSR	USSR	66.3	176.5	77 43 N	104 17 E
A054	Abisko	Sweden	Sweden	66.0	115.0	68 21 N	18 49 E
A059	Utsjoki	Finland	Finland	65.8	122.9	69 45 N	27 02 E
A060	Kiruna	Sweden	Sweden	65.3	115.6	67 50 N	20 25 E
A180	Ivalo	Finland	Finland	64.7	121.9	68 36 N	27 29 E
A092	College	Alaska	USA	64.6	256.5	64 52 N	147 50 W
A102	Big Delta	Alaska	USA	64.3	259.3	64 00 N	145 44 W
A118	Northway	Alaska	USA	64.1	263.8	62 58 N	141 57 W
A065	Sodankyla	Finland	Finland	63.8	120.0	67 22 N	26 38 E
A069	Kotzebue	Alaska	USA	63.7	242.1	66 53 N	162 36 W
A107	Healy	Alaska	USA	63.6	256.6	63 51 N	148 58 W
A074	Murmansk	USSR	USSR	63.5	125.8	68 15 N	33 05 E
A033	Dixon Island	USSR	USSR	63.0	161.6	73 33 N	80 34 E
A057	Lovozero	USSR	USSR	62.9	127.0	67 58 N	35 01 E
A140	Lerwick	Scotland	United Kingdom	62.5	88.6	60 09 N	1 11 W
A123	Dombas	Norway	Norway	62.3	100.1	62 04 N	9 07 E
A154	Meanook	Canada	Canada	61.8	301.0	54 37 N	113 20 W

Table 11-12. List of Geomagnetic Observatories (contd.)

CSAGI No.	Observatory	Location	Sponsor	Geomagnetic Lat. (°)	Geomagnetic Long. (°)	Geographic Lat. (° ′)	Geographic Long. (° ′)
A077	Cape Wellen	USSR	USSR	61.8	237.1	66 10 N	169 50 W
A130	Anchorage	Alaska	USA	61.0	258.1	61 14 N	149 52 W
A037	Tixie Bay	USSR	USSR	60.4	191.4	71 35 N	129 00 E
A149	Sitka	Alaska	USA	60.0	275.3	57 04 N	135 20 W
B038	Eskdalemuir	Scotland	United Kingdom	58.5	82.9	55 19 N	3 12 W
B009	Lovo	Sweden	Sweden	58.1	105.8	59 21 N	17 50 E
A134	Nurmijarvi	Finland	Finland	57.9	112.6	60 31 N	24 39 E
B349	Stonyhurst	England	United Kingdom	56.9	82.7	53 51 N	2 28 W
B098	Valentia	Ireland	Ireland	56.6	73.5	51 56 N	10 15 W
B259	Leningrad	USSR	USSR	56.2	117.3	59 57 N	30 42 E
B114	Rude Skov	Denmark	Denmark	55.9	98.5	55 51 N	12 27 E
B249	Agincourt	Canada	Canada	55.1	347.0	43 47 N	79 16 W
	Newport	USA	USA	55.1	300.0	48 16 N	117 07 W
B119	Hartland	England	United Kingdom	54.6	79.0	51 00 N	4 29 W
B058	Wingst	German Fed R	German Fed R	54.6	94.1	53 45 N	9 04 E
B326	Warkenhagen	German Dem R	German Dem R	54.4	96.1	54 01 N	11 04 E
B159	Victoria	Canada	Canada	54.2	293.0	48 31 N	123 25 W
B071	Witteveen	Netherlands	Netherlands	54.1	91.2	52 49 N	6 40 E
B269	Weston	USA	USA	53.9	357.1	42 23 N	71 19 W
B044	Hel	Poland	Poland	53.4	103.7	54 36 N	18 49 E
A121	Srednikan	USSR	USSR	53.1	210.6	62 26 N	152 19 E
B014	Borok	USSR	USSR	53.0	123.2	58 02 N	38 58 E
B106	Gottingen	German Fed R	German Fed R	52.3	93.7	51 32 N	9 58 E
B095	Niemegk	German Dem R	German Dem R	52.2	96.6	52 04 N	12 41 E
B132	Manhay	Belgium	Belgium	52.0	88.9	50 18 N	5 41 E
B136	Dourbes	Belgium	Belgium	52.0	87.7	50 06 N	4 36 E
B261	Casper	USA	USA	51.5	314.5	42 51 N	106 18 W
B325	Collm	German Dem R	German Dem R	51.5	96.5	51 19 N	13 00 E
	Minsk	USSR	USSR	51.5	110.4	54 06 N	26 31 E
A124	Yakutsk	USSR	USSR	51.0	193.8	62 01 N	129 43 E
B035	Moscow	USSR	USSR	50.9	120.5	55 29 N	37 19 E
B089	Swider	Poland	Poland	50.6	104.6	52 07 N	21 15 E
B161	Chambon-la-Foret	France	France	50.5	84.4	48 01 N	2 16 E
	Nantes	France	France	50.5	80.1	47 15 N	1 33 W
B101	Belsk	Poland	Poland	50.4	104.0	51 50 N	20 48 E
B143	Pruhonice	Czechoslovakia	Czechoslovakia	49.9	97.3	49 59 N	14 33 E
B269	Carrollton	USA	USA	49.6	330.4	39 22 N	93 28 W
B318	Fredericksburg	USA	USA	49.6	349.8	38 12 N	77 22 W
B182	Garchy	France	France	49.6	84.9	47 18 N	3 06 E
B028	Kazan	USSR	USSR	49.3	130.4	55 50 N	48 51 E
B137	Raciborz	Poland	Poland	49.3	100.8	50 05 N	18 11 E
B012	Beloit	USA	USA	49.2	324.9	39 28 N	98 08 W
B328	Budkov	Czechoslovakia	Czechoslovakia	49.1	96.4	49 04 N	14 01 E
B295	Boulder	USA	USA	49.0	316.5	40 08 N	105 14 W
B163	Furstenfeldbruck	German Fed R	German Fed R	48.8	93.3	48 10 N	11 17 E
	Regensburg	Switzerland	Switzerland	48.7	90.3	47 29 N	8 27 E
B054	Shatsk	USSR	USSR	48.7	123.7	53 59 N	41 51 E
B019	Sverdlovsk	USSR	USSR	48.5	140.7	56 44 N	61 04 E
C401	Burlington	USA	USA	48.5	320.1	39 17 N	102 16 W
B145	Lvov	USSR	USSR	48.0	105.9	49 54 N	23 45 E
B305	Leadville	USA	USA	48.0	315.5	39 17 N	106 17 W
B162	Wien-Kobenz	Austria	Austria	47.9	98.2	48 16 N	16 19 E
B440	Price	USA	USA	47.7	310.3	39 37 N	110 47 W
B150	Kiev	USSR	USSR	47.6	112.2	50 43 N	30 18 E
B100	Adak	Aleutian I	USA	47.2	240.0	51 52 N	176 39 W

Table 11-12. List of Geomagnetic Observatories (contd.)

CSAGI No.	Observatory	Location	Sponsor	Geomagnetic Lat. (°)	Geomagnetic Long. (°)	Geographic Lat. (° ')	Geographic Long. (° ')
B168	Nagycenk	Hungary	Hungary	47.2	98.3	47 38 N	16 43 E
B172	Hurbanovo	Czechoslovakia	Czechoslovakia	47.2	99.8	47 52 N	18 11 E
B232	Castel Tesino	Italy	Italy	46.7	92.8	46 03 N	11 39 E
B191	Tihany	Hungary	Hungary	46.3	99.1	46 54 N	17 54 E
B267	Logrono	Spain	Spain	46.1	77.2	42 27 N	2 30 W
B022	Tomsk	USSR	USSR	45.9	159.6	56 28 N	84 56 E
B236	Monte Capellino	Italy	Italy	45.8	89.5	44 33 N	8 57 E
B280	Roburent	Italy	Italy	45.8	88.4	44 18 N	7 53 E
B239	Castellaccio	Italy	Italy	45.7	89.4	44 26 N	8 56 E
B321	San Miguel	Azores I	Portugal	45.6	50.9	37 46 N	25 39 W
C329	Baja	Hungary	Hungary	45.4	99.9	46 11 N	19 00 E
C093	Coimbra	Portugal	Portugal	45.0	70.3	40 13 N	8 25 W
	Jassy	Rumania	Rumania	44.7	104.2	47 11 N	27 32 E
C001	Petropavlovsk	USSR	USSR	44.7	218.6	53 06 N	158 38 E
C406	Esparola	USA	USA	44.6	316.6	35 49 N	106 04 W
C086	Del Ebro	Spain	Spain	43.9	79.7	40 49 N	0 30 E
C098	Toledo	Spain	Spain	43.9	74.7	39 53 N	4 03 W
C018	Odessa	USSR	USSR	43.7	111.1	46 47 N	30 53 E
C028	Grocka	Yugoslavia	Yugoslavia	43.6	100.9	44 38 N	20 46 E
	Castle Rock	USA	USA	43.5	298.6	37 14 N	122 08 W
C405	Dallas	USA	USA	43.0	327.7	32 59 N	96 45 W
C063	L'Aquila	Italy	Italy	42.9	92.9	42 23 N	13 19 E
C085	La Maddalena	Italy	Italy	42.5	88.7	41 14 N	9 24 E
C215	Surlari	Rumania	Rumania	42.5	106.1	44 41 N	26 15 E
C082	Ponza	Italy	Italy	41.5	92.1	40 55 N	12 57 E
C026	Simferopol	USSR	USSR	41.2	113.3	44 50 N	34 04 E
C360	Aloushta	USSR	USSR	41.0	113.6	44 41 N	34 25 E
C143	San Fernando	Spain	Spain	41.0	71.3	36 28 N	6 12 W
C078	Capri	Italy	Italy	40.9	93.2	40 33 N	14 13 E
C059	Panagyurishte	Bulgaria	Bulgaria	40.8	103.4	42 31 N	24 11 E
B102	Irkutsk	USSR	USSR	40.7	174.8	52 10 N	104 27 E
C137	Almeria	Spain	Spain	40.6	75.3	36 51 N	2 28 W
C236	Tucson	USA	USA	40.4	312.2	32 15 N	110 50 W
C124	Gibilmanna	Italy	Italy	38.5	92.2	37 59 N	14 01 E
	Kandilli	Turkey	Turkey	38.5	107.4	41 04 N	29 04 E
C016	Yuzhno-Sakhalinsk	USSR	USSR	36.9	206.7	46 57 N	142 43 E
C364	Tbilisi	USSR	USSR	36.7	122.1	42 05 N	44 42 E
C133	Pendeli	Greece	Greece	36.6	101.5	38 03 N	23 52 E
C439	Ulan Bator	Mongolia	Mongolia	36.4	176.5	47 51 N	106 45 E
C264	Tenerife	Canary I	Spain	35.0	58.6	28 29 N	16 17 W
C425	Centro Geofisico	Cuba	Cuba	34.1	345.3	22 58 N	82 09 W
C034	Memambetsu	Japan	Japan	34.0	208.4	43 54 N	144 12 E
C050	Alma Ata	USSR	USSR	33.4	150.7	43 15 N	76 55 E
C051	Vladivostock	USSR	USSR	32.8	198.1	43 41 N	132 10 E
C361	Tashkent	USSR	USSR	32.3	144.0	41 20 N	69 37 E
C126	Ashkhabad	USSR	USSR	30.5	133.1	37 57 N	58 06 E
C416	Ksara	Lebanon	Lebanon	30.2	111.7	33 49 N	35 53 E
C300	San Juan	Puerto Rico	USA	29.6	3.1	18 07 N	66 09 W
C287	Teoloyucan	Mexico	Mexico	29.6	327.0	19 45 N	99 11 W
C163	Tehran	Iran	Iran	29.4	126.5	35 44 N	51 23 E
C339	Nitsanim	Israel	Israel	28.4	110.0	31 44 N	34 36 E
C117	Onagawa	Japan	Japan	28.3	206.8	38 26 N	141 28 E
C256	Helwan	UAR	UAR	27.2	106.4	29 52 N	31 20 E
C239	Misallat	UAR	UAR	26.9	105.9	29 31 N	30 54 E
C069	Seoul	Rep of Korea	Rep of Korea	26.5	194.2	37 35 N	127 03 E

Table 11-12. List of Geomagnetic Observatories (contd.)

CSAGI No.	Observatory	Location	Sponsor	Geomagnetic Lat. (°)	Geomagnetic Long. (°)	Geographic Lat. (° ′)	Geographic Long. (° ′)
C170	Gilgit	Pakistan	Pakistan	26.4	147.3	35 55 N	74 18 E
C147	Kakioka	Japan	Japan	26.0	206.0	36 14 N	140 11 E
C273	Tamanrasset	Algeria	Algeria	25.4	79.6	22 48 N	5 32 E
	Kanozan	Japan	Japan	25.0	205.9	35 15 N	139 58 E
E743	Midway	Midway I	USA	24.1	246.3	28 13 N	177 22 W
C214	Simosato	Japan	Japan	23.0	202.4	33 34 N	135 56 E
C220	Hachijojima	Japan	Japan	22.9	206.0	33 08 N	139 48 E
C223	Aso	Japan	Japan	22.0	198.1	32 53 N	131 01 E
	Araira	Venezuela	Venezuela	21.9	2.7	10 27 N	66 29 W
C251	Quetta	Pakistan	Pakistan	21.6	139.7	30 11 N	66 57 E
C311	M'Bour	Senegal	Senegal	21.3	55.0	14 24 N	16 58 W
C277	Honolulu	Hawaiian I	USA	21.1	266.5	21 19 N	158 00 W
C250	Sabhawala	India	India	20.5	149.7	30 20 N	77 48 E
C245	Kanoya	Japan	Japan	20.5	198.1	31 25 N	130 53 E
E575	Paramaribo	Surinam	Netherlands	17.0	14.3	5 49 N	55 13 W
E578	Fuquene	Colombia	Colombia	16.9	355.1	5 28 N	73 44 W
E532	Sokoto	Nigeria	Nigeria	15.9	77.1	13 03 N	5 15 E
E558	Freetown	Sierra Leone	Sierra Leone	14.8	57.8	8 28 N	13 13 W
E488	Lunping	Rep of China	Rep of China	13.7	189.5	25 00 N	121 10 E
E485	Zaria	Nigeria	Nigeria	13.6	79.1	11 09 N	7 39 E
E597	Kontagora	Nigeria	Nigeria	13.3	76.8	10 24 N	5 27 E
E525	Chittagong	Pakistan	Pakistan	11.4	161.9	22 21 N	91 49 E
E528	Cha-Pa	Vietnam	Vietnam	10.9	173.3	22 21 N	103 50 E
E571	Ibadan	Nigeria	Nigeria	10.7	74.7	7 26 N	3 54 E
E590	Tatuoca	Brazil	Brazil	9.6	20.8	1 12 S	48 31 W
E472	Legon	Ghana	Ghana	9.6	70.2	5 38 N	0 11 W
E538	Alibag	India	India	9.5	143.6	18 38 N	72 52 E
E542	Hyderabad	India	India	7.6	148.9	17 25 N	78 33 E
E593	Talara	Peru	Peru-USA	6.6	347.7	4 38 S	81 18 W
E586	Moca	Fernando Poo	Spain	5.7	78.6	3 21 N	8 40 E
E568	Addis Abeba	Ethiopia	Ethiopia	5.4	109.2	9 02 N	38 46 E
E574	Palmyra Island	Palmyra I	USA	5.2	265.8	5 53 N	162 05 W
E547	Baguio	Philippine R	Philippine Rep	5.1	189.2	16 25 N	120 36 E
E583	Bangui	Cent Afr Rep	Central Afr Rep	4.8	88.5	4 26 N	18 34 E
E595	Chiclayo	Peru	Peru-USA	4.5	349.2	6 48 S	79 48 W
E556	Guam	Mariana I	USA	4.0	212.9	13 35 N	144 52 E
E585	Fanning Island	Gilbert-E I	UK-USA	3.7	268.8	3 54 N	159 23 W
E553	Muntinlupa	Philippine R	Philippine Rep	3.0	189.7	14 23 N	121 01 E
E596	Chimbote	Peru	Peru-USA	2.2	350.5	9 06 S	78 36 W
E562	Annamalainagar	India	India	1.5	149.4	11 24 N	79 41 E
E561	Majuro	Marshall I	USA	1.3	239.6	7 05 N	171 23 E
E566	Kodaikanal	India	India	0.6	147.1	10 14 N	77 28 E
E611	Bunia	Congo	Congo	-0.3	99.3	1 32 N	30 11 E
E618	Jarvis Island	Jarvis I	USA	-0.6	269.1	0 23 S	160 02 W
E646	Huancayo	Peru	Peru	-0.6	353.8	12 03 S	75 20 W
	Cebu	Philippine R	Philippine Rep	-0.9	192.7	10 18 N	123 54 E
E603	Trivandrum	India	India	-1.1	146.4	8 29 N	76 57 E
E651	Curco	Peru	Peru	-2.1	357.1	13 32 S	71 58 W
E631	Binza	Congo	Congo	-3.1	83.6	4 16 S	15 22 E
E606	Koror	Palau I	USA	-3.2	203.3	7 20 N	134 30 E
E624	Lwiro	Congo	Congo	-3.8	97.2	2 15 S	28 48 E
	Davao	Philippine R	Philippine Rep	-4.1	194.5	7 05 N	125 35 E
E740	Yauca	Peru	Peru-USA	-4.1	354.5	15 32 S	74 40 W
E621	Nairobi	Kenya	Kenya	-4.4	105.3	1 19 S	36 49 E
E666	Arequipa	Peru	Peru	-5.0	357.6	16 28 S	71 29 W

Table 11-12. List of Geomagnetic Observatories (contd.)

CSAGI No.	Observatory	Location	Sponsor	Geomagnetic Lat. (°)	Geomagnetic Long. (°)	Geographic Lat. (° ')	Geographic Long. (° ')
E676	Santa Cruz	Bolivia	Bolivia	-6.4	5.5	17 48 S	63 10 W
Eu40	Luanda	Angola	Portugal	-7.2	80.6	8 55 S	13 10 E
E702	La Quiaca	Argentina	Argentina	-10.6	3.2	22 06 S	65 36 W
E629	Vassouras	Brazil	Brazil	-11.9	23.9	22 24 S	43 39 W
E625	Hollandia	D New Guinea	Indonesia	-12.5	210.3	2 34 S	140 31 E
E644	Elizabethville	Congo	Congo	-12.7	94.0	11 38 S	27 25 E
E672	Tahiti	Society I	France	-15.3	282.7	17 33 S	149 37 W
E653	Apia	Samoa I	Western Samoa	-16.1	260.2	13 48 S	171 47 W
E634	Kuyper	Indonesia	Indonesia	-17.5	175.6	6 02 S	106 44 E
	Tangerang	Indonesia	Indonesia	-17.6	175.4	6 10 S	106 38 E
E712	Easter Island	Easter I	Chile	-18.2	322.6	27 10 S	109 25 W
E686	Tsumeb	SW Africa	German Fed Rep	-18.2	82.8	19 13 S	17 42 E
E642	Port Moresby	New Guinea	Australia	-18.6	217.9	9 24 S	147 09 E
C932	Pilar	Argentina	Argentina	-20.2	4.6	31 40 S	63 53 W
C901	Tananarive	Malagasy Rep	Malagasy Rep	-23.7	112.5	18 55 S	47 33 E
C982	Las Acacias	Argentina	Argentina	-23.7	10.1	35 00 S	57 41 W
	Mauritius	Indian Ocean	United Kingdom	-26.6	124.4	20 06 S	57 33 E
C899	Plaisance	Indian Ocean	United Kingdom	-27.0	122.5	20 26 S	57 40 E
C914	Lourenco Marques	Mozambique	Portugal	-27.7	95.8	25 55 S	32 35 E
C988	Trelew	Argentina	Argentina	-31.8	3.2	43 15 S	65 19 W
C957	Hermanus	Rep S Africa	Rep S Africa	-33.3	80.5	34 25 S	19 14 E
C838	Gough Island	Gough I	Rep S Africa	-33.8	51.9	40 21 S	9 53 W
C918	Brisbane	Australia	Australia	-35.8	226.9	27 32 S	152 55 E
C925	Watheroo	Australia	Australia	-41.8	185.7	30 19 S	115 53 E
C993	Gnangara	Australia	Australia	-43.2	185.8	31 47 S	115 57 E
B966	Toolangi	Australia	Australia	-46.7	220.8	37 32 S	145 28 E
B979	Amberley	New Zealand	New Zealand	-47.7	252.5	43 09 S	172 43 E
B996	Marion Island	Marion I	Rep S Africa	-49.0	94.3	46 51 S	37 52 E
A962	Orcadas Del Sur	Orcadas	Argentina	-50.0	18.2	60 44 S	44 47 W
	G Gonzales Videla	Antarctica	Chile	-53.4	4.4	64 49 S	62 51 W
A973	Argentine Islands	Antarctica	United Kingdom	-53.8	3.4	65 15 S	64 16 W
B998	Port-aux-Francais	Indian Ocean	France	-57.3	128.0	49 21 S	70 12 E
A961	Macquarie Island	Antarctica	Australia	-61.1	247.1	54 30 S	158 57 E
A987	Sanae Station	Antarctica	Rep S Africa	-63.6	44.2	70 18 S	2 21 W
A987	Norway Station	Antarctica	Norway	-63.8	43.9	70 30 S	2 32 W
A952	Eights	Antarctica	USA	-63.8	355.3	75 14 S	77 10 W
A989	Halley Bay	Antarctica	United Kingdom	-65.8	24.3	75 31 S	26 37 W
A951	Novolazarevskaya	Antarctica	USSR	-66.2	53.6	70 46 S	11 49 E
A994	General Belgrano	Antarctica	Argentina	-67.3	15.8	77 58 S	38 48 W
A986	Roi Baudouin	Antarctica	Belgium	-68.0	63.2	70 26 S	24 18 E
A984	Syowa Base	Antarctica	Japan	-69.7	77.7	69 00 S	39 35 E
A997	Byrd	Antarctica	USA	-70.6	336.3	80 00 S	119 30 W
A980	Mawson	Antarctica	Australia	-73.1	102.9	67 36 S	62 53 E
A995	Little America	Antarctica	USA	-74.0	312.0	78 11 S	162 12 W
A988	Cape Hallett	Antarctica	New Zealand-US	-74.7	278.2	72 19 S	170 13 E
A979	Dumont D'Urville	Antarctica	France	-75.7	230.8	66 40 S	140 00 E
A978	Mirny	Antarctica	USSR	-77.0	146.8	66 33 S	93 01 E
	Plateau	Antarctica	USA	-77.2	52.5	79 15 S	40 30 E
A976	Oasis	Antarctica	USSR	-77.5	160.7	66 18 S	100 43 E
A977	Wilkes	Antarctica	Australia-USA	-77.7	179.2	66 15 S	110 35 E
A999	South Pole	Antarctica	USA	-78.5	0.3	89 57 S	13 19 W
A985	Charcot	Antarctica	France	-78.3	234.5	69 23 S	139 01 E
A991	Scott Base	Antarctica	New Zealand	-79.0	294.4	77 51 S	166 47 E
A959	Pionerskaya	Antarctica	USSR	-80.3	146.5	69 44 S	95 30 E
A996	Vostok	Antarctica	USSR	-89.2	91.4	78 27 S	106 52 E

11.8.2 Data Centers

Extensive holdings of magnetic-field data are available from two data centers in the United States:

World Data Center A (WDC-A)
for Solar-Terrestrial Physics
National Oceanic and Atmospheric Administration
Boulder, Colorado 80302
Telephone: 303-499-1000 Extension 6467
(at Rockville, Maryland, prior to 1972)

National Space Science Data Center (NSSDC)
Code 601.4
Goddard Space Flight Center
Greenbelt, Maryland 20771
Telephone: 301-982-6695

Data catalogs of their holdings are available; data (from many observatories) include normal-speed and rapid-run magnetograms, 2.5-minute digitizations, tabulation of mean values (hourly, monthly, and annual) of the field elements, files of magnetic-survey data, processed data from satellite experiments, and various other items.

Others of the World Data Centers also are of interest to geomagnetism. They are organized into WDC-A (subcenters in the U.S.A., including the one listed above), WDC-B (subcenters in the U.S.S.R., including one for solar-terrestrial physics at IZMIRAN, Moscow), and WDC-C (20 subcenters in Europe, Japan, and India). Also, some sixteen of the Permanent Services of the International Council of Scientific Unions are of interest. A listing of all of thes , with addresses, is given in STP Notes, No. 6 (October, 1969).

11.8.3 Field Measurements in Space

A "Catalog of Spacecraft and Experiments Related to Solar-Terrestrial Physics", prepared by the NSSDC in April 1970, was included in STP Notes, No. 7 (May, 1970); it has not been revised and re-issued. Active and planned spacecraft for the period 1962-1975 are included. A brief description and a reference for each experiment are given; not all spacecraft include magnetic-field measurements. Table 11-13 reproduces the list of spacecraft with their status on 1st April, 1970.

11.8.4 ELF and VLF Measurements in Space

A tabulation of ELF and VLF experiments with appropriate references has been given by Russell, et al [1972]. A condensed version is given in Table 11-14. For details and references, refer to the original.

Table 11-13. Spacecraft Carrying Experiments Related to Solar-Terrestrial Physics, as Cataloged in April 1970 [see text]

Active Spacecraft		Planned Spacecraft	
Spacecraft Name	International Designation	Spacecraft Name	Planned Year of launch
Alouette 1	62-049A	RAE-B	1972
Explorer 27, BE-C	65-032A	SSS-A	1970
Alouette 2	65-098A	IMP-I (I)	1970
Pioneer 6	65-105A	NIMBUS-D	1970
Pioneer 7	66-075A	ISIS-B	1971
ATS-1	66-110A	OSO-H	1971
VELA-4A	67-040A	SAN MARCO C	1970
VELA-4B	67-040B	Apollo 13, ALSEP	1970
Explorer 35, AIMP-2	67-070A	VELA 6A	1970
ATS-3	67-111A	VELA 6B	1970
Pioneer 8	67-123A	SOLRAD-10	1970
OGO-5	68-014A	MAGNETIC STORM SATELLITE	1971
Explorer 37, Solrad 9	68-017A	Apollo 14, ALSEP	1970
ESRO 2, IRIS	68-041A	MARINER-H, MARS-71	1971
Explorer 38, RAE-1	68-055A	MARINER-I (I) MARS-71	1971
Explorer 39, AD-C	68-066A	UK 4	1971
Explorer 40, Injun 5	68-066B	IMP-H	1972
ESRO 1, Aurorae	68-084A	HEOS A2	1972
Pioneer 9	68-100A	ATS-F	1972
HEOS-A1	68-103A	NIMBUS-E	1972
OSO-5	69-006A	GRS-A2, AEROS	1972
ISIS-1	69-009A	IMP-J	1973
ESSA-9	69-016A	Pioneer F	1972
OVI-18	69-025B	NIMBUS F	1973
OVI-19	69-025C	OSO I (I)	1973
NIMBUS 3	69-037A	VIKING A	1975
OV5-5	69-046A	Pioneer G	1973
OV5-6	69-046B	HELIOS A	1974
VELA-5A	69-046D	HELIOS B	1975
VELA-5B	69-046E		
OGO-6	69-051A		
Explorer 41, IMP-5	69-053A		
OSO-6	69-068A		
ATS-5	69-069A		
GRS-A, AZUR	69-097A		
Apollo 12, ALSEP	69-099A		
ITOS-1	70-008A		

11.8.5 Research Publications

Results, summaries, and reviews of experimental and theoretical research in geomagnetism are published principally in the following journals or series of reports (listed alphabetically):

Geomagnetism and Aeronomy, the English edition of a Russian journal, produced bimonthly by Scripta Technica, Inc., under the Russian Translation program of the American Geophysical Union, 2100 Pennsylvania Ave., N.W., Washington, D.C. 20037.

IAGA Bulletins, issued by the International Association of Geomagnetism and Aeronomy, IUGG Publications Office, 39 ter, rue Gay-Lussac, Paris (V) France.

Table 11-14. Spacecraft Carrying ELF and VLF Experiments as Cataloged by Russell et al [see text]

Spacecraft Name	Launch Date	Altitude Coverage (km or R_e)	Type of Antenna	Frequency Coverage (kHz)
Alouette 1	Sep 1962	1000	Dipole	0.6-10.0
Alouette 2	Nov 1965	500-3000	Dipole	.05-30.0
ISIS 1	Jan 1969	575-3500	Dipole	.05-30.0
Injun 3	Dec 1962	240-2800	Loop	0.5-8.8
Injun 5	Aug 1968	680-2500	Dipole Loop	.03-105 .03-10
P-11	Aug 1964	270-3700	Dipole	1.7-14.5
OGO 1	Sep 1964	1.05-24.1	3-axis Search Coil Loop	.00001-0.80 0.2-100
OGO 2	Oct 1965	400-1500	3-axis Search Coil Loop Dipole	.00001-1.0 0.2-100 0.5-18
OGO 3	Jun 1966	1.05-20.2	Same as OGO 1 plus the following: Loop Dipole	 .015-0.300 .015-100
OGO 4	Jul 1967	400-900	Same as OGO 2 plus the following: Loop Dipole	 .015-0.300 .015-100
OGO 5	Mar 1968	1.05-24.1	3-axis Search Coil Dipole 3-axis Loop	.00001-1.0 0.2-70 0.56-70
OGO 6	Jun 1969	400-1100	3-axis Search Coil Dipole 3-axis Loop Dipole	.00001-1.0 .01-400 .02-32.0 .02-32.0
OV3 3	Aug 1966	350-4500	Dipole S Coil and Dipole	.02-7.35 0.4-14.5
OV1 10	Dec 1966	647-777	Dipole	.01-1.5
Ariel 3	May 1967	500-600	Loop	3.2-16.0

Journal of Geomagnetism and Geoelectricity, published quarterly by the Society of Terrestrial Magnetism and Electricity, Geophysical Institute, University of Tokyo, Tokyo, Japan.

Journal of Geophysical Research, published three times a month by the American Geophysical Union, 2901 Byrdhill Rd., Richmond, Va. 23228.

Nature, published weekly by MacMillan Journals, Ltd., 4 Little Essex St., London WC2R 3LF, England.

Planetary and Space Science, published monthly by Pergamon Press, Ltd., Headington Hill Hall, Oxford OX3 OB W, England.

Reviews of Geophysics and Space Physics, published quarterly by the American Geophysical Union, 2901 Byrdhill Rd., Richmond, Va. 23228.

Science, published weekly by the American Association for the Advancement of Science, 1515 Massachusetts Ave., N.W., Washington, D.C. 20005.

Space Science Reviews, published monthly by D. Reidel Publishing Co., P. O. Box 17, Dordrecht-Holland, The Netherlands.

X-series reports, unpublished, issued by Goddard Space Flight Center, Greenbelt, Md. 20771.

11.8.6 Listings of Data Sources

Correlative data available at the National Space Science Data Center (NSSDC), at other centers, and in readily accessible publications are listed in the "Handbook of Correlative Data", issued by the NSSDC.

An extensive listing of data sources is provided in Annals of the IQSY, Volume 1.

Another listing of data sources is given in Appendix A of Geophysics and Space Data Bulletin, Volume IV, No. 2. (1967), published by Air Force Cambridge Research Laboratories, Bedford, Mass., 01730.

11.8.7 Gauss-Schmidt Conversion

Spherical-harmonic coefficients for the geomagnetic field which have Gaussian normalization may be converted to Schmidt normalization using the values of q listed in Table 11-15, $(\text{Gauss coefficient})_{nm} \times q_{nm} = (\text{Schmidt coefficient})_{nm}$.

11.8.8 Sources of Field Models

The National Space Science Data Center (NSSDC) has available:

1. Coefficients, for use with geodetic coordinates, on card decks, of the GSFC (12/66), POGO (10/68), POGO (8/69), and IGRF 1965.0 field models.
2. Coefficients, for use with geomagnetic dipolar coordinates, on a card deck, of the IGRF 1965.0 field model.
3. A FORTRAN program, on a card deck, to compute the field at any point in space.
4. A FORTRAN program, on a card deck, to compute the B-L coordinates of any point in space, for a given field model.
5. A FORTRAN program, on a card deck, to trace out field lines for a given field model.
6. Coefficients, on card decks, of the field model with external sources derived by Olson.

Table 11-15. Gauss-Schmidt Conversion Factors

n	m	q	n	m	q	n	m	q
0	0	1.00000	6	0	0.069264	9	0	0.0105307
1	0	1.00000	6	1	0.052901	9	1	0.0078491
1	1	1.00000	6	2	0.066915	9	2	0.0092039
2	0	0.66667	6	3	0.100373	9	3	0.0120507
2	1	0.57735	6	4	0.183256	9	4	0.0177381
2	2	1.15470	6	5	0.42977	9	5	0.029682
3	0	0.40000	6	6	1.48878	9	6	0.057478
3	1	0.32660	7	0	0.037296	9	7	0.132740
3	2	0.51640	7	1	0.028193	9	8	0.38700
3	3	1.26491	7	2	0.034529	9	9	1.64190
4	0	0.22857	7	3	0.048832	10	0	0.0055424
4	1	0.180702	7	4	0.080979	10	1	0.0041104
4	2	0.25555	7	5	0.161957	10	2	0.0047463
4	3	0.47809	7	6	0.41291	10	3	0.0060503
4	4	1.35225	7	7	1.54498	10	4	0.0085565
5	0	0.126984	8	0	0.0198912	10	5	0.0135289
5	1	0.098361	8	1	0.0149184	10	6	0.024201
5	2	0.130120	8	2	0.0178309	10	7	0.049892
5	3	0.21249	8	3	0.024143	10	8	0.122211
5	4	0.45075	8	4	0.037402	10	9	0.37668
5	5	1.42539	8	5	0.067428	10	10	1.68456
			8	6	0.145662			
			8	7	0.39891			
			8	8	1.59564			

7. A program, on a card deck, to compute the field at any point for the Olson model.

The World Data Center A (Boulder) additionally has available, on a card deck, the 168 coefficients of the World Magnetic Charts of 1970. This model is computed from ground-based data and is used for the charts issued every five years by the United States Coast and Geodetic Survey.

11.8.9 Sources of Activity Indices and Charts

At least one source is given here for each of the indices and charts described in Section 11.6.6, in the order in which they were discussed. The following abbreviations are used:

Organizations

AFCRL	Air Force Cambridge Research Laboratories, L.G. Hanscom Field, Bedford, Mass. 01730, U.S.A.
EDS-NOAA	Environmental Data Service, National Oceanic and Atmospheric Administration, Boulder, Colo. 80302, U.S.A.
ESRO	European Space Research Organization.

IACSTA	Interdisciplinary Analysis Center for Solar-Terrestrial Activity, University of Tokyo, Tokyo, Japan.
IAGA	International Association of Geomagnetism and Aeronomy, IUGG Publication Office, 39 ter, rue Gay-Lussac, Paris (V) France.
ISGI	International Service of Geomagnetic Indices, 1 (DeBilt): Royal Netherlands Meteorological Institute, DeBilt, The Netherlands. 2 (Göttingen): Institut für Geophysik, 34 Göttingen, W. Germany.
IUCSTP	Inter-Union Commission on Solar-Terrestrial Physics. Secretariat: c/o National Academy of Sciences, 2101 Constitution Ave., N.W., Washington, D.C. 20418, U.S.A.
NSSDC	National Space Science Data Center, Code 601. 4, Goddard Space Flight Center, Greenbelt, Md. 20771, U.S.A.
SDFC-NOAA	Space Disturbance Forecast Center, National Oceanic and Atmospheric Administration, Boulder, Colo. 80302, U.S.A.
WDC-A	World Data Center A for Solar-Terrestrial Physics, National Oceanic and Atmospheric Administration, Boulder, Colo. 80302, U.S.A. (formerly at Rockville, Md.)

Publications

CDSTP	Catalog of Data on Solar-Terrestrial Physics, issued by WDC-A.
GSDB	Geophysics and Space Data Bulletin, issued quarterly by AFCRL.
HGSE-65	Handbook of Geophysics and Space Environments, 1965 edition, S. L. Valley, ed., AFCRL, McGraw-Hill Book Co., New York.
IAGA-12	IAGA Bulletin No. 12, a series, issued yearly, entitled "Geomagnetic Data (Year) Indices K and C, Rapid Variations", published by North-Holland Publishing Co., Amsterdam, The Netherlands.
IAGA-18	IAGA Bulletin No. 18, a single volume, published by North-Holland Publishing Co., Amsterdam, The Netherlands.
JGR	Journal of Geophysical Research, published by the American Geophysical Union, 2901 Byrdhill Rd., Richmond, Va. 23228, U.S.A.
SGD	Solar-Geophysical Data, issued monthly by EDS-NOAA.
STP	STP Notes, a numbered series issued occasionally by IUCSTP.
TBGIRV	Three-monthly Bulletin of Geomagnetic Indices and Rapid Variations, issued by IAGA and distributed by ISGI (DeBilt).

The K index

WDC-A has K values since 1957 for many observatories on microfilm and issues a catalog which lists availability of these.

IAGA-12 lists K values for the third year prior to publication.

JGR listed K_{FR} for the month prior to publication between 1957 and 1959.

SDFC lists K_{FR} currently in its "Preliminary Report and Forecast of Solar Geophysical Activity".

The Kp index

SGD lists Kp values for the second month prior to publication.

TBGIRV contains Kp values for the 3-month interval about 8 months prior to publication.

IAGA-12 lists Kp for the 3 years prior to publication.

IAGA-18 lists Kp for the period 1932 to 1961.

JGR listed Kp for the 5th month prior to publication for the period 1951-1968 and has resumed publishing it in 1971.

HGSE-65 lists monthly means of Kp for 1932 to 1963 and daily means for 1957 to 1963.

WDC-A and NSSDC both have available a computer tape made by ESRO containing Kp values from 1932 to within one to three months of the current date.

GSDB currently lists Kp as supplied by ISGI.

See also "graphical presentations" listing.

The Kn, Ks, and Km indices

Mayaud, P.N., "Indices Kn, Ks, et Km, 1964-1967", Editions du Centre National de la Recherche Scientifique, 1968, lists numerical values for 1964-1967.

The ak and Ak indices

ak and Ak indices are not published regularly.

The ap and Ap indices

Among the sources listed for Kp, the ESRO tape at WDC-A and NSSDC, IAGA-12 and IAGA-18 contain ap for the same periods for which Kp is given.

Of the sources listed for Kp, all provide Ap as well, except for TBGIRV.

The C index

IAGA-12 lists C values for the third year prior to publication.

The Ci index

HGSE-65 lists monthly and annual means of Ci for the period 1884-1964 and daily values for the period 1957-1963.

TBGIRV, SGD, JGR, and IAGA-12 all list daily values of Ci with the same coverage as for Kp.

Terrest. Magn. Atmosph. Elec. 37, 42 (1932) lists Ci indices in 27-day recurrence sequences for the period 1906-1931.

IAGA-12 lists monthly and annual means of Ci from 1900 to the third year prior to publication.

The Cp index

Of the sources listed for Kp, all provide Cp as well, except for TBGIRV.

The C9 index

Among the sources listed for Kp, the ESRO tape at WDC-A and NSSDC contain values of C9 for the same period for which Kp is given.

SGD contains values of C9 from time to time, with intermittent coverage.

See also "graphical presentation" listing.

The Q index

WDC-A can provide the Q index for those periods (since 1957) specified in its CDSTP.

The AE Index

WDC-A and NSSDC have 2.5-minute AE values for the period 1964-1968 on a computer tape, and hourly values for the period 1957-1964 on another tape. For current additions, enquiry should be addressed to these centers. Tabulations and graphical plots of these are also available on microfilm.

The Dst Index

Hourly Dst values for 1957-1970 have been re-evaluated and listed by Sugiura and Poros in NASA/GFSC X-645-71-278, available from NSSDC. Earlier, Sugiura et al had published Dst values as follows:

(1) for July 1957-December 1968: Ann. IGY 35, 9, Pergammon Press, Oxford, 1964;

(2) for 1961-1963: NASA Technical Note TN D-4047, August 1967;

(3) for 1964-1967 NASA Technical Note D-5748, May 1970;

(4) for 1968: NASA Technical Note D-6278, March 1971;

(5) for 1969: NASA/GFSC X-645-70-345, 1970; and

(6) for early 1970: NASA/GFSC X-645-70-405, 1970.

These documents are available from NSSDC.

WDC-A and NSSDC have the Dst values of Sugiura et al available on a computer tape.

The U, u, u_1, and Δ indices

Terr. Magn. Atmos. Elec. 37, 9 (1932) lists monthly and annual means of U for 1872-1930, annual means of u for 1835-1871, and monthly and annual means of u_1 for 1872-1930.

Terr. Magn. Atmos. Elec. 51, 76 (1946) lists monthly means of u for 1940-1945.

Landolt-Börnstein, Zahlenwerte und Funktionen, Band 3, Astronomie und Geophysik, p. 871, Springer-Verlag, Berlin (1952) lists monthly means of U for 1872-1949.

HGSE-65 lists monthly and annual means of U for 1872-1949.

HGSE-65 lists the daily values and monthly and annual means of ΔH_1 for Huancayo, Peru, for the period 1933-1944.

The W measure

Terr. Magn. Atmos. Elec. 51, 184 (1946) lists monthly means of W for the period 1922-1939.

Landolt-Börnstein, Zahlenwerte und Funktionen, Band 3, Astronomie und Geophysik, p. 752, Springer-Verlag, Berlin (1952), lists two-monthly means of W for the period 1922-1947.

Graphical presentations

ISGI (Göttingen) distributes the graphical plots (27-day recurrence sequences) of Kp and C9 shown in Figures 11-53 and 11-54. GSDB currently reproduces the Kp plots supplied by ISGI.

IACSTA prepares and distributes the Solar Terrestrial Activity Charts shown in Figures 11-55 and 11-56. These are currently being reproduced in STP from time to time as they become available.

11.9 REFERENCES

Akasofu, S.I., Polar and Magnetic Substorms, D. Reidel Publishing Company, Dordrecht-Holland, 1968.

Akasofu, S.I., and C.I. Meng, A study of polar magnetic substorms, J. Geophys. Res., 74, 293, 1969.

Alfvén, H., Kungl. Sv. Vef. - Akademiens Handl. 18, No. 3, 1939.

Alfvén, H., Cosmical Electrodynamics, Oxford University Press, London, 1950.

Alldredge, L.R., Instruments and geomagnetic stations, Physics of Geomagnetic Phenomena (S. Matsushita and W. H. Campbell, ed), Academic Press, New York, 1967.

Alldredge, L.R., and L. Hurwitz, Radial dipoles as the sources of the earth's main magnetic field, J. Geophys. Res., 69, 2631, 1964.

Axford, W.I., Tail of the magnetosphere, J. Geophys. Res., 70, 1231, 1965.

Barfield, J.N., R.L. McPherron, P.J. Coleman, Jr., and D. J. Southwood, Storm-associated Pc 5 micropulsation events observed at the synchronous equatorial orbit, J. Geophys. Res., 77, 143, 1972.

Bartels, J., Geomagnetic data on variations of solar radiation: Part I - wave radiation, Terrest. Magn. Atmosph. Elec., 51, 181, 1946.

Birkeland, K., The Norwegian Aurora Polaris Expedition 1902-1903, H. Aschehoug Co., Christiana, 1913.

Bullard, E.C., The secular change in the earth's magnetic field, Monthly Notices Roy. Astron. Soc. Geophys. Suppl., 5, 248, 1948.

Bullard, E.C., The magnetic field within the earth, Proc. Roy. Soc. Ser. A, 197, 433, 1949a.

Bullard, E.C., Electromagnetic induction in a rotating sphere, Proc. Roy. Soc. Ser. A; 199, 413, 1949b.

Bullard, E.C., C. Freedman, H. Gellman, and J. Nixon, The westward drift of the earth's magnetic field, Phil Trans. R. Soc., 243A, 67, 1950.

Burlaga, L.F., Hydromagnetic waves and discontinuities in the solar wind, Space Sci. Rev., 12, 500, 1971.

Cain, J.C., Geomagnetic models from satellite surveys, Rev. Geophys. Space Phys., 9, 259, 1971.

Cain, J.C., and R. E. Sweeney, Magnetic field mapping of the inner magnetosphere, J. Geophys. Res., 75, 4360, 1970.

Campbell, W.H., Geomagnetic pulsations, Physics of Geomagnetic Phenomena (S. Matsushita and W.H. Campbell, ed.), Academic Press, New York, 1967.

Carpenter, D.L., Whistler studies of the plasmapause in the magnetosphere. 1. Temporal variations in the position of the knee and some evidence on plasma motions near the knee, J. Geophys. Res., 71, 693, 1966.

Chapman, S., and J. Bartels, Geomagnetism, Oxford University Press, London, 1940.

Chernosky, E.J., The delta measure of geomagnetic activity, Trans. Am. Geophys. Union, 37, 339, 1956.

Cox, A., R.R. Doell, and G.B. Dalrymple, Geomagnetic polarity epochs and Pleistocene geochronometry, Nature, 198, 1046, 1963a.

Cox, A., R.R. Doell, and G.B. Dalrymple, Geomagnetic polarity epochs: Sierra Nevada II, Science, 142, 382, 1963b.

Cox, A., R.R. Doell, and G.B. Dalrymple, Geomagnetic polarity epochs, Science, 143, 351, 1964.

Elsasser, W.M., Induction effects in terrestrial magnetism. 1. Theory, Phys. Rev., 69, 106, 1946a.

Elsasser, W.M., Induction effects in terrestrial magnetism. 2. The secular variation, Phys. Rev., 70, 202, 1946b.

Elsasser, W.M., Induction effects in terrestrial magnetism. 3. Electric modes, Phys. Rev., 72, 821, 1947.

Feldstein, Y.I., and G.V. Starkov, Dynamics of auroral belt and polar geomagnetic disturbances, Planet. Space Sci., 15, 209, 1967.

Fougere, P.F., Mutually consistent magnetic charts based on orthogonal functions, J. Geophys. Res., 69, 2641, 1964.

Frank, L.A., On the extraterrestrial ring current during geomagnetic storms, J. Geophys. Res., 72, 3753, 1967.

Heppner, J.P., B.G. Ledley, T.L. Skillman, and M. Sugiura, A preliminary survey of the distribution of micropulsations in the magnetosphere from OGO's 3 and 5, Ann. Geophys., 26, 709, 1970.

Hess, W.N., The Radiation Belt and Magnetosphere, Blaisdell Publishing Co., Waltham, 1968.

Irving, E., Paleomagnetism, John Wiley and Sons, New York, 1964.

Jensen, D.C., and J.C. Cain, An interim geomagnetic field, J. Geophys. Res., 67, 3568, 1962.

Kikuchi, H., and H.A. Taylor, Jr., Irregular structure of thermal ion plasma near the plasmapause observed from OGO 3 and Pc 1 measurements, J. Geophys. Res., 77, 131, 1972.

Lincoln, J.V., Geomagnetic indices, Physics of Geomagnetic Phenomena (S. Matsushita and W.H. Campbell, ed.), Academic Press, New York, 1967.

McDougall, I., and D.H. Tarling, Dating of polarity zones in the Hawaiian Islands, Natures, 200, 54, 1963.

McDougall, I., and D.H. Tarling, Dating geomagnetic polarity zones, Nature, 202, 171, 1964.

Matsushita, S., Solar quiet and lunar daily variation fields, Physics of Geomagnetic Phenomena (S. Matsushita and W.H. Campbell, ed.), Academic Press, New York, 1967.

Matsushita, S., and H. Maeda, On the geomagnetic solar quiet daily variation field during the IGY, J. Geophys. Res., 70, 2535, 1965a.

Matsushita, S., and H. Maeda, On the geomagnetic lunar daily variation field, J. Geophys. Res., 70, 2559, 1965b.

Mayaud, P.N., Indices Kn, Ks, et Km, 1964-1967, Editions du Centre National de la Recherche Scientific, 1968.

Mead, G.D., Deformation of the geomagnetic field by the solar wind, J. Geophys. Res., 69, 1181, 1964.

Midgley, J.E., Perturbation of the geomagnetic field - a spherical harmonic expansion, J. Geophys. Res., 69, 1197, 1964.

Nagata, T., Two main aspects of geomagnetic secular variation - westward drift and nondrifting components, Benedum Earth Magnetism Symposium (T. Nagata, ed.), University of Pittsburgh Press, 1962.

Nagata, T., Y. Arai, and K. Momose, Secular variation of the geomagnetic total force during the last 5000 years, J. Geophys. Res., 68, 5277, 1963.

Nagata, T., and M. Ozima, Paleomagnetism, Physics of Geomagnetic Phenomena (S. Matsushita and W.H. Campbell, Ed.), Academic Press, New York, 1967.

Nishida, A., Coherence of DP 2 fluctuations with interplanetary magnetic variations, J. Geophys. Res., 73, 5549, 1968.

Nishida, A., and S. Kokubun, New polar magnetic disturbances: Sq^P, SP, DPC, and DP 2, Rev. Geophys. Space Phys., 9, 417, 1971.

Obayashi, T., The interaction of the solar wind with the geomagnetic field during disturbed conditions, Solar-Terrestrial Physics (J.W. King and W.S. Newman, ed.), Academic Press, London, 1967.

Olson, W.P., A scalar potential representation of the tilted magnetopause and neutral sheet magnetic fields, MDAC Paper WD 1332 (unpublished), McDonnell Douglas Astronautics Company, Santa Monica, California, March, 1970.

Olson, W.P., and W.D. Cummings, Comparison of the predicted and observed magnetic field at ATS 1, J. Geophys. Res., 75, 7117, 1970.

Parkinson, W.D., and J. Cleary, The eccentric geomagnetic dipole, Geophys. J. Roy. Astron. Soc., 1, 346, 1958.

Russell, C.T., R.L. McPherron, and P.J. Coleman, Jr., Fluctuating magnetic fields in the magnetosphere. 1: ELF and VLF fluctuations, Space Sci. Rev., 12, 810, 1972.

Saito, T., A new index of geomagnetic pulsation and its relation to solar M-regions, Report of Iono. and Sp. Res., Japan, 1964.

Schindler, K., and N.F. Ness, Internal structure of the geomagnetic neutral sheet, J. Geophys. Res., 77, 91, 1972.

Silsbee, H.C., and E.H. Vestine, Geomagnetic bays, their frequency and current-systems, Terr. Magn. Atmos. Elec., 47, 195, 1942.

Speiser, T.W., and N.F. Ness, The neutral sheet in the geomagnetic tail: its motion, equivalent currents, and field line connection through it, J. Geophys. Res., 70, 131, 1967.

Sugiura, M., and S. Chapman, The average morphology of geomagnetic storms with sudden commencement, Abhandl. Akad. Wiss. Gottingen, Math. - Phys. K1. Sonderheft 3, 1960.

van Sabben, D., Ionospheric current systems of ten IGY solar flare effects, J. Atmos. Terr. Phys., 22, 32, 1961.

Vestine, E.H., The earth's core, Trans. Am. Geophys. Union, 35, 63, 1954.

Vestine, E.H., Influence of the earth's core upon the rate of the earth's rotation, Benedum Earth Magnetism Symposium (T. Nagata, ed.), University of Pittsburgh Press, Pittsburgh, 1962.

Vestine, E.H., Main geomagnetic field, Physics of Geomagnetic Phenomena (S. Matsushita and W.H. Campbell, ed.), Academic Press, New York, 1967.

Williams, D.J., and G.D. Mead, Nightside magnetosphere configuration as obtained from trapped electrons at 1100 kilometers, J. Geophys. Res., 70, 3017, 1965.

Zaytsev, A.N., and Y.I. Feldstein, Polar disturbances and current system according to data obtained in the winter season of the IGY, Geomagnetizm i Aeronomiya, 7, 449, 1967.

Zmuda, A.J., ed., World Magnetic Survey 1957-1969 (IAGA Bulletin No. 28), IUGG Publications Office, Paris, 1971.